Dynamics and Structure of Liquid Crystal Colloids

Roan Lavery

Thesis submitted for the degree of Doctor of Philosophy

Department of Physics and Astronomy

University of Edinburgh

2001

OLD MAN : " You must look for the sound of a humming birds wings.
Listen for the colour of the sky.
Search the air for the perfume of ice on a hot day.
If you find these things you will know."

YOUNG MAN : "Old man, how is it that you hear these things?"

OLD MAN : "Young man, how is it that you do not?"

SAMPLE FROM "HOW TO BE A NINJA IN ONE EASY LESSON" BY THE LONDON FUNK ALLSTARS

Abstract

This thesis sets out to investigate the dynamic and structural properties of liquid crystal colloids. In themselves the fields of colloidal and liquid crystal science have been well studied, but the combination of these produces a wealth of new physics which has provoked much interest over the past few years. The research began by investigating the dynamics of dilute suspensions of colloidal particles in the isotropic phase of a liquid crystal near the nematic transition. It was found that the particles exhibited an anomalously low diffusion which was explained in terms of the formation of an ordered layer of liquid crystal molecules surrounding the particles even when the bulk phase was disordered.

It was also discovered around this time that due to the preparation procedure the particle could become coated with a thin layer of another type of solvent which dramatically affected the particle diffusion. This lead to an offshoot study in this area, and it was found that the diffusion of these coated particles was much faster than expected because of a change to the boundary conditions at the particle surface. Latterly the nature of this coating was investigated more and a hydrodynamic model employed to compare experimental results with the predictions given by the theory. It was found that these were in good agreement.

The focus of investigations then changed, focusing on more concentrated systems of colloidal particles in liquid crystal solvents as these exhibited unusual structural phenomena. It was seen that a concentrated suspension of particles in

liquid crystal shows a huge increase in the rigidity of the material in its nematic phase, compared with the pure liquid crystal. This is due to the creation of a honeycomb-like aggregate particle network, which increases the elastic strength of the material. The network formation was observed using microscopy and the elastic modulus was measured rheologically to be many orders of magnitude higher than the pure liquid crystal. The role of cooling rate from the isotropic to nematic phase was also investigated thoroughly as this has a large impact on the final structure of the material. Finally, another liquid crystal was used which this time also featured a smectic phase, and it was again found that the ordered phases created a particle network with a surprisingly strong rigidity.

Acknowledgements

I would first of all like to thank my two supervisors ,Jason Crain and Wilson Poon, whose invaluable advice and direction helped me through this sometimes unpredictable journey. While it seems physics rarely does what is expected both Jason and Wilson were always dependable and full of wisdom and encouragement.

I would also like to thank everyone else in the department who has aided me over the past 3 years, especially the usual faces of Andy, Linda, Paul and Virginnie in the lab.

I'm perhaps obliged to give a grudging thanks to my friends outwith the university but seeing as though they've contributed nothing to the thesis and have actively persuaded me to "skive off" as much as possible I don't think I'll bother.

Contents

Abstract v

Declaration vii

Acknowledgements ix

1 Introduction 1

1.1 Liquid crystal colloids 1

1.2 Motivation for study 2

1.3 Historical overview 3

1.4 Layout of thesis 4

2 Background theory 7

2.1 Introduction 7

2.2 Liquid crystals 7

2.2.1 Building Blocks 8

2.3 The two types of Liquid Crystal 9

2.3.1 Thermotropic 9

2.3.2 Lyotropic 11

2.4 Defining order in liquid crystals 12

2.5 The isotropic-nematic transition 14

2.6 Viscosity of a nematic 17

2.7 Distortions in a nematic 18

2.7.1 Defects 20

2.7.2 Disclination lines 20

2.7.3 Point defects 20

2.7.4 Topological charges 21

2.8 Colloids 23

2.8.1 Definition of colloids 23

2.8.2 Hard spheres 25

2.8.3 Stabilisation 26

2.8.4 Core-shell colloids 27

2.8.5 Sedimentation 27

2.8.6 Polydispersity 28

2.9 Liquid crystal colloids 29

2.9.1 In the Nematic phase 30

3 Characterising the system **35**

3.1 The Colloidal Particle 35

3.2 Washing the particles 36

3.3 Determining the volume fraction 37

3.3.1 Spin-down method 37

3.3.2 Weight method 38

3.4 Dispersing particles in a liquid crystal 39

3.4.1 Dispersing dried particles 40

3.5 Determining the viscosity of a solvent 41

3.6 The Liquid crystal 43

3.7 Identifying the phases 44

3.8 Determining the boundary conditions. 47

4 Experimental techniques **51**

4.1 Light Scattering 51

4.1.1 Scattering from a particle 53

4.1.2 Scattering from many particles 55

4.2 Static Light Scattering 56

4.2.1 Scattering from the core-shell 58

4.3 Dynamic light Scattering 59
4.3.1 The Correlation function 60
4.3.2 Apparatus 62
4.3.3 Obtaining results from DLS 64
4.3.4 DLS on Liquid crystals 66
4.4 Rheology 68
4.4.1 Oscillatory rheology 69
4.4.2 The rheometer 72
4.4.3 Setting the gap 75
4.5 Microscopy 75
4.5.1 Optical Microscopy 76
4.5.2 Confocal Microscopy 77

5 Colloid dynamics in a liquid crystal **81**

5.1 Introduction 81
5.2 Dynamics of colloids 82
5.3 DLS on the liquid crystal colloids 84
5.3.1 The effect on the transition temperature 84
5.3.2 Colloidal diffusion in 5CB 86
5.3.3 Particles of different sizes 89

5.4 Discussion 92

6 Dynamics of coated colloids **95**

6.1 Introduction 95

6.2 Motivation for investigation 96

6.2.1 Preparation procedure reviewed 97

6.2.2 Size of the coating 101

6.3 The effect of time 104

6.4 Effect of particle size 105

6.5 A Hydrodynamic model 107

6.6 Using the model 111

6.7 Coated colloids in a liquid crystal 113

6.8 Discussion 116

7 Concentrated liquid crystal colloids **121**

7.1 Introduction 121

7.2 Effects of the nematic phase 122

7.2.1 Sample preparation 122

7.2.2 Direct observations and microscopy 122

7.2.3 Structural properties of network 125

7.2.4 Developing a model for network formation 127

7.3 The effect of different cooling rates 130

7.3.1 Relationship between cooling rate and microstructure . . . 131

7.3.2 Rheological study of the effects of cooling rate 134

7.4 Successive measurements 135

7.5 Confocal microscopy of particle network 138

7.5.1 Domain sizes of network 141

7.5.2 Rheology of dyed networks 141

7.6 Effects of a smectic phase 144

7.7 Microscopy images from 8CB samples 146

7.8 Rheology results from 8CB samples 147

7.9 Discussion 149

8 Conclusions **151**

8.1 Summary of results 151

8.1.1 Dynamics of colloids in isotropic phase 152

8.1.2 Dynamics of coated colloids 152

8.1.3 Structure and rheology of liquid crystal colloid composites 154

8.2 Future work 154

Bibliography **157**

List of Figures

2.1 Chemical structure for 5CB liquid crytsal molecule 9

2.2 Three possible phases of a thermotropic liquid crystal. 10

2.3 The lamellar phase of soap. 11

2.4 Diagram showing the variation in molecular alignment in a nematic. 13

2.5 Schematic demonstrating why cubic terms of Q are allowed in the free energy. 16

2.6 The schematic form of the free energy F for temperatures above, below and at the critical temperature. 16

2.7 The three geometries for viscosity measurements of a perfect nematic liquid crystal with director **n**. 17

2.8 The three types of deformation in a nematic. 18

2.9 Some examples of defects in nematic liquid crystals. 21

2.10 Colloidal particles dispersed in a continuous dispersion medium. . 23

2.11 The schematic potential for hard sphere colloids. 26

2.12 A schematic of a cross-section of a colloidal particle core and the polymer hairs grafted onto the surface so it acts as a hard sphere. 26

2.13 The refractive index profile for a typical colloidal particle with a PMMA latex core and PHSA polymer hairs grafted onto the surface. 27

2.14 A schematic diagram of liquid crystal molecules ordering at the surface of a colloidal particle 30

2.15 Examples of liquid crytsal director configurations around a colloid particle and in the pure nematic state 31

2.16 The director configurations surrounding a solid particle with homeotropic boundary conditions for weak anchoring conditions. 32

2.17 The two possible director configurations surrounding a solid particle with homeotropic boundary conditions for strong anchoring conditions. 33

2.18 Particle chaining in a nematic liquid crystal. 33

3.1 Schematic of height measurement to determine volume fraction. . 38

3.2 Schematic diagram of the preparation process for dispersing particles, initially present in one solvent, in a liquid crystal. 40

3.3 Results of Mass against volume for pure petroleum ether and the value for the density calculated. 42

3.4 Schematic of the sedimentation behaviour for a colloidal solvent. . 43

3.5 Results for the sedimentation distance against time over a period of around 6 hours. 44

3.6 Microscope image of the pure nematic phase of 8CB under crossed polarisers. 45

3.7 Microscope image of the smectic phase of 8CB. 46

3.8 A schematic of the focal-conical fan domain which gives the smectic phase its unique appearance. 46

3.9 Schematic of a LC/water emulsion where particles are suspended inside the LC. 47

3.10 Images of a liquid crystal drop, containing a colloidal particle, in water. 49

4.1 Schematic showing how the scattering vector Q is defined from light scattering from two volume elements. 53

4.2 The total light scattered from a particle is found by summing the contributions from the individual volume elements. 54

4.3 The theoretical form factor for a perfect sphere. 54

4.4 A simplified diagram of a Static Light Scattering set-up. 56

4.5 An experimentally measured form factor for a dilute system of spherical particles. 57

4.6 The fluctuating intensity signal is due to the light scattering from the particles interfering constructively and destructively as the particles move around in Brownian motion. 60

4.7 The form of $\langle I(0)I(\tau)\rangle$ against τ. 61

4.8 A schematic diagram of the Dynamic Light Scattering set-up used in this thesis. 62

4.9 An example of two possible fits to the same correlation function. . 67

4.10 Schematic of a Hookean solid undergoing deformation. 68

4.11 The profiles for stress and strain waves in a viscoelastic material subjected to oscillation. 71

4.12 A simplified schematic of the CSL^2 rheometer. 72

4.13 A close up of the cone and plate region of the rheometer. 73

4.14 3 schematic diagrams of different amounts of sample between the cone and plate. 74

4.15 A diagram showing the fundamental parts of the microscope used in this project. 77

4.16 Diagram of the simplified optics of a confocal microscope. In reality there are many different optical configurations which can be used. 78

4.17 Schematic diagram showing how the inclusion of a pinhole can greatly reduce the out of focus light that reduces images quality. . 79

5.1 The viscosity of 5CB as a function of temperature. 83

5.2 The scattering intensity as a function of temperature for samples of pure 5CB and 5CB with a dilute amount of particles. 85

5.3 The hydrodynamic radius against reduced temperature for a dilute sample of 174nm particles in 5CB. 87

5.4 The hydrodynamic radius against reduced temperature for a dilute sample of 350nm particles in 5CB. 90

6.1 Static Light Scattering results of form factors taken from samples prepared from dried particles and particles taken from a petrol stock, dispersed in cisdecalin. 98

6.2 Correlation functions obtained from DLS, at a scattering angle of 90^oC, for two samples: one prepared with dried particles and the other prepared with particles from a petroleum ether stock. . . . 99

6.3 Schematic diagram for the two-step refractive index profile of the colloidal particle. 102

6.4 Two different examples of experimental data compared with the theoretical form factor for coated spheres. 103

6.5 A graph of the correlation function for the same sample of coated colloids two weeks apart. 105

6.6 Comparison of the physical and hydrodynamic radii for a number of different sized particles. 106

6.7 Diagram of the 2 zone model used for the hydrodynamic calculations of the coated colloid dynamics. 108

6.8 A plot of l ($\frac{R_c}{R_p}$) against the slip factor S for 2 values of ξ:15 and 64. For a 2.5nm coating we can see that $\xi = 15$ gives a value for S of around 5.4 while for $\xi = 64$ produces a S value of 4.9. 113

6.9 Measurements of hydrodynamic radius against reduced temperature $(T - T_c)$ for 312nm coated particles in a liquid crystal. 115

6.10 Intensity against temperature for 3 samples. The sample containing uncoated particles shows a delayed phase transition temperature while the samples prepared with coated particles have a transition which is practically identical to the pure liquid crystal. . . . 116

7.1 A slice of colloid liquid crystal composite. 123

7.2 Microscope image of the honeycomb-like structure of aggregated particles 124

7.3 Oscillatory viscoelastic measurements of the storage and loss modulii of the liquid crystal colloid compound as it is cooled from the isotropic phase to the nematic phase. 126

7.4 A series of schematic diagrams describing the formation mechanism of the particle network. 129

7.5 Close-up schematic of the cell wall of particle network. 130

7.6 Two microscopy images of the particle network taken in the isotropic phase after reheating. 132

7.7 Two microscopy images taken just below 35^oC when the nematic domains nucleate in the isotropic and eventually coalesce to completely form the nematic phase. 133

7.8 Rheology results for the storage and loss modulii for samples cooled at 3 different rates. 135

7.9 Rheological measurements of the storage modulus taken from the same sample where reheating into the isotropic phase and vigorously shearing for 5 minutes occured between each run. 136

7.10 Storage and loss modulii measurements for a 5% volume fraction sample with successive measurements and varying cooling rate. . . 137

7.11 Confocal microscopy images taken from 5% volume fraction liquid crystal colloid composites for a variety of different cooling rates. . 140

7.12 Domain size against cooling rate as measured from the averaging of over 100 domains in each sample. 142

7.13 Rheology results for measurements of G' and G'' made on a sample of dyed particles in 5CB. 143

7.14 Viscosity measurements as a function of temperature for pure 8CB. 145

7.15 Two microscopy images of a 5% volume fraction liquid crystal colloid composite prepared with 8CB, and taken into the nematic phase and then back to the isotropic. 146

7.16 Microscopy image taken in the isotropic phase of the liquid crystal after the sample had been previously cooled into the smectic phase then reheated. 147

7.17 Rheological measurements of $G'$and G'' taken as the sample of 8CB and particles is cooled from the isotropic to the smectic phase. . 148

List of Tables

2.1 Various common colloidal systems with their constituents 24

6.1 Table showing a series of results taken from SLS and DLS showing the physical radius of particles alongside the measured hydrodynamic radius, and the slip factor implied. 107

6.2 Comparing experimentally measured values of S with the theoretical predictions made for a 2.5nm coating of solvent surrounding. . 112

Chapter 1

Introduction

1.1 Liquid crystal colloids

Independently the fields of liquid crystals and colloids have been well studied over the years. Liquid crystals have been of interest to scientists since their discovery in the second half of the ninetinth century. However it wasn't until much later that research into the possibilities these fascinating materials presented began seriously. Today of course, the liquid crystal industry is huge with it's most famous application, the Liquid Crystal Display, utilised in watches,calculators and even modern televisions. Likewise, colloids are an equally important part of our everyday lives with their use in everything from shampoo's to food. With the proliferation of use for both liquid crystals and colloids it is not unreasonable to think that the two separate systems have been completely studied. While this is only partially true, and there are many areas in each field that are the subject of ongoing research, it is true that simple colloid and liquid crystals are today well understood. However as is often the case in physics combining two apparently simple and well understood systems results in a third state which is more complex than the sum of its parts and contains a wealth of new physics. Such is the case

with liquid crystal colloids.

1.2 Motivation for study

Studying the combination of liquid crystals and colloids can be useful in understanding either of the two fundamental constituents. From the liquid crystal standpoint, including a colloidal particle into the nematic state introduces defects, and so the nature of defects and crucially how they interact with one another can be studied. Using colloidal particles to do this is easy as they allow for a well defined and controlled amount of defects to be added. We will also find that the inculsion of colloidal particles into the nematic states has a profound effect on the elasticity of the overall composites. From the colloidal point of view, there is the oppourtunity to study the behaviour of a particle in an anisotropic solvent where the forces between particles are much more complex than in a normal solution.

These considerations are all of a fundamental nature but there has also been great interest in liquid crystal colloids from a practical standpoint. It has been suggested that making liquid crystal displays that are doped with particles would create a number of advantages over the traditional displays [1]. The effects that colloidal particles have on the elasticity of the nematic phase are also of interest in the field of Liquid Crystal Displays as it creates the possibility for a new kind of display with strong mechanical strength combined with a flexibility that would allow for very thin displays that could be rolled up. Some of the practical considerations for this technology will be discussed in later chapters.

1.3 Historical overview

The first instance of somebody intentionally trying to add particles to a liquid crystal for scientific purposes was probably by de Gennes and Brochard [2] who were studying the effect of an external magnetic field on the molecular orientation of the liquid crystal. In order for there to be sufficient coupling between the liquid crystal molecules and the external field it was first necessary to "dope" the liquid crystal with ferromagnetic grains. While there were problems with clustering of the grains the work was later continued more sucessfully by a couple of groups [3,4]. In 1987 Bottger *et al* examined the dynamics of colloidal particles in the isotropic phase of a liquid crystal as it was cooled towards the nematic [5], and suggested that a change in the colloidal dynamics was due to molecular ordering at the surface of the particles, and there have been other studies of colloidal motion in a liquid crystal that suggested that particles may become "frozen" in the nematic phase and cease to diffuse [6,7]. While we have given here some brief examples, there has been many attempts to include particles of various natures in liquid crystals and some of these can be found in references [8–10] and will expanded upon later in the thesis.

From a theoretical stance there has also been considerable progress in our understanding of liquid crystal colloids. Considerable effort has gone into understanding the director field surrounding a particle in the nematic phase, and the solution has turned out to be much more complex than would perhaps first be anticipated. Terentjev and Ruhwandl studied the frictional drag on a particle in a liquid crystal [11] and later the director configurations of liquid crystal molecules surrounding particles in nematics [12], as well as the novel forces between particles in nematics [13]. Meanwhile Lubensky *et al* was also analysing the topological defects that colloidal particles create in nematics [14]. The picture that emerged from all of this work was one where the director structure around particles in nematics can take on a number of possible configurations and is very sensitive

to factors such as the anchoring strength at the particle surface. While much knowledge has been gained from these studies it seems as though there is still some way to go before the simple case of a single particle in the nematic phase is completely understood.

If the case of a single particle in a nematic liquid crystal is complicated then the case for a concentrated amount of colloidal particles might at first seem impossibly so. However, these systems have provided some fascinating new physics and possible industrial applications. Meeker *at al* [15] reported the formation of a "soft solid" when sufficient amounts of colloidal particles were included in the nematic phase. These materials, names liquid crystal colloid composites, exhibited extremely high elastic modulii and were so rigid that they could be cut with a knife. Further work has gone on to examine these materials further by Terentjev and others, in part focusing on the role of particle concentration on the final elasticity of the materials and providing a theoretical explanation for the strength of these structures [16–18].

1.4 Layout of thesis

This thesis details two main areas of experimental research: the case of dilute colloids in a liquid crytsal, and more concentrated liquid crystal colloids. There is a third chapter dedicated to an off-shoot study which began a result of some unusual experimental results.

Chapter 2 contains some background information on the fundamentals of this project. It begins with some basic theory regarding the separate issues of liquid crystals and colloids before proceeding to discuss the somewhat more complicated case when the two are combined.

Because of the importance of preparation procedure in the following experiments,

the entirety of Chapter 3 is devoted to the various methods that were used in sample preparation, as well as some preliminary results concerning the identification of colloidal behaviour in a nematic. This was crucially done at this stage so as to justify assumptions used later in the project.

Chapter 4 details the various experimental techniques that were employed. These included static and dynamic light scattering, microscopy and rheology and in each case a simplistic overview of the principles behind each and how they are used in my experiments is given.

Chapter 5 is the first main results section where the dynamics of particles in the isotropic phase of a liquid crystal are examined and how this effects the phase transition of the liquid crytsal itself.

Chapter 6 is the offshoot study of the coated colloid dynamics, where some unusual experimental results are examined more throughly with the aid of a hydrodynamic model.

The final results are presented Chapter 7, where the behaviour of concentrated systems of liquid crystal colloids are studied. Both nematic and smectic crystals are used and many different aspects of their remarkable behaviour are investigated.

Chapter 8 concludes the thesis with summary of all the work contained in the thesis as well as some suggestions for further work.

Chapter 2

Background theory

2.1 Introduction

This thesis deals with the effects of a combination of liquid crystals and colloids, two very separate fields of physics which have very different ideas describing their behaviour. As such, this introductory chapter shall be split into three sections: the first two sections shall give a brief theoretical background for the separate cases of pure thermotropic liquid crystals and colloids in simple solvents, and the third is then primarily concerned with the "new" physics that is obtained when these two are combined.

2.2 Liquid crystals

Everybody is familiar with the three fundamental states or "phases" of matter : solid, liquid and gas and the corresponding molecular or atomic behaviour which essentially defines that particular phase. A solids rigidity arises because the molecules or atoms are set in fixed positions and cannot move, while in a

liquid they have a certain degree of mobility and so allow the substance to flow.

As the name suggests liquid crystals are a class of materials that exist somewhere between liquids and solids [19], and to explain this further the molecular behaviour must be examined further. Liquid crystals are materials that have extra phases of matter somewhere between the solid and liquid states, and the molecular ordering in these "mesophases" exhibit some characteristics of the two extremes. There are many different mesophases that liquid crystalline materials can have, each corresponding to a different type of molecular ordering, and one of the most important factors in determining the mesophases is the shape of the molecules that make up the material.

2.2.1 Building Blocks

Generally speaking, to create a liquid crystalline material the building blocks (molecules or groups of molecules) must be anisotropic in shape and usually this means they fall into either the rod-like or disc-like categories [20]. It is the anisotropic shape of the molecules which means it is possible for the material to demonstrate a liquid crystal phase. While there are many different shapes of molecules that give rise to liquid crystalline phases, all materials used in this study are of the rod-like variety so the discussion here shall be focused on those. An example of one of the most common rod-like molecules can be seen in Fig 2.1. The shape of the molecules is very important in ensuring that liquid crystal mesophases are possible in the first place but there are other controlling factors that determine the particular type of phases, and at this point it is important to realise that there are two fundamentally different types of liquid crystals.

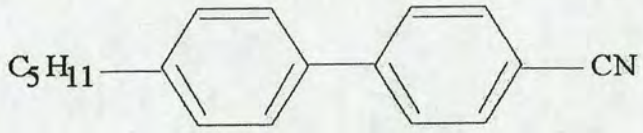

Figure 2.1: The chemical structure for $4' - n - Pentyl - 4 - cyanobiphenyl$. Two Benzene rings connect to a alkyl side chain group and a cyano terminal group giving the molecule its rod-like shape.

2.3 The two types of Liquid Crystal

2.3.1 Thermotropic

Thermotropic liquid crystals are of great research interest because it is these types that are used for devices such as liquid crystal displays which are found in calculators, lap-top computers and even some modern televisions [21].

In these types of liquid crystals it is the temperature which controls the ordering of the molecules and consequently what mesophase the liquid crystal is in. There are roughly 3 types of thermotropic liquid crystal mesophases: nematic, smectic and cholesteric. Using an example with rod-like molecules, we can examine some of the most common phases in a liquid crystal.

At high enough temperatures the molecules are completely randomly oriented and the fluid resembles any normal liquid. This is known as the isotropic phase. As the temperature decreases at some point it will become energetically favourable for the substance to undergo a phase transition, where the molecules align somewhat, thereby gaining a measure of order. In this phase, which is called the nematic, the molecules have a preference over what direction they want to point in (known as orientational ordering), and this direction is given by the director $\hat{n}$, a unit vector. Note however that although the molecules will tend to align parallel to each other, there is no positional ordering for each molecule and they still move

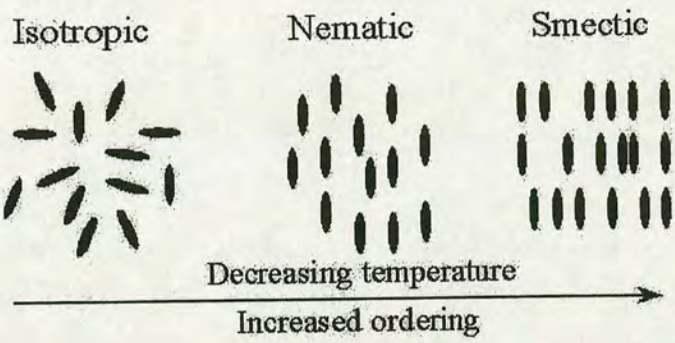

Figure 2.2: Three possible phases of a thermotropic liquid crystal. At the highest temperature the molecules are randomly orientated. As the temperature is cooled a nematic phase is seen where the molecules now have some degree of orientational order and if the temperature is cooled even further we see a smectic phase where the molecules now have orientational and positional ordering.

around relatively freely.

As the temperature is lowered even further another phase transition may take place in certain LC's. This phase is known as a smectic phase, and now the molecules not only have a larger degree of orientational ordering but also positional ordering as well. Here well-defined layers are formed and the material begins to diagramatically resemble a solid, but the layers are still individually fluid and there is the opportunity for molecules to diffuse from one layer to another so the material retains its liquid-like characteristics. There are different sub-types of smectic phases, as there can be a variety of molecular arrangements within each later, and the type described above is known as a Smectic A structure.

There is a third type of mesophase called the cholesteric phase where the director rotates in a helical fashion throughout the bulk but the discussion here shall be limited to those 2 listed above which have particular relevance to the experimental study at hand.

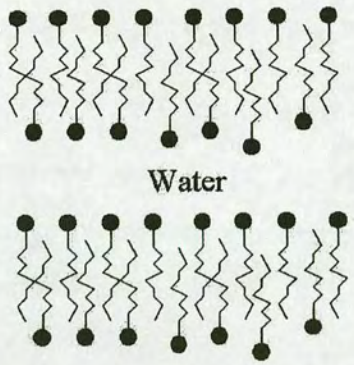

Figure 2.3: The lamellar phase of soap.

2.3.2 Lyotropic

The second type of liquid crystals are called Lyotropics and these are of great biological interest because many seem to be important in living processes [22]. Examples of these are DNA, certain viruses (tobacco mosaic virus) and cell membranes.

Lyotropic liquid crystals are made up of two or more components. This usually consists of a solution of rod-like building blocks suspended in a normal isotropic solvent. The rod-like building blocks are often an amphiphile with a polar head group attached to a long hydrocarbon tail and the solvent is often water. If the concentration of water is high enough, liquid crystalline mesophases may be obtained, and changing the concentration of the rods often allows the transition between various different mesophases. The most common example of this type of lyotropic liquid crystal is ordinary soap.

2.4 Defining order in liquid crystals

Now that the common types of liquid crystal have been introduced it is necessary to examine more closely what we mean by molecular ordering. The simplest form of liquid crystalline ordering is that found in the nematic where the molecules wish to align their axis to a generally preferred direction, so it is this example which shall be discussed first.

As described before, a nematic liquid crystal differs from its normal liquid counterparts because the molecules have a degree of orientational order. The centres of mass of the molecules are distributed at random throughout the liquid but there is a symmetry axis or director to which the molecules align parallel. This cylindrical symmetry means that the properties of the phase are different depending on whether you are looking parallel or perpendicular to the director. Optically this is seen as birefringence where rays of light propagating parallel to the director encounter a different refractive index to those travelling perpendicular.

Although the molecules prefer to align perfectly along the director, thermal fluctuations in the material will prevent this and as such the molecules shall be distributed with a range of orientations to the director. It is here where the notion of an order parameter becomes useful. A material where all the molecules lie perfectly along the director is obviously more ordered than one where there is a large variance in the orientations and it is possible, and indeed necessary, to quantify this in order to gain a greater understanding of liquid crystals. The order parameter is what we use to quantify the symmetry or order of the system, and this must be large for a highly ordered system and zero for a completely disordered isotropic one.

One of the commonest descriptions for the long-range order in a nematic was first introduced by Tsvetkov. It applies for a system for a system of rod-like molecules where:

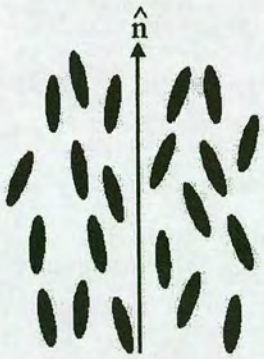

Figure 2.4: Diagram showing the variation in molecular alignment in a nematic. While there is a preferred direction for the molecules most are orientated at a small angles to this because of thermal fluctuations.

(1) The distribution function is cylindrically symmetric around the long axis of the molecules.

(2) The directions of n and -n are equivalent ie a 180^o rotation of a rod makes no difference.

Taking these considerations into account we can define the scalar molecular order parameter [23] as

$$S = \frac{1}{2} < 3\cos^2\theta - 1 > \tag{2.1}$$

where θ is the angle between the long axis of the molecule and the director $\hat{n}$, and the brackets denote a statistical average over all the molecules in the bulk. It is clear that in a sample where all molecules lie perfectly along the director (ie $\theta = 0$) then S=1. However in a completely random case the average $< \cos^2\theta >= \frac{1}{3}$ and S = 0. Therefore we can use S as a measure of alignment.

The overall order of the liquid crystal has a direct bearing on certain experimentally determinable quantities. Many of these macroscopic properties, such as magnetic moment, are tensor properties so a tensor order parameter (as opposed to the previous scalar version) is also useful in describing their behaviour.

Take a general molecular tensor property M and for simplicity choose the z-axis parallel to the nematic axis. In the isotropic phase this will have the form

$$M_{\alpha\beta} = M\delta_{\alpha\beta}. \tag{2.2}$$

This means that $M_{xx} = M$ while $M_{xy} = 0$ for example. In the uniaxial nematic phase M will be

$$M_{\alpha\beta} = \begin{pmatrix} M_\perp & 0 & 0 \\ 0 & M_\perp & 0 \\ 0 & 0 & M_\parallel \end{pmatrix} \tag{2.3}$$

where $\alpha, \beta = x, y, z.$ and $M_\perp$ and $M_\parallel$ refer to the tensor properties perpendicular and parallel to the symmetry axis respectively, and summation over repeated indices is implied.

Extracting the anisotropic part of this tensor will give us the tensor order parameter.

$$Q_{\alpha\beta} = G(M_{\alpha\beta} - \frac{1}{3}\delta_{\alpha\beta}\sum_\gamma M_{\gamma\gamma}) \tag{2.4}$$

Where G is a normalization constant and can be chosen. It can be seen that in the isotropic phase this goes to zero as any order parameter should. However as the next section shall show even in the isotropic phase small amounts of order can still exist.

2.5 The isotropic-nematic transition

We have assumed thus far that in the isotropic phase the molecules are randomly oriented with no positional or orientational ordering. But if the isotropic phase was to be examined closely it would be found that locally molecules still align parallel to one another in small regions that are often called swarms. Between different swarms there is no correlation of ordering but within each the ordering

is nematic. The size of these swarms is known as the coherence length $\zeta(T)$ as it is obviously a function of temperature. Typically $\zeta(T)$ will be of the order of 10^{-8}m (ten times the length of the molecules) just above the phase transition [5]. The nearer the temperature is to the isotropic-nematic transition the larger the swarms of nematic become. This gives an insight into the nature of the isotropic-nematic phase transition.

It is clear that a more rigorous description of the phase transition must involve the determination of the order parameter and its fluctuations for every temperature, and to do this we expand the free energy F in powers of the tensor order parameter which was described previously. We can write this [20] as

$$Q_{\alpha\beta} = Q(T)(n_\alpha n_\beta - \frac{1}{3}\delta_{\alpha\beta}) \tag{2.5}$$

which is essentially a different form of equation 2.4 for a uniaxial nematic.

There are a number of limitations for the terms when expanding F in powers of Q, and these shall listed here along with explanations as to why they are allowed or disallowed.

(1) There can be no linear terms in Q. This is to ensure that the state of minimum F is the state when Q=0 ie the isotropic state.

(2) Cubic terms in Q are allowed however. This is because the states $Q(\vec{r})$ and -$Q(\vec{r})$ represent different states with potentially different energies as shown in Fig 2.5.

Taking these considerations into account the free energy F takes the form [20]

$$F = F_0 + \frac{1}{2}A(T)Q_{\alpha\beta}Q_{\beta\alpha} + \frac{1}{3}B(T)Q_{\alpha\beta}Q_{\beta\gamma}Q_{\gamma\alpha} + \frac{1}{4}C(T)(Q_{\alpha\beta}Q_{\beta\alpha})^2 + O(Q^5) \tag{2.6}$$

which has the graphical form shown in Fig 2.6. Looking at the graph it can be seen that above the isotropic-nematic (I-N) transition temperature T_c the state of minimum F corresponds to Q=0 (the isotropic state as is expected). When

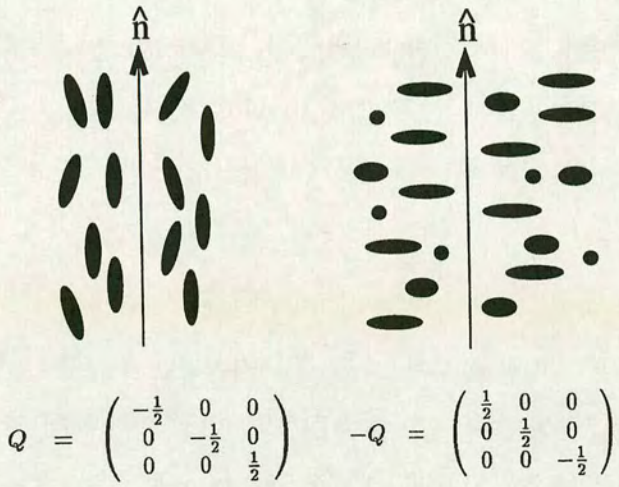

Figure 2.5: Schematic demonstrating why cubic terms of Q are allowed in the free energy. In the first case the molecules have a preferential alignment along the director. In the second the preferred alignment is in the two planes perpendicular to the director. The black dots symbolise molecules that have their long-axis coming out of the page. These two states are not equivalent and may have different energies.

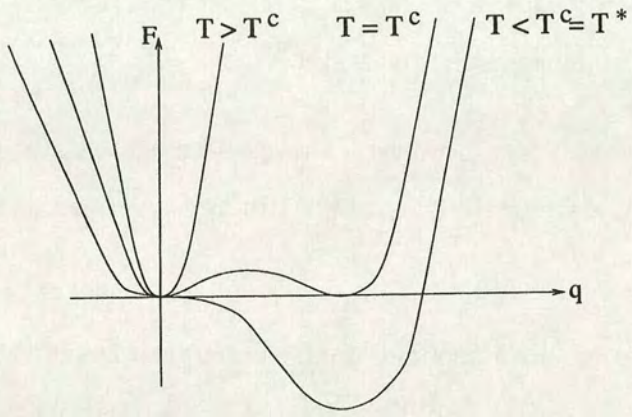

Figure 2.6: The schematic form of the free energy F for temperatures above, below and at the critical temperature. The temperature at which the liquid crystal becomes completely unstable with regards to nematic ordering is T^*.

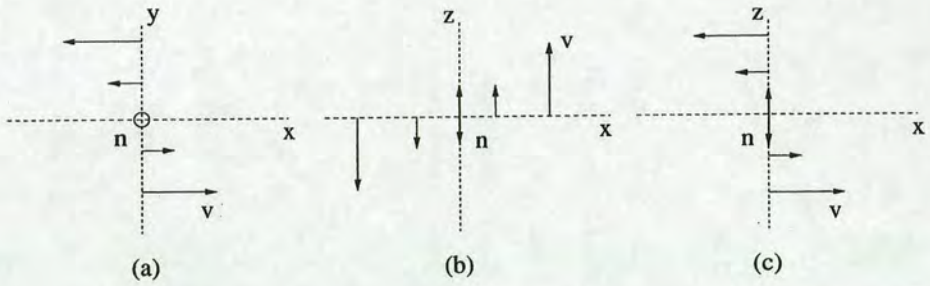

Figure 2.7: The three geometries for viscosity measurements of a perfect nematic liquid crystal with director **n**.

T=T_c there exists stable states for both Q=0 and $Q \neq 0$. This means that isotropic and nematic phases can coexist here. For lower temperatures below the transition temperature the free energy becomes completely unstable with respect to nematic ordering and only the nematic phase exists. At the transition there are discontinuites in many properties meaning the transition is first order. However, because the discontinuities are small and both isotropic and nematic phases can coexist means that the transition is only weakly first order.

2.6 Viscosity of a nematic

Any examination of the nematic state will reveal that many properties will depend on the direction of observation. The refractive index is one such anisotropic example, where light will experience a different refractive index depending on whether it propagates parallel or perpendicular to the director. Another example is the viscosity, but here there are three possible values depending on the particular direction of flow of the liquid crystal and the orientation of the director. If we apply a flow to the liquid crystal with velocity **v** then the three possible viscosities are shown in Fig 2.7 (a) shows the case where the director **n** is perpendicular to both the flow and the velocity gradient, (b) depicts the case where **n** is parallel to the flow and (c) describes the case where **n** is parallel to the velocity gradient,

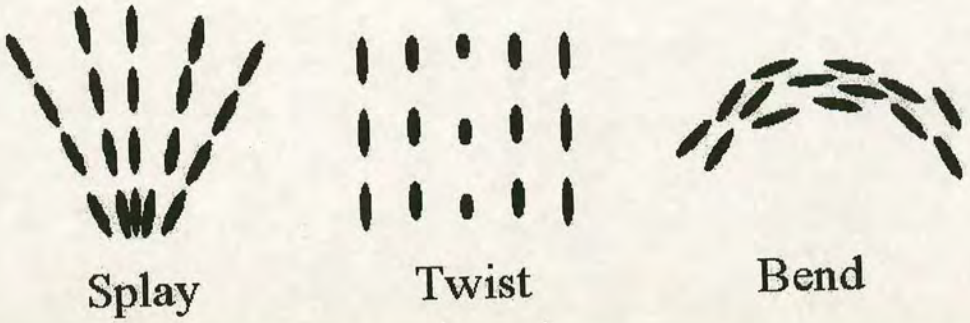

Figure 2.8: The three types of deformation in a nematic. Note that for twist the director rotates in out of the plane of the page

and they are called η_a, η_b and η_c respectively. These are know as the Miesowicz viscosities and in general $\eta_c > \eta_a > \eta_b$ for typical nematics [20].

2.7 Distortions in a nematic

Up to now it has been assumed that the director is perfectly uniform throughout the liquid crystal. This is not the case in practice as many circumstances will cause the director to vary from point to point. These deformations can be caused when the liquid crystal comes in contact with a wall or any solid surface within the bulk or simply because of thermal fluctuations. This is of particular relevance to this thesis as the inclusion of colloidal particles into a liquid crystal induces a number of possible defects and these can have profound effects on the behaviour of the liquid crystal. There are three main types of deformation that commonly occur in nematic liquid crystals [24] and these can be seen in Fig 2.8. In these cases small changes in $\hat{n}$ occur over relatively large distances (much larger than the molecular length) and so have no significant effect on the overall order parameter, and so the deformations can be described by continuum theory.

Examining our liquid crystal, even when it is disordered, will reveal numerous

regions of localised ordering. Within each region the ordering is well defined, but the orientational ordering will vary from region to region. If each of these regions is associated with a local director we can think of the bulk sample as composed of a large number of local directors and so we can build up a director field $\hat{n}(\vec{r})$. The tensor order parameter $Q_{\alpha\beta}$ now becomes a function of **r** as the order varies from region to region and new terms must be added to the free energy involving gradients of $Q_{\alpha\beta}$.

In the unperturbed nematic equilibrium state there is a complete parallel alignment of all molecules and consequently directors. If perturbations are now added to this system the local directors will no longer be invariant and the free energy will increase. Deformations of the director from its equilibrium state are similar to deformations of a spring and they are described in terms of the free energy as a function of the spatial derivatives of the director.

However as with the tensor order parameter there are restrictions of what free energy terms are allowed:

(1) The free energy must be invariant under the interchange of $\hat{n}$ and -$\hat{n}$ as these states are indistinguishable.
(2) No linear terms are allowed (except in chiral LC's) as these give different free energy terms if the coordinate system is rotated.
(3) In many cases terms that are of the form **div u** may be ignored because they can also be written as surface integrals which do not play an important part in the volume energies.

Taking these considerations into account the distortion energy can be written as follows.

$$F_d = \frac{1}{2}K_1[\nabla \cdot \hat{n}]^2 + \frac{1}{2}K_2[\hat{n} \cdot (\nabla \times \hat{n})]^2 + \frac{1}{2}K_3[\hat{n} \times (\nabla \times \hat{n})]^2 \qquad (2.7)$$

The first term in this equation represents the contribution to the deformation energy arising from splay, the second from twist and the third from bend. The

constants K_1, K_2 and K_3 are the elastic constants (called Frank constants) which are analogous to spring constants. They typically have values of the order of $10^{-11}\ Jm^{-1}$ [25].

2.7.1 Defects

In the previous section the situation where small perturbations of the director affect the free energy has been examined, but there is another, more dramatic form, of perturbation. These are called defects and in these cases the changes in the director are not smooth at all points. There are two main types of defect which have relevance to this thesis and they shall be discussed in the next sections.

2.7.2 Disclination lines

When a nematic liquid crystal is viewed under crossed polarisers a large number of black thin thread-like filaments are seen crossing the sample. Indeed it is this thread like structure which gives the nematic liquid crystal its name (it comes from the Greek for thread). These threads are examples of disclination lines; discontinuities in the director field $\hat{n}(\vec{r})$ that run in lines throughout the sample and the patterns are called Schlieren textures [26].

2.7.3 Point defects

The second kind of defect that can occur in a nematic liquid crystal is the point defect. Here there is a point singularity at the centre of a defect structure, and perhaps the simplest example of this can be found when a drop of pure nematic liquid crystal is suspended in water. The director is normal to the surface at all points at the bubble/water interface. This means that the director is radiating

outwards from the centre of the bubble, and a point disclination forms here. This would be an example of pure splay, but in reality pure splay is not seen as the twist constant of the nematic is smaller than the splay so the free energy is minimised by forming a twisted centre arrangement [14]. Examples of different types of defects can be seen in Fig 2.9.

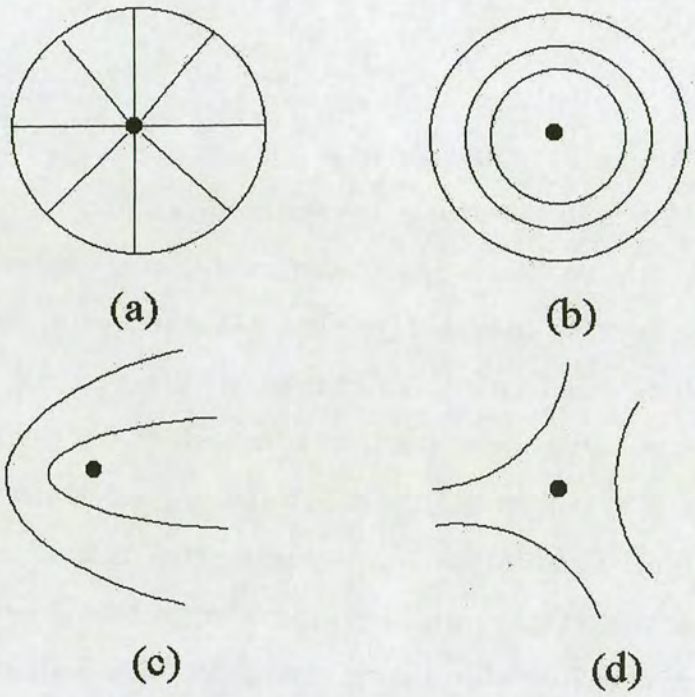

Figure 2.9: Some examples of defects in nematic liquid crystals. (a) and (b) both show point defects whereas (c) and (d) show line defects where the black dot represents the line coming out of the plane of the page.

2.7.4 Topological charges

Recognising different types of defect is relatively easy due to the unique optical patterns associated with them but quantifying them is a more involved process and one that will shed light on important issues later in this thesis.

To understand the nature or "strength" of any defect further we have to under-

stand the behaviour of the director in the vicinity of the defect. For a nematic liquid crystal containing a defect, the function [25]

$$\theta(\phi) = m\phi + \theta_0 \tag{2.8}$$

describes the orientation of the director as a function of the rotation angle ϕ where θ_0 is the function in its unperturbed state and m is a number. In a typical nematic liquid crystal the two states described by **n** and **-n** are indistinguishable so $\theta(\phi)$ must change by some multiple of π when ϕ is increased by 2π i.e. going one full loop around the disclination. This means $m = \pm\frac{1}{2}, \pm 1, \pm\frac{3}{2}$ etc, and m is referred to as the strength of the disclination because it describes how often director rotates in a 360^o loop around the defect. The sign of m merely refers to the direction in which the director rotates. A positive sign means it rotates anti-clockwise when an anti-clockwise path round the defect is taken, and a negative sign means it rotates clockwise when the same anti-clockwise path is taken. For example, radial defects like the one in Fig 2.9(a) and (b) have a strength m=1 because the director rotates 360^o every full loop of the defect, while in Fig 2.9(c) the director only rotates by 180^o so it has a strength of $m = \frac{1}{2}$. It is found that the only stable disclination lines have strength $m = \pm\frac{1}{2}$.

Determining what happens when two or more defects are present requires the introduction of topological charge. Similar in definition to the strength of a defect the topological charge q specifies the number of times the unit sphere is wrapped by the director on any surface enclosing the defect core. In liquid crystals the directions **n** and - **n** are equivalent so defects with positive or negative charges are indistinguishable and we can calculate total topological charge simply by using $q_a + q_b$ or $\mid q_a - q_b \mid$. This then allows us to calculate the total topological charge for a system of defects.

2.8 Colloids

Because this thesis revolves around the inclusion of colloidal particles into a mesogenic solvent, the theory of simple colloids is just as relevant as the preceding discussion of liquid crystals, and in the next sections some of the basic principles of colloidal physics shall be reviewed. However, the discussion here shall be brief and centred only around single colloidal particle behaviour and dilute colloid regimes as they are the only ones of interest in this thesis.

2.8.1 Definition of colloids

Colloidal systems are ones with at least 2 components [27], where a dispersed phase is uniformly and finely distributed in a dispersion phase (see Fig 2.10).

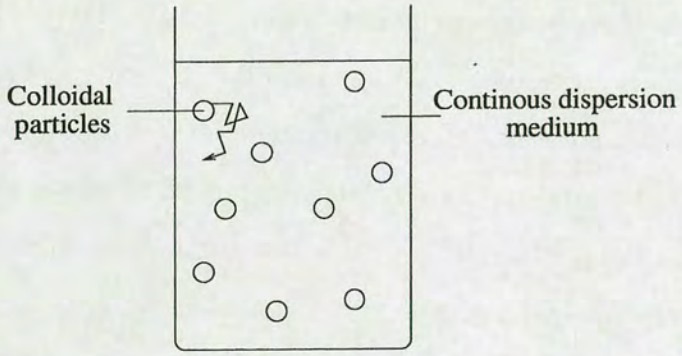

Figure 2.10: Colloidal particles dispersed in a continuous dispersion medium.

The nature of these dispersed and dispersion phases could be an entire thesis in itself as there are millions of possibilities including emulsions, aerosols and foams, and some of the commonest systems are listed in Tab 2.1.

Although the examples above show the wide variety of combinations that make up colloidal systems the term is generally only used for systems of hard particles

Colloidal system	Dispersed phase	Dispersion phase
Mist	Water droplets	Air
Milk	Fat droplets	Aqueous solution
Paint	Solid particles	Liquid medium

Table 2.1: Various common colloidal systems with their constituents

in a solvent and this thesis shall use this definition from here. While this provides a starting point for the discussion of colloids there are other considerations that must be taken into account. The statement that the dispersed phase must be uniformly and finely distributed can be clarified further by discussing the behaviour of the particulates suspended in our continuous dispersion medium.

For the system to be classed as colloidal, the particles must be large enough so that they are distinct from the solvent so that it can be treated as continuous, while small enough so that their behaviour is not dominated by gravity. Under these conditions the particles move under "Brownian motion" where their movement is controlled by random collisions of the solvent molecules on the particle. The particle then appears to move randomly, "zig-zagging" throughout the sample in a random walk. The range of particle sizes which fufill these criteria is thought to be from around 1nm to 500 nm [28].

The diffusion of hard colloidal particles which move under Brownian motion is described by the Stokes-Einstein expression [29]

$$D = \frac{kT}{6\pi\eta R} \tag{2.9}$$

where D is the diffusion coefficient, a measure of the speed at which the particles move, T is the temperature of our system, η the viscosity of the solvent and R is the hydrodynamic radius of our particle. The hydrodynamic radius is a measure of the physical radius of the particle and an amount of solvent which the particle drags around with it. Usually the hydrodynamic and physical radii are almost

equivalent but because the hydrodynamic radius is defined through the Stokes-Einstein relation this is not always the case as other considerations can come into play as will be shown later.

The time taken for a particle to diffuse a distance the size of its own radius is called the "structural relaxation time" and is given by

$$\tau_R = \frac{R^2}{D}. \tag{2.10}$$

The relaxation time for colloidal particles is typically of the order 10^{-2} seconds whereas for the molecules of the solvent it is approximately 10^{-11} seconds. This means the solvent can be treated as continuous for the timescales that are of interest when studying colloids.

2.8.2 Hard spheres

One of the most commonly used assumptions in colloidal science is probably the notion of the hard sphere. The term hard referring to the fact that there is a infinitely strong repulsion between two particles as they touch. Theoretically the potential here should be infinite but in practice this is not the case as the electron clouds of each particle can overlap slightly. If the particles are not charged then there will be no long-range interaction and the particles analogously act as "billiard balls" as the schematic potential in Fig 2.11 shows. In reality the is still some degree of attraction due to **Van-der-Waals** forces. These originate from the interaction between the fluctuating elctron clouds of molecules and are strong enough to have a significant effect on particle interactions. The force is attractive and the potential near particles surface can be many k_bT. This is much larger than the normal thermal energies that the particles have of $\approx k_bT$ so the particles will aggregate unless other measures are taken to prevent this. This is done by stabilising the surface of the particles, ensuring they act as hard spheres.

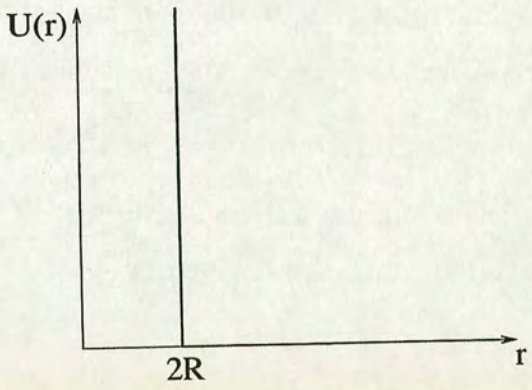

Figure 2.11: The schematic potential for hard sphere colloids. For $r \leq 2R$ the potential is infinite (definition of hard) and for $r > 2R$ the potential is zero as there is no long range attraction.

2.8.3 Stabilisation

To avoid aggregation of particles they are sterically stabilised by grafting polymer chains onto their surface [29] (see Fig 2.12). The free end of the polymer chain which is in contact with the solvent is a lyophilic group meaning that it prefers to be in contact with the solvent rather than other polymers. When two particles touch the polymer chains will then cause a repulsive force as any entanglement or compression of the polymers is entropically unfavourable and therefore the particles act as hard spheres.

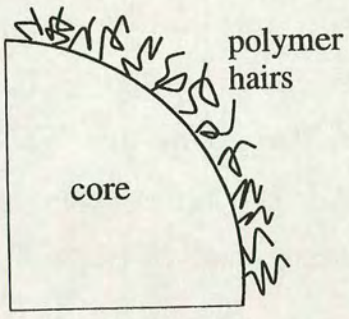

Figure 2.12: A schematic of a cross-section of a colloidal particle core and the polymer hairs grafted onto the surface so it acts as a hard sphere.

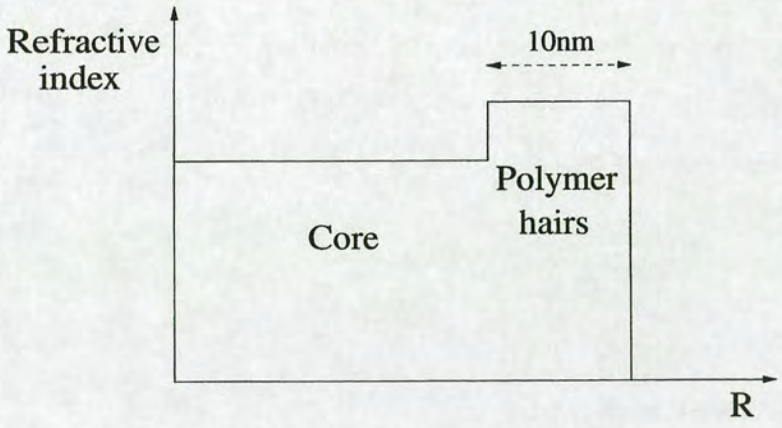

Figure 2.13: The refractive index profile for a typical colloidal particle with a PMMA latex core and PHSA polymer hairs grafted onto the surface.

2.8.4 Core-shell colloids

Although the grafting of polymer hairs onto the surface of the colloidal particles is necessary in order that they work as hard spheres it has the side effect that the particle now has a refractive index profile which steps at the boundary between the PMMA core and the PHSA hairs, as can be seen in Fig 2.13. The refractive index of PMMA is 1.484 and the refractive index of PHSA is 1.51 [30]. This has implications when light scattering is performed on these particles as the light is effectively scattering from two different objects, and this shall be discussed further in the next chapter.

2.8.5 Sedimentation

While the particles are small enough so that their motion is unaffected by gravity over short timescales, for longer timescales this assumption no longer holds. Given a suitably long period of time the particles will gradually begin to sink to the bottom of the container if they are of a greater density than the solvent. The time it takes for the particles to sink or sediment depends on factors such as the

size and density of the particles as well as the viscosity of the solvent. The two forces acting on the particle as it sinks are the downwards force of gravity and the viscous drag force exerted by the liquid. These are

$$\begin{aligned} F_{grav} &= m_B g \\ &= \frac{4}{3}\pi R^3 \Delta\rho g \end{aligned} \tag{2.11}$$

where m_B is the buoyant mass, and

$$F_{drag} = 6\pi\eta R V_{sed} \tag{2.12}$$

The velocity of sedimentation is then found by equating these two forces and solving for V_{sed}.

$$V_{sed} = \frac{2}{9}\frac{R^2\Delta\rho g}{\eta} \tag{2.13}$$

where $\Delta\rho$ is the difference in densities between the solvent and the particle and g is the acceleration due to gravity. Typically this will be of the order of a few millimeters a day for standard particles and solvents.

2.8.6 Polydispersity

When theoretically discussing systems of colloidal hard spheres it is often assumed that the particles are all of identical size and shape. Practically this is never the case and the variation in size (or shape) from particle to particle, known as the polydispersity, can have profound effects on phase behaviour [31]. While this is more important for studies of concentrated systems it does have experimental consequences for some of the techniques employed in this thesis and shall be defined briefly here. Polydispersity is defined as the standard deviation of the distribution in size divided by the mean.

$$\sigma = \frac{(\bar{R^2} - \bar{R}^2)^{\frac{1}{2}}}{\bar{R}} \tag{2.14}$$

Obviously polydispersity is kept to a minimum in as much as the preparation process will allow as it can make otherwise simple measurements unduly complicated. Typical polydispersities are usually of the order of $\sigma < 0.10$ and these pose little problems for the type of experiments performed here.

2.9 Liquid crystal colloids

Now that background theory has been given on the separate cases of colloids and liquid crystals it is possible to proceed to the situation where the two are combined. This throws up many more topics of discussion which have been the subject for much investigation both experimentally and theoretically in the last few years and the salient points shall be discussed here.

It was known for some time that the presence of a solid surface affected the orientation of liquid crystal molecules in its close vicinity [32]. Namely that even in the disordered isotropic phase the presence of a solid surface, like a wall, will induce local ordering of the molecules. If this solid surface is a colloidal particle then there should also be some ordering around its surface. The nature of this ordering depends greatly on the type and strength of anchoring at the colloidal particle/liquid crystal interface [12]. Two types of anchoring are theoretically possible: homeotropic anchoring, where the molecules attach with their long axis perpendicular to the surface and planar alignment where the molecules align with their long-axes tangential to the surface. Out of these two it appears that homeotropic alignment is favoured in most cases similar to ours [5] and so the discussion shall focus on this case primarily. As the temperature is cooled from the isotropic phase to the nematic the ordered layer of molecules surrounding our particle will begin to increase in thickness. Because the nematic phase has a higher viscosity than the isotropic the particle is now effectively diffusing inside a small region of liquid crystal which has a higher viscosity than the bulk. If the

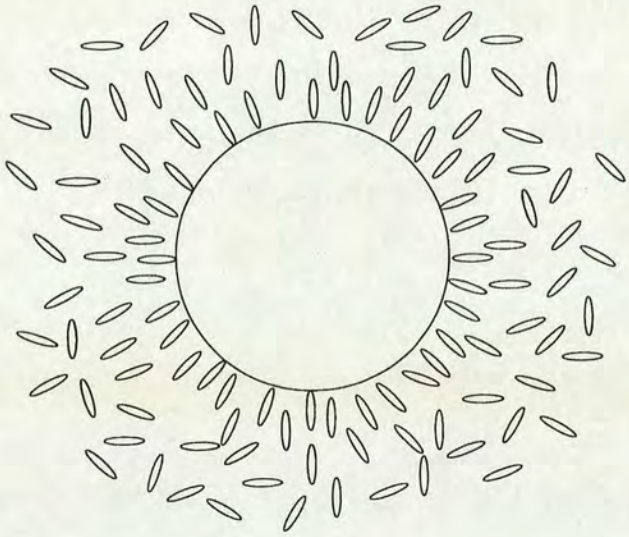

Figure 2.14: A schematic diagram of liquid crystal molecules ordering at the surface of a colloidal particle in the isotropic phase. Far from the particle the molecules are still disordered.

Stokes-Einstein relation (Eqn (2.9) is recalled we can see that a higher viscosity will have the effect of giving an anomalously low diffusion constant. When the hydrodynamic radius is then calculated using the viscosity of the bulk isotropic, at that given temperature, it will then be higher than it should be. Ordering of liquid crystal molecules at the particle surface can therefore be detected by an measuring an increase in the hydrodynamic radius of the particle.

2.9.1 In the Nematic phase

When the nematic phase is entered there are more considerations to be taken into account. In the pure ideal nematic phase the molecules align perfectly with the director, and because there are no defects in this structure and it has a uniform far-field $\hat{\mathbf{n}}$ we can say it has a total topological charge of 0. Introducing a spherical particle into this unperturbed state will change the director locally to the sphere creating a defect structure and topological charge $\neq 0$. If we assume that the molecules attach homeotropically at the surface of our particles then the

director structure surrounding the particle is the simple radial hedgehog structure described in Fig.2.15 (a) and as described earlier this has a topological charge of 1. The overall far field topological charge of 0 must conserved so the radial hedgehog must be balanced with another accompanying defect. To give an overall charge

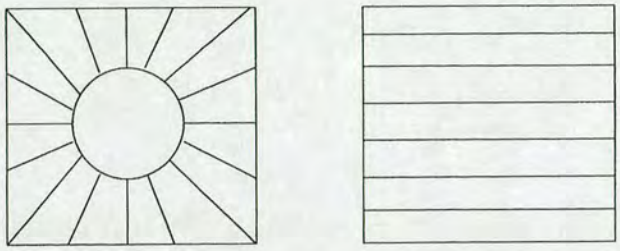

Figure 2.15: (a) shows the radial hedgehog arrangement of molecules at the surface of a colloidal particle in the nematic phase with a topological charge of 1. In (b), the unperturbed pure nematic state, there is a topological charge of 0.

of 0 requires an additional defect structure of q = ±1 to be formed. It appears that there are three possibilities [33] depending on the anchoring conditions at the surface of the particle and the free energies associated with them. Recall the free energy for slow varying spatial distortions

$$F_d = \frac{1}{2}K_1[\nabla \cdot \hat{n}]^2 + \frac{1}{2}K_2[\hat{n} \cdot (\nabla \times \hat{n})]^2 + \frac{1}{2}K_3[\hat{n} \times (\nabla \times \hat{n})]^2$$

the additional free energy surface term arising from the spherical particle has the form [13]

$$F_s = -\frac{1}{2}W \int (\hat{n} \cdot \hat{\nu})^2 dS \tag{2.15}$$

where $\hat{\nu}$ is the surface normal and W is the anchoring energy. There are the possibilities of other surface-like terms in the free energy but these are ignored in the present discussion for simplicity. Defining the strength of anchoring conditions is crucial in our understanding of the boundary conditions at the surface of the particle and anchoring conditions are said to be strong if the factor $\frac{WR}{K} \gg 1$ or weak if $\frac{WR}{K} \ll 1$, so while the anchoring energy is important, of equal importance are the bulk elastic energy K and the particle size R.

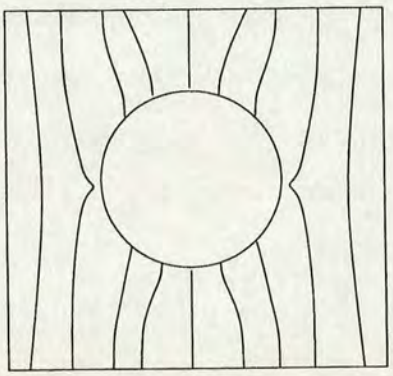

Figure 2.16: The director configurations surrounding a solid particle with homeotropic boundary conditions for weak anchoring conditions. The director is only slightly perturbed by the presence of the particle.

Now if there are weak molecular anchoring conditions at the surface of the particle then the particle will not have a huge effect on the surrounding nematic and the director field will be relatively unaffected. Such an example can be seen in Fig 2.16 . However, if the molecular anchoring is much stronger at the particle/liquid crystal interface then two possible director configurations emerge as possibilities. The two defect structures which give an overall topological charge of zero, and so conserve the far-field charge, are seen in Fig 2.17 .

In the first case the radial structure nucleated when a sphere is included into the nematic is accompanied by a disclination ring encircling the equator of the particle in a "Saturn-ring" manner. This disclination ring structure has a linear strength of -$\frac{1}{2}$ but an overall charge of q = -1 effectively "cancelling out" the radial hedgehog created by the particle, and giving an overall topological charge of zero. The second choice shows the radial hedgehog being joined by a companion "hyperbolic" hedgehog in a dipole configuration. Similarly this companion hedgehog also cancels out the radial hedgehog surrounding the particle.

There has been much debate over which of these two configurations is favourable in certain situations but it appears that both cases are theoretically possible under similar conditions, and that the cooling mechanism is important in determining

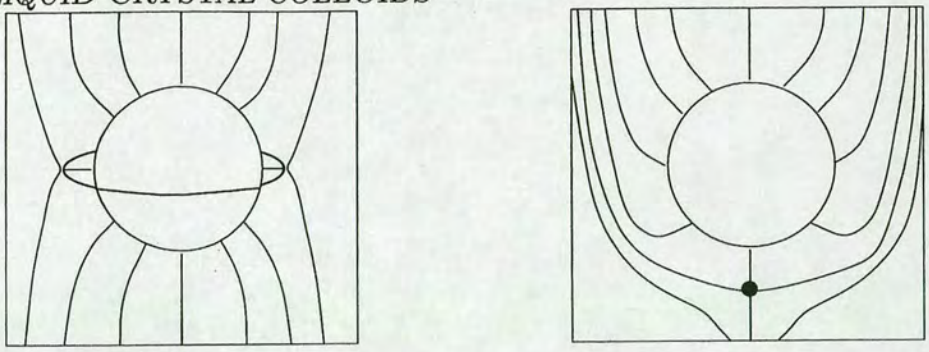

(a) (b)

Figure 2.17: The two possible director configurations surrounding a solid particle with homeotropic boundary conditions for strong anchoring conditions. In (a) the particle is surrounded by a "Saturn" disclination ring and in (b) it is joined by a satellite defect forming a dipole structure.

which one forms although it seems experimentally that the dipole configuration is preferred. There is no evidence of shifting between the two configurations once they have formed because of the large amounts of energy needed to do this.

If more than one colloidal particle, and their corresponding dipole defects, are present within a nematic host then there are attractive forces between dipoles and the particles begin to form chains as shown in Fig 2.18. Examples of colloidal particle chains in liquid crystals have been seen experimentally [34]and they give and insight into the forces controlling colloidal behaviour which become important later in this thesis.

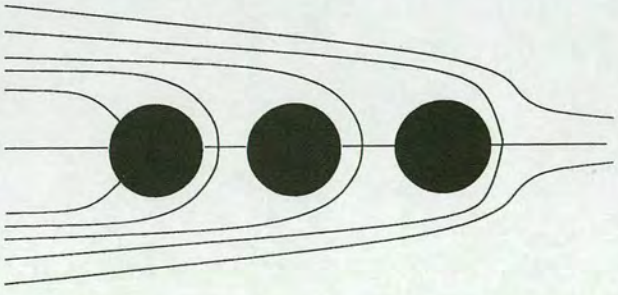

Figure 2.18: Particle chaining in a nematic liquid crystal. The particles form chains because the dipolar particle/hedgehogs attract each other.

Chapter 3

Characterising the system

Because the preparation of colloids in a liquid crystal solvent is difficult, and because complications in the preparation lead on to a whole new field of study, an entire chapter shall be devoted to the methods of making and characterising the samples used in the following investigation. This will cover the standard procedures used when preparing any colloid sample and will go on to discuss the complications arising from using a liquid crystal and what methods were taken to overcome these.

3.1 The Colloidal Particle

The particles used in this study are all made up of an essentially solid core of the tightly coiled polymers Poly(methylmethacrylate) (PMMA) surrounded by a mono-layer of poly-12-hydroxystearic acid (PHSA) grafted to the surface. The PHSA polymer chains or "hairs" are generally around 10-15nm long and have a large surface coverage on the sphere. The solvents for the colloids are often chosen so that they are good solvents for the PHSA in that the polymer wants to be in contact with the solvent. This means the polymers extend outstretched

into the solvent and any other particles that comes close will be repelled. Typical good solvents that are used for dispersing PMMA particles with PHSA hairs are *cis*-decahydronapthalene (cis-decalin) and dodecane . When the particles are initially prepared [35] (In house by Dr Andrew Schofield) they are dispersed in dodecane, but while this solvent is a good solvent for PHSA its refractive index is very different from that of the particles meaning that a number of complications, which will be described later, arise when light scattering is performed on these samples and more appropriate solvents can be found. Cis-decalin is one of the preferred solvents because it acts as a good solvent for the polymer hairs and has a refractive index which is similar to the particles making light scattering experiments easier.

3.2 Washing the particles

To transfer the colloids from one solvent to another is not a trivial task but one that is crucial during the course of many experimental investigations. The colloids, dispersed in their original solvent of dodecane, are placed in plastic cells and centrifuged at high angular velocities. The particles have a higher density than the solvent and so sink to the bottom of the container in a random close packed structure which resembles a stack of marbles. Once the sedimentation has been completed (a process which takes a matter of hours [36]) the supernatant dodecane can be poured away and the new solvent added. However when the particles are re-dispersed by vigorous shaking the dodecane which was trapped in the sediment will be as well. The procedure of spinning down the particles, removing the supernatant solvent and adding a new solvent must be repeated approximately 7 times before all of the old solvent has been replaced by the new solvent. This can be checked by measuring the refractive index of the final solvent and comparing it to the known values of the pure solvents.

3.3 Determining the volume fraction

Once the particles have been dispersed in the final solvent it is often necessary to find the concentration of the particles in relation to the amount of solvent. This is generally quantified by the volume fraction

$$\phi = \frac{4}{3}\pi R^3 \rho \tag{3.1}$$

where R is the particle radius and ρ is the number density of the particles. The volume fraction can be found by a variety of techniques which will be summarised here.

3.3.1 Spin-down method

With the spin-down technique the sample of colloids dispersed in solvent is centrifuged until the particles have formed a random close packed solid at the bottom of the cell. It is known that this structure has a $\phi_{cp} \approx 0.64$ depending on the polydispesity and slight compressibility of the particles [37]. By measuring the heights of the close packed particles and the supernatant liquid the total volume fraction can be found with

$$\phi_{total} = \frac{h_1 \phi_{cp}}{h_1 + h_2} \tag{3.2}$$

where h_1 and h_2 are the heights of particle sediment and solvent respectively as shown in Fig 3.1, and ϕ_{cp} is the volume fraction of the random close packed structure. This method is only useful for measuring volume fractions of very concentrated systems as it relies on large amounts of particles present for accurate measurements. For much more dilute systems another method is needed.

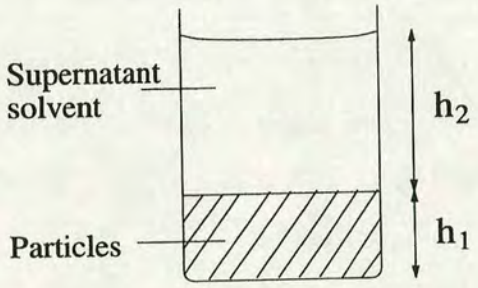

Figure 3.1: After centrifuging the sample contains a 'solid' region of random close packed particles and a supernatant solvent. Measuring the heights of these allows calculation of the volume fraction.

3.3.2 Weight method

Another method of determining the volume fraction is to measure the mass fraction. Here the colloidal solution is weighed accurately, and is then dried in a vacuum oven until all of the solvent has been removed. This is verified by repeated mass measurements until no change is seen. The final particle residue mass is then measured and by using the density values of the solvent and the particles the volume fraction can be found. The difficulty here is two-fold. It is necessary that the densities of both the solvent and the particles must be known, and while finding the density of the solvent is easy the density of the colloidal particles is more difficult to accurately determine. The PMMA particle core may be porous and consequently have a different density to the bulk form of PMMA, and it is possible that the polymer hairs may also be solvated changing the density of the particle. Secondly the particles have to be re-dispersed with exactly the same amount of solvent if they are to be used again.

Calculating the volume fraction is then determined by the formula

$$\phi_{total} = \frac{1}{1 + \frac{\rho_p}{\rho_{sol}}\left[\frac{M_{total}}{M_p} - 1\right]} \tag{3.3}$$

where ρ_p and ρ_{sol} are the densities of the particles and the solvent, and M_{total} and M_p are the total masses and mass of particles respectively.

It is clear that if we have an known amount of initially dried particles then it is simple to add a measured amount of solvent to give any desired volume fraction and it is this method that is employed when dispersing particles in a liquid crystal solvent.

3.4 Dispersing particles in a liquid crystal

It has now been discussed how particles can be dispersed in a solvent of our choice and how the volume fraction can be accurately measured. When the solvent is a liquid crystal this becomes much more complicated as added considerations need to be taken into account.

As described in the previous chapter, the presence of colloidal particles in a nematic phase introduces defects [10]. While this can be compensated for by the emergence of other defects if the boundary conditions are suitable, it is also possible that the nemtic phase will simply try to expel the particles for a more energetically favourable state. This means that particles may be forced into large aggregates which will not re-disperse [38]. It has also be found that the presence of dipole defects lead to attractive interactions which cause the chaining of particles [34,39] and this too may well contribute to the aggregation of particles seen in the nematic phase. As shall be later in the thesis it is these phenomena which leads to some striking rheological behaviour, but initially the discussion shall be focused on the difficulties this introduces into the preparation procedure. The fact that particles aggregate in the nematic phase means that preparation of many particle/LC systems must be done purely in the isotropic phase. As the isotropic phase exists at temperatures significantly above room temperature (5CB has $T_{NI} = 35^oC$) this means that all the sample preparation must also be performed above this temperature.

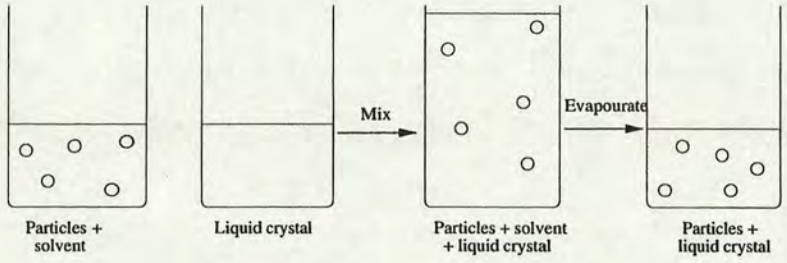

Figure 3.2: Schematic diagram of the preparation process for dispersing particles, initially present in one solvent, in a liquid crystal.

There are additional complications that arise when the colloidal particles must be transferred from the stock solvent, dodecane, into the new liquid crystal solvent. Because of the high financial cost of pure liquid crystal it is not practical to wash the particles with the liquid crystal solvent in the manner described above, as this would require large amounts. Rather it is necessary to first wash the particles with a solution of heptane or petroleum ether, both of which have very low boiling points. This means that when an amount of particles in heptane is added to the liquid crystal solvent the heptane can be evaporated off at a high enough temperature in a vacuum oven leaving only the particles suspended in liquid crystal as seen in Fig 3.6. It is found that this preparation process has some complications of its own which affect the particles diffusion and this lead to the offshoot study of Chapter 6.

3.4.1 Dispersing dried particles

When it was necessary to disperse large accurate amounts of particles in a liquid crystal another method had to be used, which is basically an adaptation of the weight method used to determine volume fractions. The particles, which are initially prepared in their solvent stock, are first dried and then weighed accurately. The desired volume fraction is then decided upon, and the appropriate amount of liquid crystal is added at room temperature, in the nematic phase. Because

the dried particles are essentially stuck together in huge aggregates, completely re-dispersing them takes time and effort. To do so, the sample is placed upon a tumbler inside an oven at a temperature high enough so that the liquid crystal is well into the isotropic phase, where there is no tendency for the particles to aggregate, and the sample is tumbled continuously until the particles are fully re-dispersed. To ensure complete re-dispersal the sample periodically removed from the tumbler and sonicated for up to 15 minutes. This entire process of re-dispersing particles can take up to a week.

3.5 Determining the viscosity of a solvent

While the viscosity determination of many solvents is easily performed with a rheometer it is the case that for some low viscosity solvents it is not possible due to the constraints of the equipment itself. In these cases the viscosity must be determined by other means, of which there are many. In my experiments it was necessary to know the viscosities of heptane and petroleum ether, as these were to become crucial in the understanding of our system. Values for the viscosity of heptane can be found readily in data books [40] but data on petroleum ether is much rarer and more difficult to come by. Because of this the viscosity of petroleum ether had to be calculated experimentally by measuring the sedimentation time for a colloidal suspension in petrol and using Eqn 2.13 to calculate the viscosity.

Because there are some unknowns in this equation the first stage in the determination of the viscosity was to calculate the density of the solvent. This is simply done by measuring out a precise volume and weighing it accurately. The results of this can be seen in Fig 3.3, and from this we can deduce a density of $0.63 gcm^{-3}$.

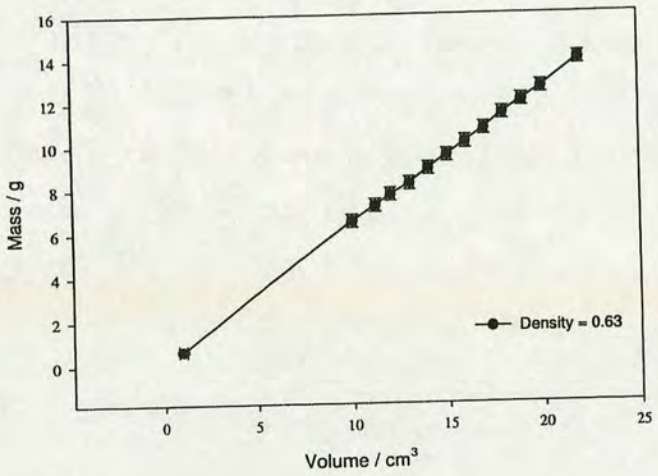

Figure 3.3: Results of Mass against volume for pure petroleum ether and the value for the density calculated.

Knowing the density of petrol, the density of the colloidal particles (which we assume is the same as pure PMMA at $1.188gcm^{-3}$) and the radius of the particles (found by SLS) means that all of the unknowns in Eqn 2.13 are known and the sedimentation velocity can be measured and the viscosity found.

The sedimentation velocity is found by first preparing a dilute suspension (ϕ = 0.025) of colloidal particles (R= 350nm) in petrol. Because the refractive index difference between petrol (n=1.366) and the particles (n=1.5) is large the sample appears relatively cloudy even at this very low volume fractions. The sample is then shaken and left for a couple of hours until a distinct phase separation between the clear liquid at the top and the cloudy colloidal suspension below is seen as in Fig 3.4. Over 6 hours repeated measurements of the height of the suspended phase were made to determine the speed of sedimentation of the particles, and once these results had been taken a graph of sedimentation distance against time was drawn from which the sedimentation velocity could be easily found (see Fig 3.5). It is important to realise however, that the sedimentation velocity is affected

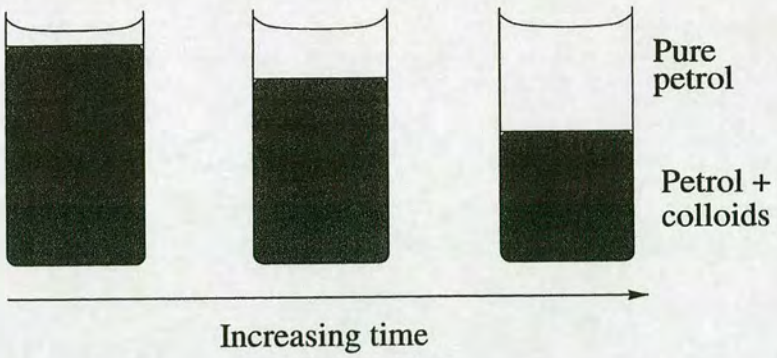

Figure 3.4: Schematic of the sedimentation behaviour for a colloidal solvent.

by the concentration of the suspension as more concentrated systems will sediment slower than extremely dilute ones due to the collisions between particles. In order to determine the viscosity we have to find the sedimentation velocity of a single sphere in our fluid and this can be found by using the equation [41]

$$\frac{v(\phi)}{v(0)} = 1 - 6.55\phi. \tag{3.4}$$

It is then trivial to find the viscosity of the liquid, and for petroleum ether this was found to be 0.22 cp at room temperature.

3.6 The Liquid crystal

Two different types of liquid crystal were used in the experiments described in this thesis. The first is $4' - n - Pentyl - 4 - cyanobiphenyl$, commonly known as 5CB. This is a very well characterised liquid crystal that exhibits a nematic phase below $T_{NI} = 35^oC$ and an isotropic phase above this. The second liquid crystal used also belongs to the same cyano-biphenyl family. It's chemical formula is $4' - n - Octyl - 4 - cyanobiphenyl$, but it is more commonly known as 8CB and it exhibits a nematic phase at around $T_{NI} = 40.5^oC$ and a smectic A phase at approximately $T_{SN} = 34^oC$ [42]. Both types of liquid crystal are of the rod-like

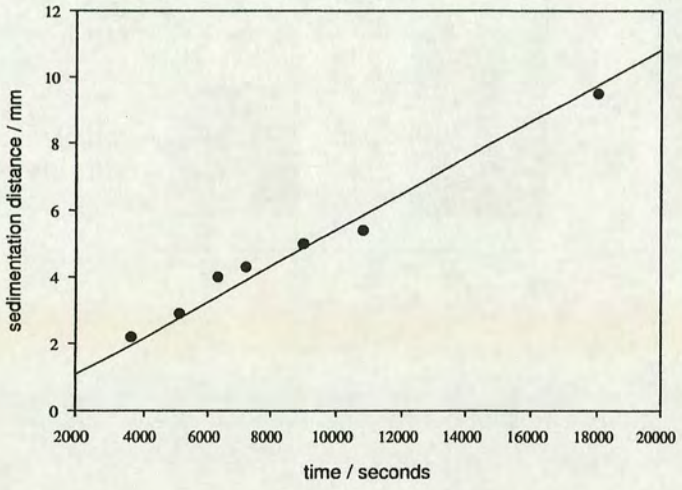

Figure 3.5: Results for the sedimentation distance against time over a period of around 6 hours.

variety described in the background chapter.

3.7 Identifying the phases

On the most basic of levels it is possible to tell roughly what phase the liquid crystal is in simply by looking at it . The isotropic phase is clear to the eye whereas ordered liquid crystal phases are cloudy because of the director fluctuations, and generally speaking the more opaque the sample the more ordered the liquid crystal phase. For example, the smectic phase is cloudier than the nematic. While this information is useful in sample preparation it is imperative that the optical appearance of the phases is understood more as well as how they relate to the molecular structure.

The name nematic comes from the Greek for thread and when the phase is viewed with a powerful microscope it appears to be made up a criss-crossing series of

black thread-like filaments. These threads are the disclination lines that run throughout the sample and they make observations of particles in the nematic phase difficult, although this can be avoided by the use of confocal micrscopy and dyed particles which is described in a later section.

Figure 3.6: Microscope image of the pure nematic phase of 8CB under crossed polarisers. The disclination lines are predominately visible throughout the structure

In the smectic phase the molecules formes ordered individual layers stacked on top of one another. In 1917 Grandjean viewed droplets under a microscope and noticed the stepped edges of these lamellar layers which have come to be known as Granjean terraces [24].

From an optical polarising microscope point of view the phase can have two characteristic textures which result from two different molecular structures. When the molecules are all aligned homeotropically then polarised light is extinguished and the texture will appear dark because the light is passing down the optical axis. But when the molecules are not aligned homeotropically then a texture called a focal-conic fan texture is seen as Fig 3.7. This arises because it is energetically favourable for the lamellar structure to form a system of curved equidistant layers. The molecular packing gives rise to concentric circles which merge together unsymmetrically creating the characteristic fan texture as seen in Fig 3.8.

Figure 3.7: Microscope image of the smectic phase of 8CB. The fan regions are easily evident and small regions where the molecules have aligned homeotropically can also seen as blank patches.

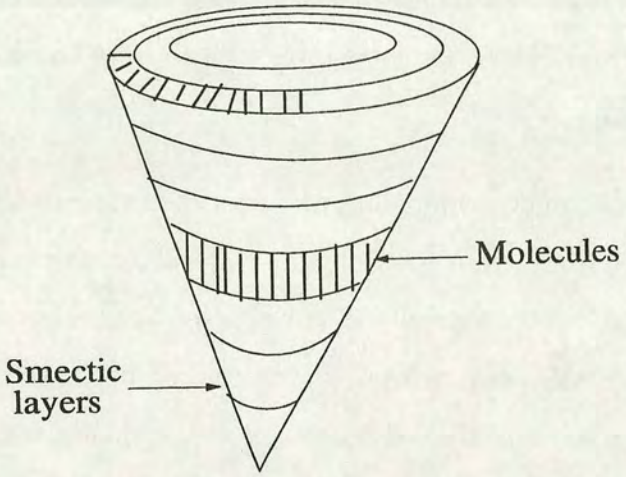

Figure 3.8: A schematic of the focal-conical fan domain which gives the smectic phase its unique appearance.

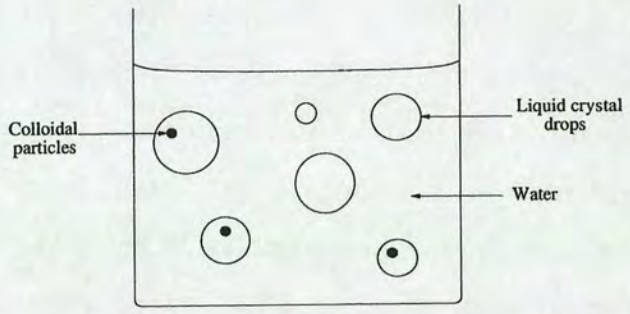

Figure 3.9: Schematic of a LC/water emulsion where particles are suspended inside the LC. The normal boundary conditions at the surface of the drop ensure that the particle remains inside even in the nematic phase.

3.8 Determining the boundary conditions.

Previously we have talked about how the presence of a sphere in a nematic phase affects the director field locally, and how extra defects are sometimes needed to balance the overall topological charge. In these discussions it was assumed that the boundary conditions at the surface of the particle were homeotropic i.e. the molecules aligned with long-axis perpendicular to the surface of the particle. To check whether or not this assumption is valid for our system we first need to suspend a particle in a nematic phase. Because it is energetically unfavourable for a particle to exist in the normal nematic phase the particles are often expelled making it difficult to observe particles. This problem can be overcome by making a liquid crystal/water emulsion [43] as shown in Fig 3.9.

If a liquid crystal/water emulsion is made, where we have spherical drops of liquid crystal, with particles inside, suspended in water then the new boundary conditions at the liquid crystal/water interface mean the particle will not be expelled and we can examine the molecular behaviour of the liquid crystal at the particle surface. This is achieved by first preparing a sample of particles suspended in the isotropic phase of our liquid crystal (5CB) in the manner described above. This is then added to a solution of water and sodium dodecyl sulfate ($\approx 1\%$),

and the entire solution is then shaken. The duration of the shaking determines the final size of the liquid crystal drops suspended in the water and a process of trial and error is required to find droplets of an appropriate size. The sample is finally examined under a powerful brightfield microscope, to try and find any liquid crystal drops that have particles suspended inside them. Once one of these is found the temperature can be lowered into the nematic phase and the director configuration examined under cross ploarisers. Using this method it was possible to suspend particles with a radius of approximately 1 micron inside LC drops of around 10 microns, and view these with our microscope.

It was observed that in the isotropic phase, the particles diffuse inside the liquid crystal drops in normal Brownian motion as is expected. As the nematic phase is entered a point defect forms at the outer edges of the drop and then immediately moves into the centre. The particle then rapidly moves towards this defect where it is finally fixed, with the whole process taking a matter of seconds. Viewed under crossed polarisers the particle is clearly visible in the centre of a nematic droplet, with a "four-armed star" radiating out from it's surface to the edge of the drop, and no other defects are seen. This does indeed confirm that there are homeotropic boundary conditions present at the surface of the particle as a brief examination of the topology involved reveals. Images of this process can be seen in Fig 3.10.

For the case of a pure nematic drop the molecules are aligned normal to the surface of the drop. This gives the drop an overall topological charge of 1, unlike the case for unrestrained nematic which has a charge of 0. This is achieved by a twisted radial hedgehog point defect radiating from the centre of the drop. Now, if a colloidal particle is placed inside this drop the topological charge of 1 must be conserved and the particle moves to the centre of the drop where it effectively acts as a point defect with a radial hedgehog defect structure, assuming there are homeotropic boundary conditions at the particle surface. This is verified by the

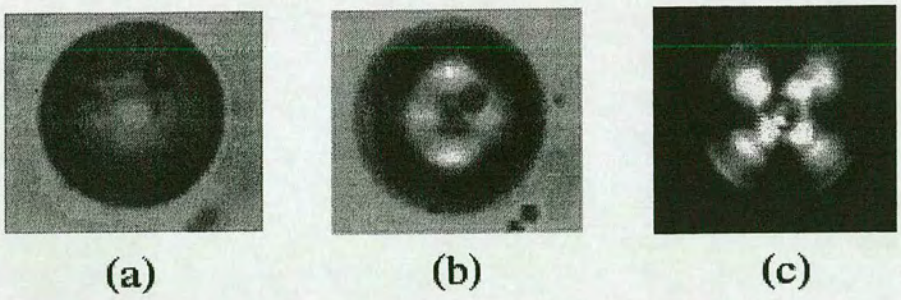

Figure 3.10: In (a) the colloidal particle can be seen diffusing in Brownian motion inside the isotropic droplet. As the nematic phase is initially entered in (b) the defect can seen in the centre of the drop and the particle moves towards this. In (c), deep into the nematic phase and viewed under cross polarisers, the particle is fixed in the centre of the drop with a radial director configuration around it.

presence of the "four-armed star" pattern which is characteristic of homeotropic boundary conditions and a radial director structure.

Chapter 4

Experimental techniques

The research involved in this project has utilised a relatively large number of experimental techniques in order to gain an understanding of many of the different aspects of liquid crystal colloids. The experimental methods used in this project shall be briefly introduced here but focus will be on only the points which have direct relevance to the results obtained.

4.1 Light Scattering

For an object to be visible it must clearly scatter light [44] , and the nature of this scattered light can tell us information about that object. This can be as simple as its colour but it can also give us much more complicated information about the system. Indeed when light scattering is performed on systems of colloidal particles a great deal can be revealed about how the particles are behaving [28, 45, 46].

According to classical electromagnetic theory light can be represented by a wave where an electric field and a magnetic field at right angles to each other propagate at the speed of light. The radiation interacts with matter through the effects of

the electric field on the electrons present in the molecules or atoms. *Absorption* of light means that the system is transferred from its ground state into a higher energy state by the absorption of photons. When the system returns to its ground state the energy is emitted again and if the amount of energy absorbed and emitted is the same the scattering is said to be *elastic.*

If a linearly polarised electric field is incident on a particle a dipole monent will be induced inside the particle, and if the particle is significantly smaller than the wavelength of light (a condition known as the Rayleigh limit) then all parts of the particle essentially experience the same field. As the wave propagates and the field at that point fluctuates so does the dipole, and a linearly polarised field will induce a dipole in the plane of the electric vector.

If our light (with a wavelength λ) has an electric field amplitude $\mathbf{E_0}$, linearly polarised along the $\mathbf{x}$ axis then the intensity of the scattered light is given by

$$I_s = \frac{16\pi^4\alpha^2 E_0^2}{r^2\lambda^4}\sin^2\phi\ . \tag{4.1}$$

where α is the polarisability of the particle, r is the distance from the scatterer and ϕ is the angle between the scattering direction and the direction of polarisation.

The treatment for a larger object, where the Rayleigh limit does not hold, means the object now has to be thought of as a collection of small volume elements, where each one scatters as above. The total scattered field is the found by the coherent sum of the fields scattered by each of the volume elements. Now if we assume that the incident plane wave front is not distorted by the presence of other volume elements (the Rayleigh-Gans-Debye criteria) then the phase difference between two different volume elements at $\mathbf{r_i}$ and $\mathbf{r_j}$ is simply $e^{-i\mathbf{Q}.(\mathbf{r_i}-\mathbf{r_j})}$. Looking at Fig 4.1 shows how the scattering vector $\mathbf{Q}$ can be defined as

$$Q = \frac{4\pi n_s}{\lambda_0}\sin\left(\frac{\theta}{2}\right)\ , \tag{4.2}$$

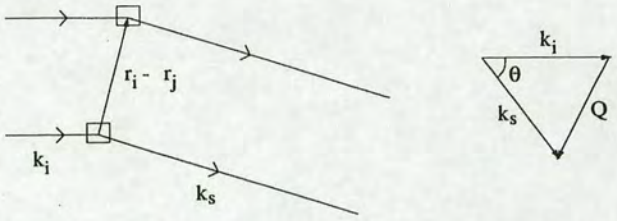

Figure 4.1: Schematic showing how the scattering vector Q is defined from light scattering from two volume elements.

where λ_0 is the wavelength of light *in vacuo*, n_s is the refractive index of the propagating medium and θ the angle between the incident and scattered light.

4.1.1 Scattering from a particle

The total electric field amplitude $\mathbf{E(Q)}$ is the sum of the fields scattered by each volume element. This means that for a single particle with position of centre at $\mathbf{r_j}$ and volume element $\mathbf{s}$ as shown in Fig 4.2, and ignoring the terms not involved with the phase shift of the light, the electric field can be written as

$$\begin{aligned} E(Q) &\propto \Delta n \int_{V_j} dV e^{-i\mathbf{Q}.\mathbf{r}} \\ &= \Delta n \left[\int_{V_j} dV e^{-i\mathbf{Q}.\mathbf{s}} \right] e^{-i\mathbf{Q}.\mathbf{r_j}} \\ &= \Delta n b_j(Q) e^{-i\mathbf{Q}.\mathbf{r_j}} \end{aligned} \tag{4.3}$$

where $b_j(Q)$ is known as the scattering amplitude and Δn is the difference in the refractive indices between the particle and the dispersion medium.

For a homogenous sphere of refractive index n_c and radius R the scattering amplitude $b_j(Q)$ is found to be

$$b(Q,R) = 4\pi R^3 (n_c - n_s) \left(\frac{\sin QR - QR\cos QR}{(QR)^3} \right) . \tag{4.4}$$

Another more experimentally useful quantity is the *form factor* which is the

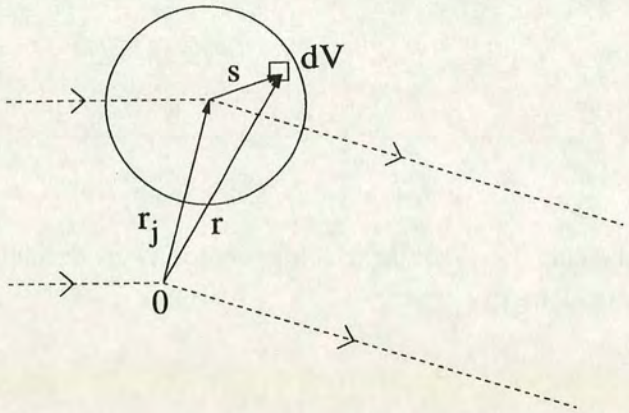

Figure 4.2: The total light scattered from a particle is found by summing the contributions from the individual volume elements.

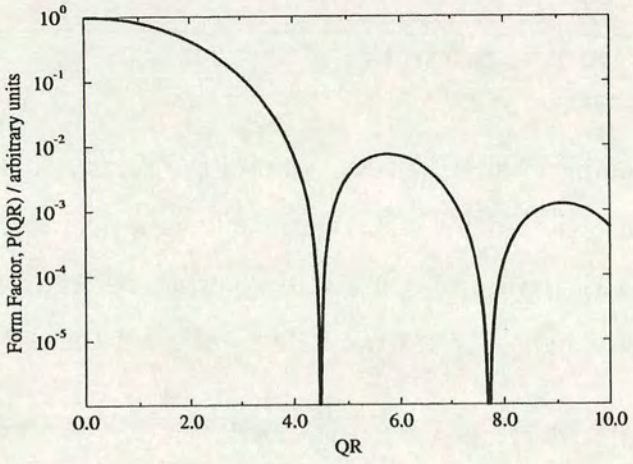

Figure 4.3: The theoretical form factor for a perfect sphere.

normalised intensity scattered by a single particle, deifned as

$$P(Q,R) = \frac{|b(Q,R)|^2}{|b(0,R)|^2}. \tag{4.5}$$

In the case of the uniform sphere examined above this becomes

$$P(QR) = 9\left(\frac{\sin QR - QR\cos QR}{(QR)^3}\right)^2. \tag{4.6}$$

which has the form shown in Fig 4.3. This has minima at QR=tan QR and this leads to solutions of $Q_{min}R = 4.493, 7.725, 10.904...$ The form factor for a system of polydisperse spheres shows that the minima are not as pronounced as the case

for perfect spheres but are still relatively distinct assuming the polydispersity is smaller than roughly 0.10. Indeed the change in the depth of the minima can be used as an indicator to the degree polydispersity as shall be seen later.

4.1.2 Scattering from many particles

As the number of particles is increased we must begin to consider the correlation effects of light scattered from different particles. We previously stated that the electric field scattering from one particle is

$$E(Q) \propto b_j(Q)e^{-i\mathbf{Q}\cdot\mathbf{r_j}}$$

so when scattering from N particles this becomes

$$E(Q) \propto \sum_{j=1}^{N} b_j(Q)e^{-i\mathbf{Q}\cdot\mathbf{r_j}} \tag{4.7}$$

where we have again ignored the prefactors not relating to particle scattering. Now if all the particles are identical then the scattering amplitudes will likewise be equal, allowing us to take the scattering amplitude factor outside of the summation. This means

$$E(Q) \propto b(Q) \sum_{j=1}^{N} e^{-i\mathbf{Q}\cdot\mathbf{r_j}} \tag{4.8}$$

As the particles move around in Brownian motion the phase angle $Q \cdot r_j(t)$ fluctuates randomly meaning an average scattered field must be found, and the time or ensemble average is simply

$$\langle E(Q) \rangle = b(Q) \sum_{j=1}^{N} \left\langle e^{-i\mathbf{Q}\cdot\mathbf{r_j}} \right\rangle . \tag{4.9}$$

Now the scattered intensity I(Q) is

$$I(Q) = E(Q)E^*(Q) = \mid E(Q) \mid^2 \tag{4.10}$$

and the average intensity is

$$\langle I(Q) \rangle = b^2(Q) \sum_{j=1}^{N} \sum_{k=1}^{N} \left\langle e^{-i\mathbf{Q}\cdot(\mathbf{r_j}-\mathbf{r_k})} \right\rangle . \tag{4.11}$$

For a dilute suspension of particles there is no correlation in the position of different particles. This means that the contribution to the scattered intensity from the $j \neq k$ terms is zero leaving only the $j = k$ term. This gives a final scattered intensity (ignoring some constants) of

$$\langle I(Q) \rangle = \Delta n^2 b^2(Q) N \tag{4.12}$$

and so experimentally measuring the intensity as a function of Q to obtain the form factor, and using the known positons of the minima, allows the particle radius to be measured. This is one of the main uses of Static Light Scattering.

4.2 Static Light Scattering

Static Light Scattering is essentially the process of measuring scattered intensity as a function of angle (or Q) to determine information about the system. It does not reveal the dynamics of the particles but can provide information on the particle radius, polydispersity and structure of a colloidal system [31]. A schematic experimental set-up is seen in Fig 4.4. A laser is focus by a lens

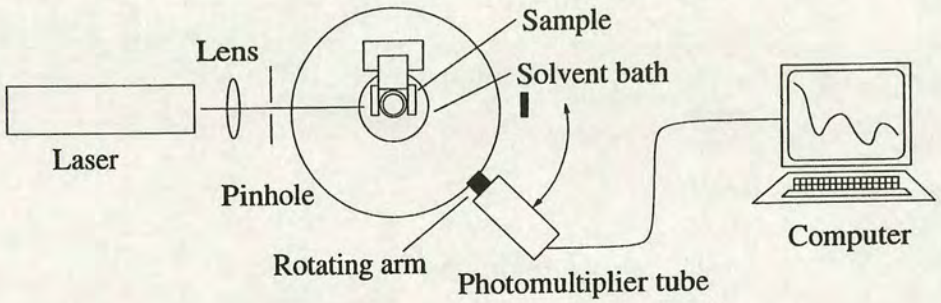

Figure 4.4: A simplified diagram of a Static Light Scattering set-up.

through a pinhole and onto the sample which subsequently scatters light in all directions. The sample sits in a high quality glass bath containing a solvent with a refractive index similar to the glass to reduces any reflection of the laser beam

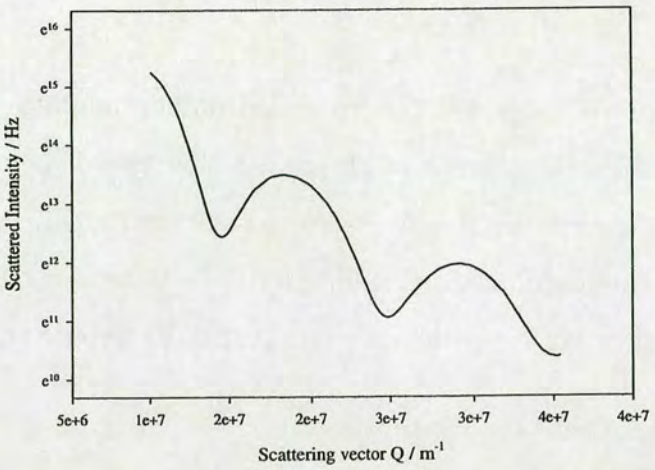

Figure 4.5: An experimenatally measured form factor for a dilute system of spherical particles. The various minima can clearly be seen but the polydispersity of the particles means they are shallower compared with the theoretical case. Here, the radius of the particles is calculated to be 307nm from the position of the first minima.

caused by a large refractive index difference at an air/glass interface. By then rotating a photomultiplier tube around the sample the scattered intensity as a function of Q is measured. For the case of dilute spherical colloids, where the positions of different particles are uncorrelated, this should simply be the form factor shown above. Using the fact that

$$R = 4.493/Q_{min} \tag{4.13}$$

for the first minimum means the radius of the particles is easily found. However, practically all the particles are not exactly the same size and this polydispersity "smears out" the minima as can be seen in Fig 4.5. A quick method for quantifying the polydispersity, developed by Pusey and van Megen [47], involves the height measurements of the first maxima and minima in the form factor. By expanding the expression for the intensity around a minimum in the form factor

they found that small polydispersities can be approximated using the formula

$$\sigma \approx \frac{1}{\sqrt{57.4\frac{I_{max}}{I_{min}}}} \tag{4.14}$$

where I_{max} and I_{min} are the heights of the first maxima and minima in the form factor. A more accurate measurement of the radius and polydispersity can be achieved by fitting the experimental form factor to the analytical expression of $P(Q, R)$ with the variable parameters R and σ but this is time consuming and for the accuracy needed in my experiments was not usually necessary.

It also important to note that the concentration of the particles in the solvent directly affects the measured values for the radius and polydispersity [36]. As the concentration is increased the measured radius decreases and the polydispersity apparently increases. To avoid inaccurate measurements the sample is repeatedly diluted until no further change in either of these measurements is seen while still maintaining a high enough particle concentration so that a decent scattering intensity is observed, generally a process of trial and error.

4.2.1 Scattering from the core-shell

As previously mentioned, the practical necessity that particles act as hard spheres means PHSA polymer hairs are grafted onto the surface of the PMMA core sterically stabilising them and preventing aggregation. Because the polymer hairs have a different refractive index to the core, any light scattering from this system effectively comes from two different objects. The form factor experimentally obtained therefore contains information about both the core and the shell. The scattering amplitude for this system is simply the sum of the scattering from two spheres: one from the core and the other the shell. This gives

$$b_{cs}(Q, R) = 4\pi R^3(n_c - n_{shell})\left(\frac{\sin QR - QR\cos QR}{(QR)^3}\right) + \tag{4.15}$$

$$4\pi(R+\Delta)^3(n_{shell} - n_s)\left(\frac{\sin Q(R+\Delta) - Q(R+\Delta)\cos Q(R+\Delta)}{(Q(R+\Delta))^3}\right)$$

where n_{shell} is the refractive index of the shell and Δ is the shell thickness. It is also worth noting that in this case R refers to the core radius and not the radius of the entire particle. An experimentally obtained form factor can now be fitted to this expression with parameters of core radius and shell thickness. It is seen that if the refractive index of the shell is significantly different to that of the core then even very small shells can dramatically affect the form factor, and this will prove important in later discussions [48].

4.3 Dynamic light Scattering

While Static Light scattering allows us to determine the size and structure of our particle system it tells us nothing of the behavioural motion of the individual particles. To do this requires the analysis of the time dependence of the scattered light intensity.

As the particles move about in Brownian motion the light scattering from them combines in phase and out of phase depending on their individual positions. The resultant intensity therefore fluctuates as the particles continue on their random walk and analysing this fluctuation provides information on the particle movement. This is the basic premise of Dynamic Light Scattering, and in the following sections details on the basic principles of DLS, and how it can be used to gain information about a colloidal system, will be discussed. Should the reader desire, more information can be found in a number of excellent texts [45, 49–51].

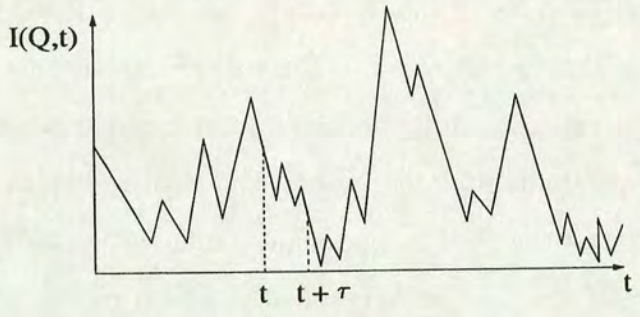

Figure 4.6: The fluctuating intensity signal is due to the light scattering from the particles interfering constructively and destructively as the particles move around in Brownian motion.

4.3.1 The Correlation function

If we recall the scattered intensity for a dilute system of identical particles and now consider its time dependence we find

$$\langle I(Q,t)\rangle = b^2(Q)\sum_{j=1}^{N}\sum_{k=1}^{N}\left\langle e^{-i\mathbf{Q}\cdot(\mathbf{r_j(t)}-\mathbf{r_k(t)})}\right\rangle \tag{4.16}$$

where the particle movement changes the phase of the electric fields scattered from them and results in a fluctuating intensity as can be seen in Fig 4.6.

Investigating the particle motion requires the comparison of the intensity at a time t and at a later time $t+\tau$. This is known as the *time correlation function* and is defined as

$$\langle I(t)I(t+\tau)\rangle = \lim_{T\to\infty}\frac{1}{T}\int_0^T I(t)I(t+\tau)dt. \tag{4.17}$$

The choice of starting time t is arbitrary and so can be set to 0 allowing the time correlation function to be written as $\langle I(0)I(\tau)\rangle$. In the limit as $T \to 0$ then

$$\langle I(0)I(\tau)\rangle = \left\langle I^2\right\rangle \tag{4.18}$$

and in the limit $T \to \infty$, $I(t)$ and $I(t+\tau)$ now fluctuate completely independently so

$$\langle I(0)I(\tau)\rangle = \langle I(0)\rangle\langle I(t)\rangle = \langle I\rangle^2 \tag{4.19}$$

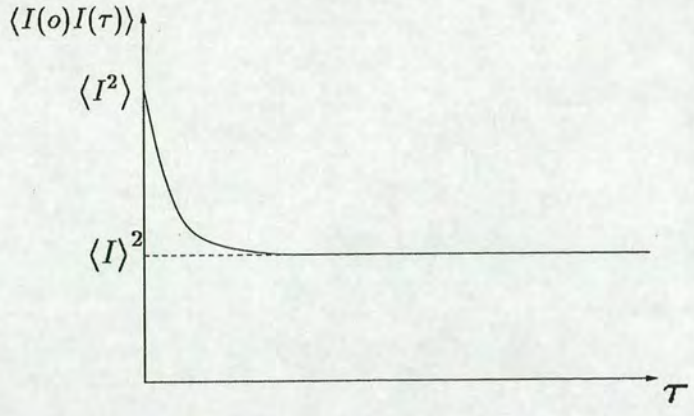

Figure 4.7: The form of $\langle I(0)I(\tau)\rangle$ against τ.

The form of $\langle I(0)I(\tau)\rangle$ can be seen in Fig 4.7 and it is clear that the initial time dependent part of the time correlation function is closely related to the diffusion of the particles. The time correlation function is usually normalised, and it can be found that, for a dilute suspension of nearly identical particles, it is related to the motion of the particles by the following expression.

$$\left[\frac{\langle I(0)I(\tau)\rangle}{\langle I\rangle^2} - 1\right]^{\frac{1}{2}} = e^{-DQ^2\tau} \tag{4.20}$$

where the left hand side of the expression can be measured experimentally and the right hand side is connected with the motion of one particle, where D is the diffusion coefficient. For convenience this is often written as

$$\sqrt{g^{(2)}(Q,\tau) - 1} = g^{(1)}(Q,\tau) \tag{4.21}$$

which is known as the intermediate scattering function, where

$$g^{(2)}(Q,\tau) = \frac{\langle I(t)I(t+\tau)\rangle}{\langle I\rangle^2} \tag{4.22}$$

and for a dilute suspension of nearly identical hard spheres

$$g^{(1)}(q,\tau) = \exp -DQ^2\tau. \tag{4.23}$$

Plotting $\ln\sqrt{g^{(2)}(Q,\tau) - 1}$ against $Q^2\tau$ should then yield a straight line with gradient D, allowing us to determine the diffusion coefficient of the particles. If the

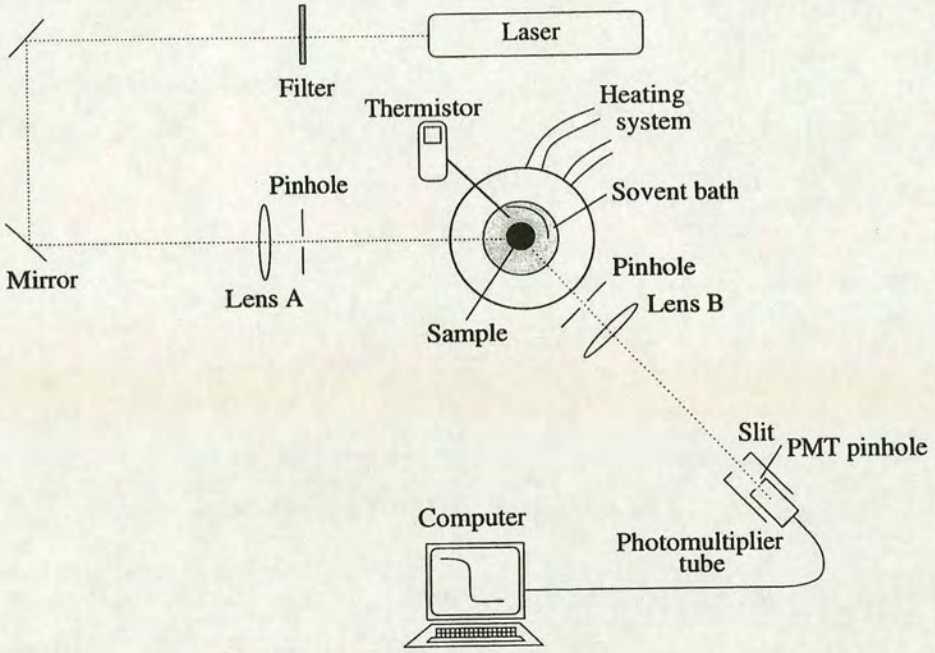

Figure 4.8: A schematic diagram of the Dynamic Light Scattering set-up used in this thesis.

Stokes-Einstein expression is recalled then we can now determine the hydrodynamic radius of the particles, as long as the temperature and viscosity of the solvent are known. This what is achieved when Dynamic Light Scattering is performed.

4.3.2 Apparatus

A schematic diagram of the DLS set-up used can be seen in Fig 4.8, and the main components of the system shall now be discussed.

(1) A Coherent Innova 90 Argon-Ion laser is used to illuminate the sample, used in the green mode which has light with a wavelength of 514.5 nm. This is then passed through a variety of neutral density filters which can be used to control the intensity of the beam. In general the laser beam intensity is kept at as low a value as possible to reduce the effect thermal lensing which gives anomalous diffusion

readings. However the intensity must be such that the signal-noise ration is still high enough to give a good correlation function, and it was found that intensities of around 100mW seem to satisfy both criteria.

(2) Lens A is used to focus the laser beam directly onto the centre of the sample contained in the sample bath. An additional pinhole is also placed before the sample bath which "cleans" the laser beam before it enters the sample.

(3) The sample container consists of a holder for the sample cell and a high quality glass bath filled with a mixture of cis-decalin and tetralin. The mixture is chosen such that the refractive index is as close as possible to that of the glass ($n_{glass} \approx 1.5$.) therefore reducing any light reflections at the cell surface. A beam stop is also placed within the sample bath to reduce any reflection from the back of the bath at the glass/air interface. The entire sample container and bath is fixed inside a temperature control system. Water of a desired temperature is circulated around the bath and a thermistor placed inside the bath accurately measures the temperature. The temperature regulator for the water heater allows sample temperatures in the range of $15^oC - 50^oC$ to be obtained easily to within an accuracy of 0.1^oC. However, when the temperature is changed a few minutes should be left before the temperature can be considered to have stabilised at its new value. At high temperatures evaporation of the bath mixture is also a factor so the bath must be regularly checked to ensure there is enough solvent to completely cover the sample cell. Changing the bath solvent periodically also means any impurities or dust that have built up over time are removed.

(4) The scattered light is first passed through another pinhole to reduce any further stray light and then through lens B which focus it onto the slit in front of the photomultiplier tube.

(5) The size of the slit and the photomultiplier pinhole effect the size of the scattering volume obtained and this has large implications for the experimental

procedure and shall be discussed in the next section. The photomultiplier tube itself is surrounded by a light shield to remove any stray light from outside sources and is connected to a computer which then allows for the correlation function to be obtained. The PMT is in itself a complicated piece of apparatus and there are numerous considerations to be taken into account when it is used, however these shall not be detailed here but can be found in certain texts [52].

Because of the relatively large amount of apparatus in the Dynamic Light Scattering rig the alignment procedure is lengthy and requires great care if good results are to obtained. A thorough explanation of this can be found in the reference [36].

4.3.3 Obtaining results from DLS

When the light scattered from a colloidal suspension is viewed in the far field a collection of rapidly fluctuating bright and dark spots is seen. This "speckle pattern" is caused from the light scattered from the diffusing particles interfering constructively and destructively. To obtain information about the diffusion of the individual patterns the speed of the fluctuation must be measured, and this involves measuring the intensity of, at most, a single speckle by controlling the scattering volume. This is done by varying the size of the slit in front of the photomultiplier and the photomultiplier pinhole as well.

Once we have ensured that the photomultiplier is detecting the light scattered from one speckle only it is possible to obtain the correlation function and so determine the diffusion coefficient.

It has already been mentioned before that any real sample of colloidal particles will be polydisperse. That is, there is a variance in the radii of the different particles due to the preparation procedure. When DLS is performed on such a sample a range of diffusion coefficients will be measured as different sized particles

diffuse with different speeds. To determine the average diffusion coefficient of the particles requires the analysis of the data via the use of the method of cumulants [45].

For the case of a polydisperse system it is clear that the correlation function consists of a sum or distribution of exponentials,

$$\mid g^{(1)}(\tau) \mid = \int_0^\infty G(\Gamma) e^{-\Gamma\tau} d\Gamma \tag{4.24}$$

where $\Gamma = DQ^2$ and is known as the decay rate.

To determine information on the system we can now take the logarithm of both sides and expand the right hand side in a power series of τ.

$$ln \mid g^{(1)}(\tau) \mid = 1 - K_1\tau + \frac{1}{2}K_2\tau^2 - \frac{1}{3!}K_3\tau^3 + \frac{1}{4!}K_4\tau^4 ... \tag{4.25}$$

where

$$K_n = \left[(-1)^n \frac{d^n}{dt^n} ln \mid g^{(1)}(\tau) \mid \right]_{t=0} \tag{4.26}$$

are the n^{th} cumulants of the correlation function. The first two cumulants are

$$K_1 = < \Gamma > \tag{4.27}$$

$$K_2 = < (\Gamma - < \Gamma >)^2 >$$

and it is clear that they represent a means of finding the diffusion coefficient and its variance, which is essentially another form of the polydispersity. By using the method of cumulants on DLS data we can therefore accurately find the average diffusion coefficient and the polydispersity of the particles, and consequently, by use of the Stokes-Einstein expression, the hydrodynamic radius [53].

In practise fitting the data to high orders of the cumulants is laborious and unnecessary so usually it is only fitted to linear, quadratic and cubic orders. The linear fit has the least statistical error from run to run but this is perhaps unrealistic as the actual correlation function might be better described by a higher

order polynomial. On the other hand fitting to a high order polynomial, while potentially giving good fits, has the disadvantage of introducing a larger statistical error since the number of unknown parameters is greater. To obtain the most accurate results the data is usually fitted simultaneously to a linear, quadratic and cubic fits and the results given by each for the diffusion coefficient compared. Similar values for D from all 3 fits is indicative of good quality data and accurate analysis.

There are other factors which determine how accurate the analysis is, and it is important to realise over what range of time scales the data should be fitted to. For example at very low time scales there is a large effect from noise so it is often necessary to ignore these points. Similarly the data at very large timescales may not contain accurate information on the short time diffusion of the particles that we are interested in. In practise this amounts to finding a range of timescales over which an accurate value of D can be found and relies largely on experience and judgement. A typical example of a correlation function and the fitting range can be seen in Fig 4.9

4.3.4 DLS on Liquid crystals

Because liquid crystals have unique properties performing DLS on them has a few added complications, even in the isotropic phase. It has been mentioned that even in its disordered phase a liquid crystal can possess *locally* a degree of molecular ordering. This leads to a light scattering contribution from the collective orientational fluctuations of the solvent, and as the nematic phase is approached, and the size of the fluctuations grows, this will clearly increase. However, the characteristic timescales over which these director fluctuations take place are very short, typically being of the order of $10^{-6}s$ compared with $10^{-2}s$ for the colloids [5]. The scattering from the director fluctuations will not therefore

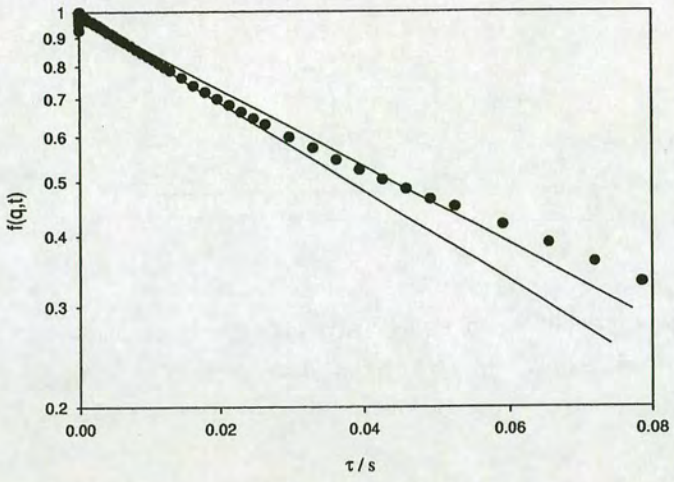

Figure 4.9: An example of two possible fits to the same correlation function. It is clear that the value obtained for the diffusion coefficient depends greatly on which points are chosen to fit over. In general the diffusion coefficient is given by the short time decay rate and so fitting over this range gives the most accurate results for fairly monodisperse spheres.

interfere with the measurement of the diffusion coefficient of the colloids but it will still greatly reduce the signal-to-noise ratio of the correlation function, and as the scattering from the liquid crystal increases near the isotropic-nematic transition taking any results around this region is extremely difficult. Because the light scattered from the director contribution is depolarised, whereas the light scattered from the colloids is not, including a high quality polaroid sheet on the detection arm of the DLS rig will ensure a reduction in the light detected from the molecule fluctuations leading to a better signal-to-noise ratio.

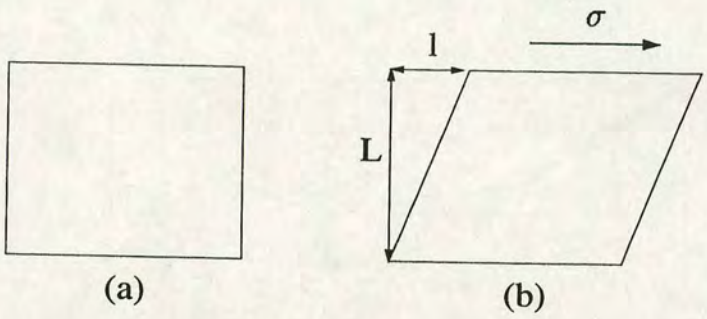

Figure 4.10: Schematic of a Hookean solid undergoing deformation. (a) shows the unperturbed block in equilibrium. In (b), as a shear stress σ is applied the block deforms with a shear strain of γ. This strain persists until the stress is removed.

4.4 Rheology

Broadly speaking rheology is the study of deformation and flow of matter [54–56]. In doing this the material is perturbed somehow and its response to this deformation measured. The simplest case of this is that of simple shear seen in Fig 4.10.

A shear stress σ is applied to the material which consequently "flows". If the material is a perfect Newtonian liquid the flow persists for as long as the stress is applied, but if it is a Hookean solid the material will deform and stay fixed in this state for as long as the shear stress is applied. For an elastic material the shear stress is given by

$$\sigma = G\gamma \tag{4.28}$$

where G is known as the rigidity modulus and $\gamma = \frac{l}{L}$ is called the shear strain.

In the case of the liquid, the Newtonian description of ideal viscous behaviour states that

$$\sigma = \eta\dot{\gamma} \tag{4.29}$$

where η is obviously the viscosity of the liquid and $\dot{\gamma}$ is the shear rate.

For a solid, the strain returns to zero after the stress has been stopped, whereas

with a liquid the strain remains non-zero after the stress has been removed because the material has flowed. Indeed these observations allow for definitions of the solid and liquid states, but in reality most materials fall somewhere between these two ideal cases and are known as *viscoelastic.* Modern rheology is concerned with determining the viscous and elastic components of a material to see which properties dominate, and there are a number of ways to do this.

4.4.1 Oscillatory rheology

One of the most common ways of deforming the material to be studied is to apply an oscillatory stress or strain in a sinusoidal manner and measure the materials response [57, 58].

In oscillatory rheology a sinusoidal stress wave is applied to the material and its resultant strain wave measured.

For a Hookean solid this means

$$\sigma = Asin\omega t$$

$$\gamma = Bsin\omega t$$

as stress is proportional to strain and a sinusoidal stress wave produces an in phase sinusoidal strain wave response.

For the Newtonian liquid

$$\sigma = Asin\omega t$$

$$\gamma = -Bcos\omega t$$

Because the resultant strain wave is now 90^o out of phase with the stress wave.

Because most materials are viscoelastic the resultant strain wave is always between 0^o and 90^o out of phase with the initially stress wave and measuring this

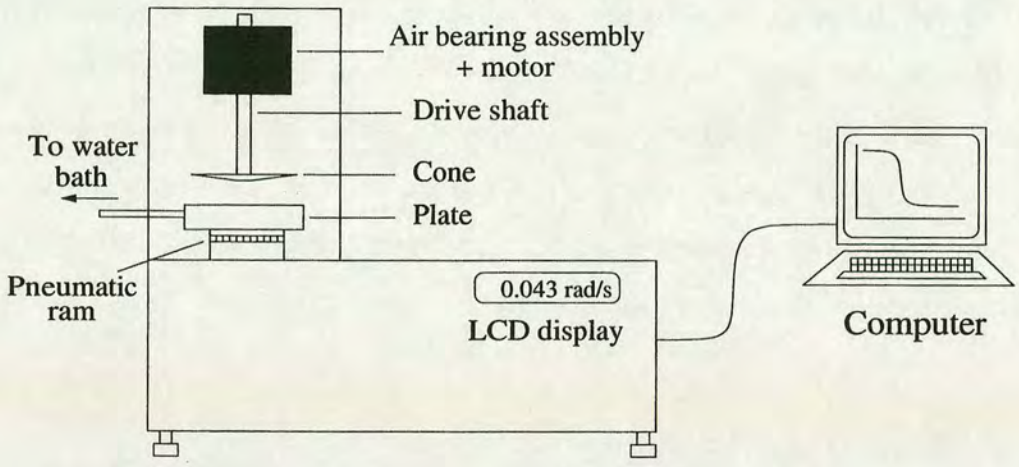

Figure 4.12: A simplified schematic of the CSL^2 rheometer.

4.4.2 The rheometer

The rheometer used in the following investigations was a CSL^2 Rheometer from TA Instruments and a diagram of this can be seen in Fig 4.12.

A brief description of the main components of the apparatus shall now be given.

(1) The air bearing assembly ensures that there is a minimum of friction when the electronically controlled induction motor is used to rotate the dive shaft. The pressure of the air used in the bearing is critical for ensuring the safe usage of the rheometer because a low pressure could mean the possible risk of damage to the equipment.

(2) The drive shaft passes through the air bearing and is finally connected to the geometry. This is the part of the apparatus that comes into contact with the material being analysed, and in this case a truncated cone and plate system were used as can be seen in Fig 4.13.

Here the material being studied is contained between the truncated cone and plate. The rotational motion of the cone is then controlled by the drive shaft and known stresses can be applied to the material allowing for rheological mea-

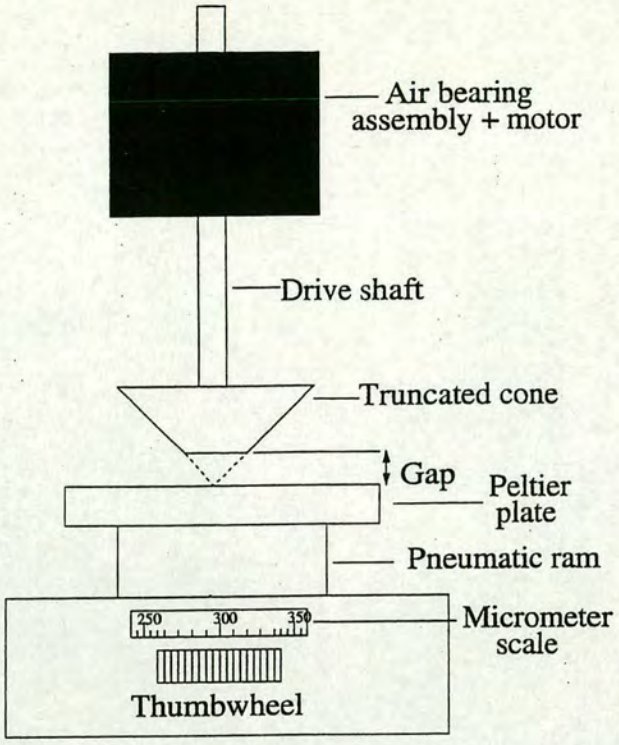

Figure 4.13: A close up of the cone and plate region of the rheometer with a greatly exaggerated angle for the cone. The gap between the cone and the plate is set at the point where the cone tip would have been. The exact experimental process for setting the gap is described later.

surements. The gap between the cone and the plate is especially important for obtaining good quality data and for the case of the truncated cone this must be set at the position where the point of the cone would have touched the plate had it not been truncated. This is unique to the particular geometry and can easily be set by manually altering the position of the plate using the thumbwheel and micrometer scale connecting to the pneumatic ram. A more detailed description of this process is given in the next section.

(3) Once the gap between the cone and plate has been successfully set the plate is lowered via a pneumatic ram and the sample can now be loaded. The amount of fluid which is added to the plate is also important as too much or too little will lead to inaccurate results. Examples of over-filling and under-filling and the

correct amount of fluid needed can be seen in Fig 4.14.

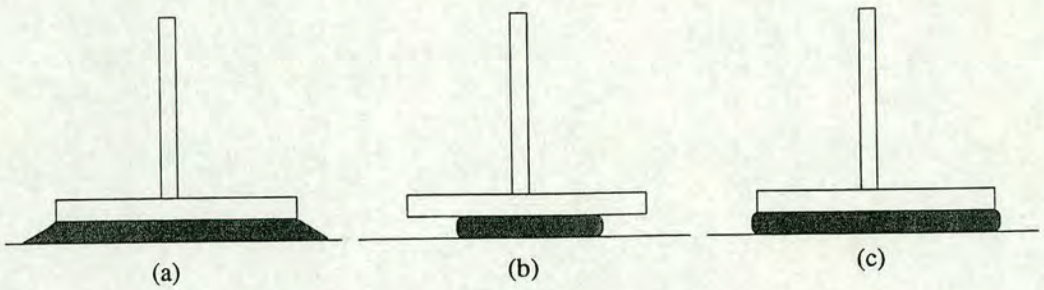

Figure 4.14: 3 schematic diagrams of different amounts of sample between the cone and plate. (a) shows the case for over-filling where too much material is added, (b) shows under-filling and (c) shows the appropriate amount of material needed for accurate results. Over-filling carries the risk of some of the sample leaking on top of the geometry and under-filling effectively changes the diameter of the cone so any measurements will be flawed. In general though under-filling is more of a problem than over-filling and if too much sample has been loaded onto the plate some of the excess can be carefully removed by wiping with a tissue.

Once the correct amount of material has been transferred onto the plate it is raised again via the ram to the correct height which has previously been found.

(4) The temperature of the plate can be controlled by a Peltier system which uses a thermo-electric effect to rapidly and accurately heat or cool the plate. It works by controlling the magnitude and direction of the electric current supplied to the plate and functioning as part of a heat pump. Consequently a heat sink must also be present and this takes the form of a large water bath which removes any unwanted heat from the plate.

(5) The measurements are obtained with the use of an optical encoder device, which can measure very small angular displacements. It consists of a light source and a photo-cell arranged on either side of a transparent disc attached to the drive shaft. Fine radial lines are etched onto the edges of the disc effectively turning it into a diffraction grating, and there is also another stationary diffraction grating between the light source and the disc. The interference of the light which

passes through the two diffraction gratings causes diffraction patterns which are detected by the photo-cell. As the drive shaft moves and the encoder disc rotates as the sample strains the diffraction patterns change. Analysing the change in the patterns then allows for the strain of the sample to be measured. Other rheological information can then be found and plotted by the computer.

4.4.3 Setting the gap

To set the correct distance between the cone and the plate is a relatively easy procedure but one that is crucial for precise results. To do this the pneumatic ram is first raised to a position where it is considerably lower than the cone. A small shear rate is then applied to the cone, and the plate is raised slowly using the thumbwheel until there is contact between the cone and plate. The reading on the micrometer is then taken (this is known as the zero point), and the plate is lowered again. This procedure is repeated a number of times until a consistent value for the zero point is found. The correct position for the plate is then calculated using the gap distance known for the particular geometry and the zero point. The plate is then finally placed at the point with the correct gap distance using the thumbwheel, and the rheometer can now be used.

4.5 Microscopy

While the techniques previously described can be usefully in determining all sorts of quantitative data from our sample it is often helpful to simply observe our materials under a high powered microscope to see what is happening. Firstly, as a means of checking phenomena suggested by other techniques and secondly because observing the structure of materials can often yield interesting results which are not possible using other methods. Two types of microscopy were used

in the course of these experiments: conventional bright field optical microscopy [59,60] with crossed polarisers and confocal microscopy.

4.5.1 Optical Microscopy

The most common form of microscopy is brightfield microscopy where the sample is illuminated with a plain white light source. In this thesis an Olympus BX50 microscope was used with long working distance objectives and crossed polarisers as can be seen from the schematic in Fig 4.15 A number of possible long working distance lens were available meaning magnifications of X10, X20 or X50 were available and two different camera lens of X2.5 or X5 gave a large number of possible overall magnifications . The microscope was connected to a CCD camera and a PC allowing either real time video or snapshots to be taken of the samples under study. The samples were generally held in a Linkam LTS 359 hotstage which allowed for the samples to be held at a constant temperature or subject to a constant temperature ramp. This was crucial for this project as much of the liquid crystal investigation had to begin in the isotropic phase, at a temperature significantly above room temperature.

Polarisers are also a crucial component of the microscope when viewing liquid crystals. When the isotropic phase is viewed under crossed polarisers it will appear black the same as any other normal liquid. However, as the liquid crystal undergoes a phase transition into an ordered phase then characteristic textures will be seen due to the birefringence of the liquid crytsal phase, and as has already been discussed it is possible to determine the molecular behaviour of the liquid crytsal from observing the birefringent textures.

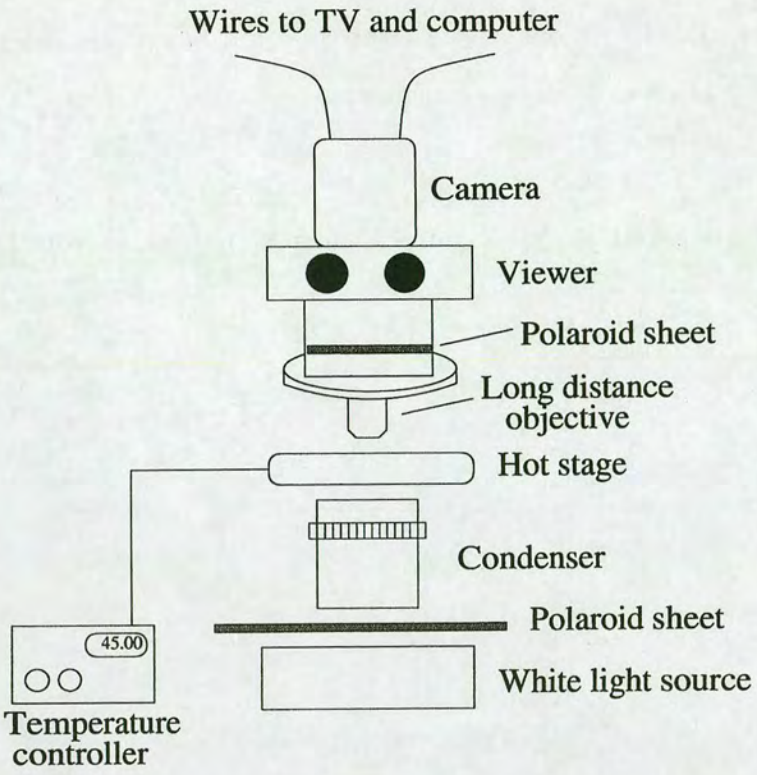

Figure 4.15: A diagram showing the fundamental parts of the microscope used in this project. The sample is illuminated by the white light source focused by the condenser onto the sample itself which is placed inside the temperature controlled hotstage. There are a number of long distance objectives with different magnifications which are available, and the sample can be viewed either directly or on a monitor where still images can be taken or footage recorded onto video. The two polaroid sheets that were also used were placed just above the light source and before the viewing apparatus.

4.5.2 Confocal Microscopy

A different kind of microscope is the confocal microscope, which was initially developed by Minsky in 1955 but it took until the invention of the laser and powerful computers until the technique was practically useful. It has a number of advantageous over conventional microscope because it allows for a very small depth of field as it blocks much more of the out of focus light than a normal microscope does, which leads to a better resolution. There are a number of ways

that this can be achieved with one of the most common being the scanning laser microscope which was used in these experiments .

A simplified diagram of the basic optics of the confocal microscope can be seen in Fig 4.16. The main advantage of the confocal microscope comes from the use of

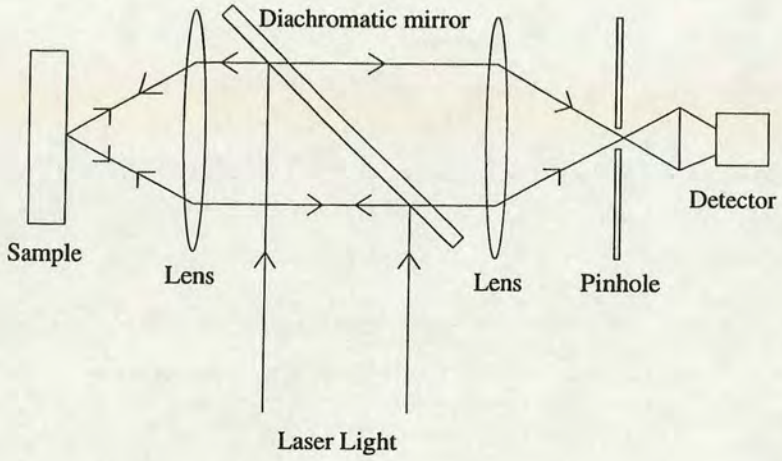

Figure 4.16: Diagram of the simplified optics of a confocal microscope. In reality there are many different optical configurations which can be used.

the pinhole as can be seen in Fig 4.17. In a normal system the microscope will be set-up to image at a single depth with sample placed at the focal point. However light will also be imaged from points in front and behind this focal point. Now these light rays are not in focus at the screen and so reduce the overall imaged quality but they can be reduced by the inclusion of the pinhole which greatly reduces the out of focus light while allowing the in-focus light through, and so improving the image. In practice the laser is scanned quickly across the sample and the pinhole and PMT only detect one point of the sample at any one time, but as the laser is scanned a picture of the entire sample can be built up. The use of the pinhole has the effect of giving the confocal microscope a very small depth of field and the image comes from only a very thin section of the sample. This is exploited as it allows for 3D images to be constructed of a sample by adding the thin sections together.

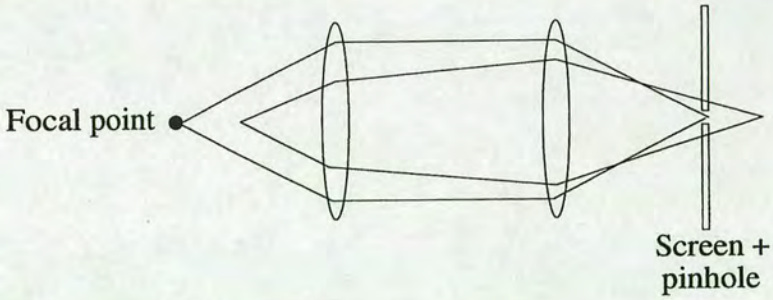

Figure 4.17: Schematic diagram showing how the inclusion of a pinhole can greatly reduce the out of focus light that reduces images quality.

Another feature that commonly goes hand in hand with the optical principles of the confocal microscope is the practice of fluorescent dying of materials. When light is directed onto a molecule it is often common for that molecule to aborb photons sending it into a higher energy state. When the molecule returns to its original lower state some of the energy may be lost internally so the emitted photon is of a lower energy. In practice this means that blue light, for example, may be directed onto a certain molecule but that green light is emitted. There are numerous materials that have such properties and one of them is the fluorescent dye Fluorescene. This is a property which is sometimes exploited by confocal microscopy as we shall see.

Using the knowledge of fluorescent materials along with the dichromatic mirror, which reflects light above a certain wavelength and passes light below that wavelength, gives the confocal microscope an added advantage. If the correct combination of laser and mirror is used then it is possible to shine light onto a material which as been dyed with a suitable dye and to view only the emitted light. This means it is possible to dye part of the sample and only that part will be visible with the confocal micrscope.This will be exploited later when combining colloids and liquid crystals as only the colloids are dyed allowing them to be isolated from the liquid crystal.

Chapter 5

Colloid dynamics in a liquid crystal

5.1 Introduction

Over the last few years investigations into colloidal behaviour in a liquid crystal medium have been common, but most of these studies have focused on the nematic phase. This is perhaps unsurprising as this is where the most obvious liquid crystalline effects take place. However, even in the isotropic phase of a liquid crystal short range order can still be seen and because the isotropic-nematic transition is first order, molecular ordering of the liquid crystal can be observed above the transition temperature.

The effects of adding a colloidal particle into this complicated situation are numerous. Because the molecules will attach homeotropically at the surface of the colloidal particle as previous shown, the liquid crystal will effectively order itself around the particles even in the isotropic phase, an effect known as orientational pre-wetting . As the temperature is cooled towards the nematic phase the ordering around the particles will increase, altering the dynamics of the particles further. Secondly, the radial ordering of molecules at the surface turns the particle into a defect site in the bulk liquid crystal. Because this disrupts the overall

order of the nematic slightly it is possible that this will have the effect of "delaying" the isotropic-nematic transition to a lower temperature as more disorder has been introduced into the system.

This chapter deals with an experimental investigation of dilute colloidal suspensions in the isotropic phase of a liquid crystal, examining both the altered dynamics of the particles and how this can be related to orientational pre-wetting, and the effect on the isotropic-nematic transition temperture when defects are artificially introduced. These results are primarily a combination of Static and Dynamic Light Scattering but some preliminary rheology was also involved.

5.2 Dynamics of colloids

A nematic liquid crystal has a unique symmetry and therefore certain properties can have different values depending on which direction you are looking along. Viscosity is one such property and liquid crystals have a number of different viscosities for different directions with respect to the director. These factors can be combined though to give a "average" value for the viscosity in either the isotropic or nematic phase.

In the isotropic phase of a liquid crystal the increased molecular ordering around colloidal particles creates a small region of nematic liquid crystal around the particles which is of a higher viscosity than the bulk isotropic. Any particle diffusing will then exhibit an anomolously low diffusion coefficient and consequently a high hydrodynamic radius when it is determined via the Stokes-Einstein expression. Molecular ordering at the particle surface is therefore detected by measuring an anomolously high hydrodynamic radius, and this should increase further as the nematic phase is approached. A second effect may also contribute to a higher hydrodynamic radius. The thickness of the ordered molecular layer surrounding

the particles is of the order of the coherence length $\zeta(T)$, which in the case of a nematic liquid can be of the order of 10-40 nanometers. As the particle moves it may drag about this layer contributing further to the increase in its hydrodynamic radius.

In order to calculate the hydrodynamic radius in the first place there are other factors in the Stokes-Einstein expression that must be known, including the viscosity of the bulk liquid crystal. This was done using a rheometer and a sample of pure liquid crystal, which in this chapter was exclusively 5CB. Results of the viscosity measurements can be seen in Fig 5.1.

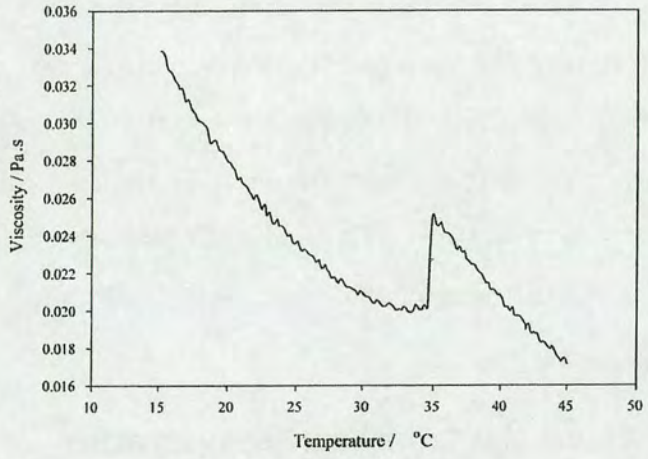

Figure 5.1: The viscosity of 5CB as a function of temperature. The isotropic-nematic phase transition is seen as a sharp dip in viscosity around 35^oC. It should be noted that measuring the viscosity of a nematic liquid crytsal in this manner is not without complications as this is an average viscosity which contains contributions from the three Miesowitz viscosities. Using an oscillatory flow means that the molecules will naturally align with the direction of flow and consequently any measurement of the viscosity will reflect the viscosity of molecular flow parallel to the director more than the other two viscosities. Consequently the nematic viscosity measured here may not accurately reflect that experienced by a colloidal particle diffusing in the nematic. However, as this experiment was principally carried out to measure the isotropic viscosity the results are still useful.

These results agree well with the known values for the viscosity of 5CB.

5.3 DLS on the liquid crystal colloids

Now that the viscosity of 5CB is known it is possible to perform Dynamic Light Scattering on samples of dilute colloids in 5CB and calculate the hydrodynamic radius. The samples were prepared in the manner described in the previous chapter, where the colloidal particles, initially suspended in heptane, are added to the liquid crystal. This mixture is then kept at a high temperature under vacuum to remove only the heptane leaving the particles suspended in the liquid crystal. Once the process was finally completed the refractive index of the samples was checked against that of the pure liquid crystal to check that the bulk of the heptane had been removed. From this we could say that the sample was made up from less than 1 percent heptane, and the samples were very dilute, typically having a volume fraction of $\approx 10^{-3}$. The radius of the particles was checked by performing Static Light Scattering of the particles in cis-decalin.

5.3.1 The effect on the transition temperature

The first experiment to be done was to investigate the effect that the presence of colloidal particles have on the position of the isotropic-nematic transition temperature [61]. This was done by simply measuring the scattering intensity as a function of temperature going from the isotropic phase to the nematic phase. Because the director fluctuations in the isotropic phase increase as the temperature is decreased the scattering intensity also increases. At the transition there is a peak in the scattering intensity as nematic domains form, allowing for the accurate determination of the transition temperature.

Fig 5.2 shows the measured scattering intensity with the detector arm of the DLS

rig at 90^o for a sample of 5CB with 310 nm radius particles with a volume fraction of 10^{-3} as well as the scattered intensity for the pure liquid crystal. The samples were first introduced in the isotropic phase and cooled at a rate of approximately 0.1^oCmin^{-1} in steps of 0.5^oC with runs lasting 10 minutes at each temperature.

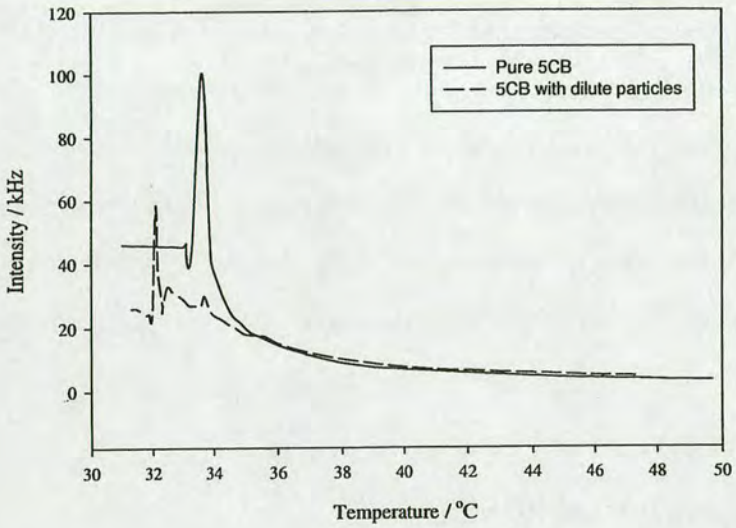

Figure 5.2: The scattering intensity as a function of temperature for samples of pure 5CB and 5CB with a dilute amount of particles. As the temperature is decreased the scattering intensity increases due to the growing director fluctuations until it peaks as the nematic phase forms. The sample containing particles has a significantly lower transition temperature than the pure liquid crystal. The difference in apparent scattering magnitude between the two samples can be explained as follows. At the start of the second experiment, with liquid crystal and particles, the laser intensity was changed so that the initial scattering intensity was equal in both cases. The light scattered from samples containing particles includes a large contribution from the particles alone. This means that the liquid crystal director fluctuations do not contribute as much compared with pure 5CB samples, so a smaller increase in scattering intensity is seen as they are cooled.

The graph shows the characteristic increase in scattering intensity for both samples as the director fluctuations increase and the sharp peak in intensity as the nematic phase is reached. The intensity then decreases sharply after the peak

when the forming nematic domains strongly scatter light. Clearly the particles have an effect on the isotropic-nematic transition as it appears that the peak in intensity which signifies the transition is "depressed" by approximately 2^oC. This can be explained by looking at the molecular behaviour of the liquid crystal surrounding the particles. If the molecules attach homeotropically to the surface of the particles in the isotropic phase and some degree of local molecular ordering exists then the particles effectively act as defect sites which inhibit the ordering of the nematic phase. This means the system has to be cooled to a lower temperature before it becomes favourable for the liquid crystal molecules to begin ordering, and the phase transition temperature decreases. However a depression of 2^oC is quite large for such a small amount of particles and it is possible that any left over heptane dispersed in the sample would also contribute to this effect.

5.3.2 Colloidal diffusion in 5CB

Clearly the presence of colloidal particles has an effect on some of the bulk properties of the liquid crystal but how are the colloids themselves affected? To examine this the diffusion coefficients of colloidal particles in 5CB were measured as a function of temperature starting in the isotropic phase and decreasing towards the nematic. The particles used were 175nm particles sized by Static Light Scattering and suspended in 5CB at a volume fraction of approximately 10^{-3}. The samples were then loaded into the Dynamic Light Scattering rig in the isotropic phase of 5CB and measurements of the diffusion coefficient were made for a range of temperatures down to the nematic phase. Using the Stokes-Einstein expression and the known values for the viscosity of 5CB the hydrodynamic radius could then be determined. Results for the hydrodynamic radius of the particles against temperature can be seen in Fig 5.3.

As Fig 5.3 shows, at high temperatures, well into the isotropic phase, the calcu-

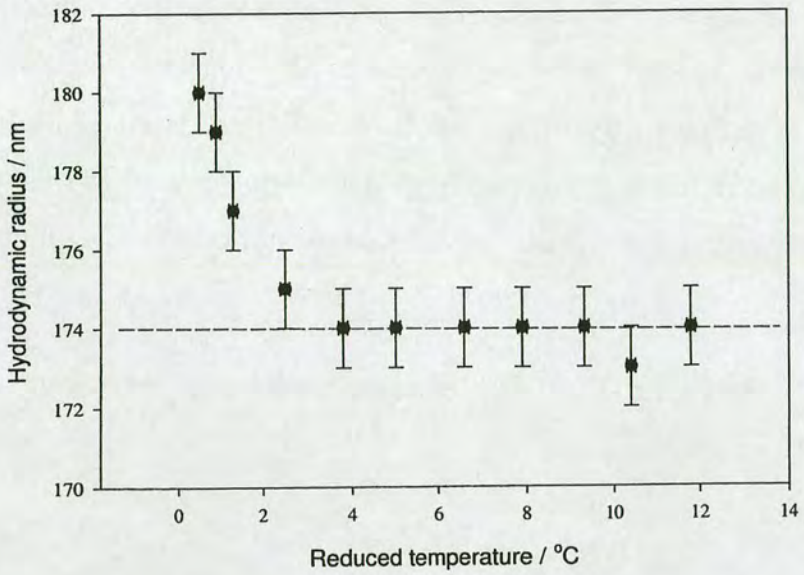

Figure 5.3: The hydrodynamic radius against reduced temperature for a dilute sample of 174nm particles in 5CB with a dotted line showing the physical radius . The increased radius is indicative of molecular ordering at the surface of the particles. The reduced temperature is defined as $T - T_{I-N}$ where T_{I-N} is the position of the nematic isotropic transition in this sample.

lated hydrodynamic radius is equal to that of the physical radius as expected. However, as the temperature is decreased we see an increase in the hydrodynamic radius which continues until the nematic phase is approached and measurements are no longer possible. Like the effect on the bulk transition temperature this is also cause by the ordering of 5CB molecules at the surface of the particle even in the isotropic phase, an effect known as orientational pre-wetting.

If we recall the Stokes-Einstein expression (Eqn 2.9) then we can see how the calculated radius is dependent on the other factors in the equation when the diffusion coefficient is experimentally measured. The viscosity for pure 5CB in the isotropic phase is already known and used in the equation, but orientational pre-wetting at the particle surface will change the local viscosity experienced by

the particle changing its rate of diffusion. A higher local viscosity around the particles will lead to a lower diffusion and a higher hydrodynamic radius when the Stokes-Einstein is applied. One such cause of this higher viscosity could be a small region of ordered nematic molecules surrounding the particles in the isotropic phase, and Fig 5.3 suggests this is what is happening. However, there are other considerations as the viscosity of a liquid crystal can have a number of possibilities depending on direction of flow.

The orientational ordering of the molecules cause anisotropic behaviour of the viscosity local to the particles giving

$$\eta_{eff} = \eta_{iso} + K(Q_{ij}) \tag{5.1}$$

where η_{eff} is the effective viscosity, η_{iso} the isotropic viscosity and $K(Q_{ij})$ is some function of the tensor order parameter. For 5CB the Miesowicz viscosities η_b and η_c differ from η_{iso} significantly with η_b 10 % less than η_{iso} and η_c 20 % more than η_{iso}. Thus, the nature of the viscosity close to the particle is greatly dependent on the local flow pattern, something which is impossible to determine with DLS.

Another contribution to the increased R_H could come from the fact that the particle will drag about more solvent with it when there is an ordered layer of molecules that wish to align parallel to one another. Both these effects come from the same basic principle of orientational pre-wetting in the isotropic phase and the increased R_H with decreasing temperature is evidence of this.

There are other important points to note in Fig 5.3, and one of these is relevant to how the data is obtained and interpreted. Performing DLS allows for the diffusion coefficient of the particles to be measured, and from this the hydrodynamic radius calculated with the use of the Stokes-Einstein expression. Also part of the Stokes-Einstein expression is the viscosity of the fluid as measured experimentally in Fig 5.1. However when the particles are present there arises an additional complication. As we have previuously seen the presence of particles

directly affects the position of the isotropic-nematic transition and in the case samples from Fig 5.2 and Fig 5.3 we see a reduction in the phase transition by 2^oC. This menas that we have no known value for the viscosity of the isotropic liquid crystal at temperatures between that of the pure liquid crystal and that at which the actual transition takes place in samples with particles. We overcome this problem by extrapolating a viscosity from the isotropic part of the curve in Fig 5.1 to the appropriate temperature.

Once the sample has been taken into the nematic phase it was re-heated again into the isotropic and diffusion coefficient measurements were performed again. It was found that the hydrodynamic radius was much higher than when cooling was taken place giving a value of approximately 205nm, and that this value stayed even at temperatures 10^oC above the transition. Molecular ordering around the particles would not survive at such temperatures so the increased radius is probably due to aggregation of the particles in or near to the nematic phase which would lead to an increased hydrodynamic radius. This is supported by the fact that the correlation functions obtained by DLS show evidence of more than one timescale suggesting there were different sized objects diffusing inside the sample.

5.3.3 Particles of different sizes

Frenkel *et al* [5] suggested that the size of the colloidal particles would have a direct bearing on the extent of orientation pre-wetting with larger particles showing a larger ordering effect at their surface, but their experiments used particles which were much smaller than the ones used in this thesis and the results were inconclusive. A number of different samples were made using various sizes of particles and investigated in the manner described above to see if there was indeed any correlation between particle size and the extent of orientational pre-wetting. It was found that this was indeed the case but that some unusual results lead to

a whole new area of research.

Samples of 350nm radius particles were prepared at volume fractions of 10^{-3} in 5CB as before. Diffusion coefficient measurements as a function of temperature were then performed on the samples and the corresponding hydrodynamic radii calculated. It was immediately noticed that this radius was much *lower* than expected. This was particular unusual as, if anything, it should be higher due to orientational pre-wetting. This initiated an investigation of the preparation procedure which eventually lead to the findings of the next chapter.

In the meantime however, the experiments measuring the diffusion coefficient continued and results of D vs reduced temperature for these samples can be seen in Fig 5.4.

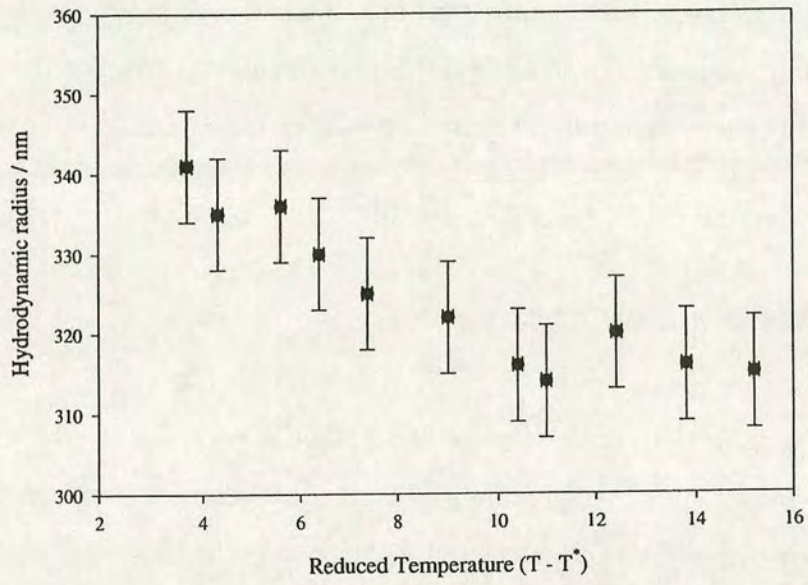

Figure 5.4: The hydrodynamic radius against reduced temperature for a dilute sample of 350nm particles in 5CB. The hydrodynamic radius increases by a greater amount when larger particles are involved. The discrepancy between the nominal physical radius and hydrodynamic radius is discussed in the next section.

Like the case of smaller particles, these results show a dramatic increase in the hydrodynamic radius as the temperature decreases towards the nematic phase transition. However, the magnitude of this increase is much larger compared to the smaller particles, with an increase of 30nm for the larger particles compared to only 7nm for the smaller ones, implying a greater ordering at the particle surface. The ordering also seems to occur at a much higher temperature for the larger particles, beginning at around 9^oC above T_{I-N} compared with only 3^oC for the smaller particles. This would all seem to agree with the predictions of Frenkel where larger particles exhibit a greater molecular ordering. When these samples were taken into the nematic phase and then re-heated again it appeared that the aggregation seen in the smaller case was much more pronounced and it was impossible to obtain any meaningful data from the samples and they had to be discarded.

One thing which cause great surprise was the value for the hydrodynamic radius far into the isotropic phase. The particles physical radius was measured using SLS to be around 350nm, but a hydrodynamic radius of around 310nm was measured as can be seen from the graph. An exhaustive study of the possibilities for this lead to the conclusion that the preparation process of first having the particles suspended in heptane and then transferring them to the liquid crystal lead to the particles becoming coated with a layer of heptane while dispersed in the liquid crystal. These coated colloids have altered dynamics and behave differently compared to their normal uncoated counterparts, and a full study of this can be found in the next chapter alongside some implications for coated colloids in a liquid crystal.

5.4 Discussion

In this chapter we have presented the results of Dynamic Light Scattering experiments on dilute systems of colloidal particles in the isotropic phase of 5CB. This has shown that the particles show a significant change in their dynamics which is interpreted in the framework of molecular ordering at their surface. The particles in turn act as defect sites which affects the position of the isotropic-nematic phase transition. It was also seen that once the samples had been taken into the nematic phase and re-heated into the isotropic phase that the calculated hydrodynamic radius of the particles was permanently higher than initially measured, and it is thought that this can be explained in terms of aggregation of the particles.

The size of the particles also seems to effect the magnitude of the ordering at the surface, with larger particles showing evidence of greater ordering at the surface. However, it is difficult to determine the exact thickness of the ordered layer just from the increase in the hydrodynamic radius, as a number of factors are involved. The ordered layer clearly has a different viscosity from the bulk isotropic but because the nematic phase has 3 different viscosities depending on the direction of flow it is impossible to predict this without understanding the nature of the flow around the particles. The particle may also drag around the ordered layer more than it would the isotropic solvent, which would again affect the diffusion of the particles. These combined effects make it difficult to interpret the exact nature of the molecular ordering at the surface.

There has been previous theoretical evidence that the interaction between spherical particles in the isotropic phase is complicated with both repulsive and attractive forces at work. Stark [62] described that for small interparticle distances ($d \approx \zeta$) then the particles would strongly attract however for larger d a repulsion barrier appears which has a height of several kT near the isotropic-nematic transition. This repulsion then decays exponentially for higher d. There has also

been experimental and theoretical evidence for the aggregation of colloidal particles in the nematic phase of a liquid crystal due to elastic forces present and the anchoring conditions at the surface of the particle. These two effects could explain the results observed in the DLS experiments. In the isotropic phase the particles are initially far apart in our dilute system, and due to the repulsive force at long ranges do not attract. However as the liquid crystal enters the nematic phase the particles aggregate, and on return into the isotropic phase they remain fixed together due to the short range attraction. These forces together with orientational pre-wetting have important consequences for the more concentrated systems of liquid crytsal colloids which will be examined later.

Chapter 6

Dynamics of coated colloids

6.1 Introduction

During the course of the investigation into the dynamics of colloids in a liquid crystal solvent it was noticed that some samples gave an anomalously low value for the hydrodynamic radius that could not be accounted for. It was subsequently discovered that the preparation process, which involved the particles being transferred from one solvent to another, may have been responsible for this and an offshoot project was undertaken to understand this process more. This entails a detailed experimental study of the altered dynamics of these special colloids and the conditions under which it is possible to create them. The results presented here are evidence of a novel type of colloidal behaviour that has so far not been documented and one that could prove extremely important for the everyday practical use of particles in soft condensed matter.

Latterly, a hydrodynamic treatment is used to compare experimental results to those given from a theoretical model which is also introduced. The model itself was initially developed as part of a study into Stokes-Einstein violation in glass-forming liquids, however here it is used in a completely new context to explain

the altered dynamics of the colloids found in our systems.

Because performing measurements of colloidal dynamics in a liquid crystal solvent has numerous complications it was decided that this investigation should centre on more conventional solvents used in soft condensed matter, however the results discovered have some interesting implications for liquid crystal solvents and these shall be discussed at the end of this chapter.

6.2 Motivation for investigation

After it was initially discovered that many samples prepared with our liquid crystal solvent gave values for the diffusion coefficient that were much higher than expected and so values for the hydrodynamic radius that were much lower than the physical radius it was necessary to look again at the Stokes-Einstein expression in order to understand why. It is clear that a number of parameters lie between the measurement of the diffusion coefficient and the value of the hydrodynamic radius. The temperature is easily measured and the viscosity of the solvents are also well known so the only remaining factor that could effect the calculated diffusion coefficient of the particles is the 6π factor. This represents the boundary conditions at the surface of the particle and is equivalent to saying that there are *stick boundary conditions* at the colloid/solvent interface, where the solvent molecules attach at the surface. It has been well known for many years that drops of one solvent in another have different boundary conditions to solid particles because of the internal flow of the drop. This leads to *slip boundary conditions* and the factor in the Stokes-Einstein expression becomes a 4π.

If it was somehow possible to alter the boundary conditions at the surface of our solid colloidal particle from *stick* to *partial slip* then the dynamics of the colloids would change and so would the calculated hydrodynamic radius. In fact

boundary conditions that were more "slip-like" would result in a faster diffusion for the particles and a lower hydrodynamic radius as was seen in our earlier experiments with liquid crystals.

6.2.1 Preparation procedure reviewed

Because the method which goes into making up the samples is so crucial to the resultant effects on the behaviour of the particles, it shall be reviewed here for the more general case of dispersing particles suspended in one solvent in another solvent. In the experiments described here the particles were all initially dispersed in petroleum ether because of its low boiling point and so easy evaporation, but heptane was also used in some cases as shall be seen. The particles in petroleum ether were then added to cis-decalin at a suitable temperature to remove only the petrol in a vacuum oven for a period of a few days. Once this was done the referactive index of the final solution was measured, as this could be checked with the refractive indexes of the individual solvents to make sure that the petrol had been removed. Once it was discovered that less than 1% of the final solution contained petroleum ether and that this would not decrease on further heating the samples were deemed prepared.

If this method of preparation was responsible for producing unusual and anomalous behaviour for the dynamics of the particles it is also necessary to compare it to a system of "normal" colloids of the same size and type. To this end a solution of dried particles, of the same stock as the previous samples, were dispersed in cis-decalin. This involved first taking an amount of the particles in petroleum ether and completely evaporating all of the petrol in a vacuum oven, a procedure itself which has a number of complications. Obviously the temperature must be above the boiling point of petrol however it cannot be too high so as to damage the colloidal particles and a temperature of around 50^oC is suitable for this . When

the evaporation has finished the residue is a white powdery mass of aggregated colloidal particles, and trying to disperse an accurately known dilute amount of them in another solvent is difficult. This was done by adding the dried particles to the cis-decalin and then shaking them vigorously for many days, along with intermittent sonication of the samples, which would hopefully result in the particles being completely re-dispersed in a new solvent.

Once the two types of samples were prepared it was possible to compare results given by both Static and Dynamic Light Scattering as these measure the physical and hydrodynamic radius of the particles respectively. The results of Static Light Scattering measurements, with a laser wavelength of 647.1 nm, on two samples of 316nm particles prepared in the two methods described above can be seen in Fig 6.1.

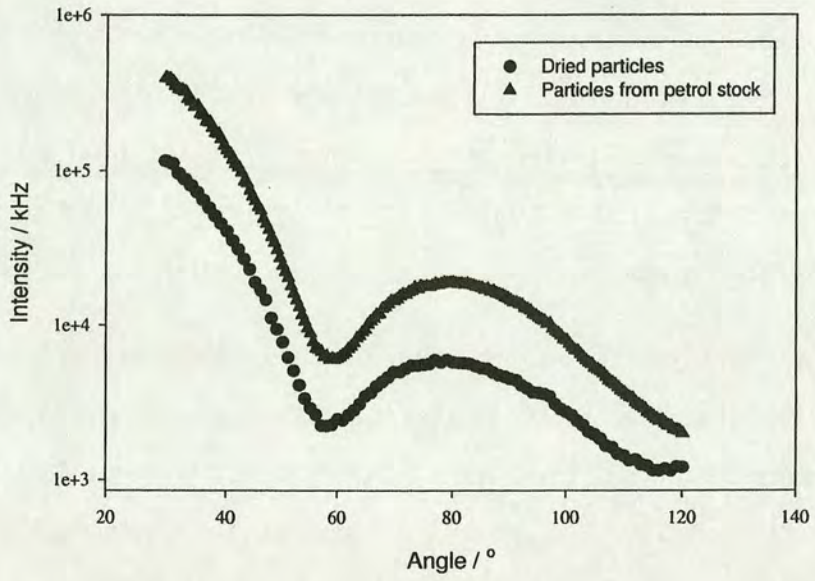

Figure 6.1: Static Light Scattering results, with a laser wavelength of 647.1nm, of form factors taken from samples prepared from dried particles and particles taken from a petrol stock, dispersed in cisdecalin. The form factors are practically identical proving that the particles are the same size and polydispersity.

The graph shows that as expected the form factors are identical, demonstrating that, as expected, the particles are the same in both cases.

The interesting results appear when Dynamic Light Scattering is performed on the same samples, and because DLS first measures the diffusion coefficient it is possible to detect any changes to the diffusion of the particles that might result from unusual circumstances. The results of the correlation functions measured for the same two samples above can be seen in Fig 6.2. Clearly the diffusion of

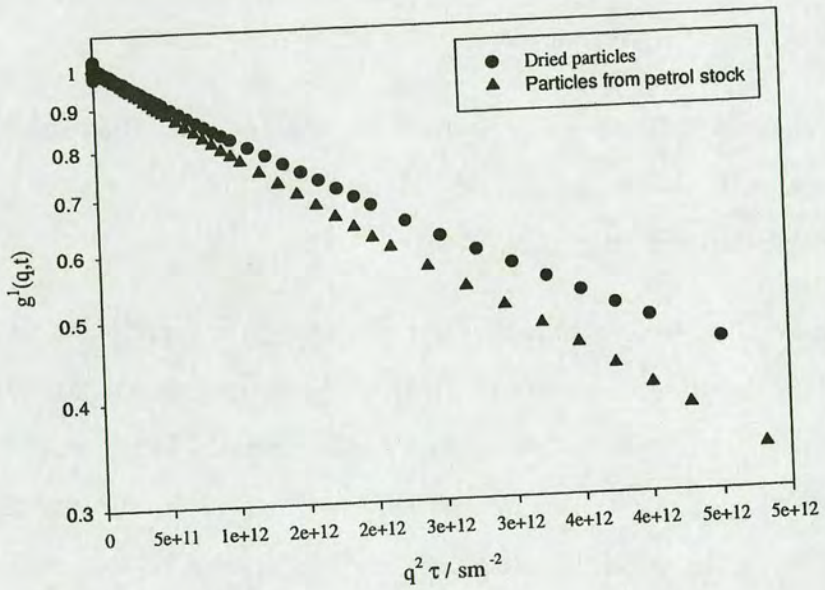

Figure 6.2: Correlation functions obtained from DLS, at a scattering angle of 90^oC, for two samples: one prepared with dried particles and the other prepared with particles from a petroluem ether stock. The colloidal dynamics of the two samples are extremely different with the particles from the petroluem stock diffusing faster.

the particles in the two different samples is drastically different. The correlation for the particles taken from the petrol stock has a significantly larger gradient than the particles that were dried first meaning they have a faster diffusion.

The Static Light Scattering results show that the particles are almost exactly the

same size, so any difference in the diffusion must be a result of altered boundary conditions at the surface of the particle. This is supportive of the suggestion that the preparation procedure coats the particles with a thin layer of solvent which persists even when the particles are re-dispersed in a second solvent. This creates "semi-slip" boundary conditions at the surface of the particles which affects the diffusion.

This motivated us to re-write the Stokes-Einstein equation as follows

$$D = \frac{kT}{S\pi\eta R} \tag{6.1}$$

where S is now a slip factor and has a value between 4 and 6.

The exact value for S will depend on a number of factors including the thickness of the coating and the viscosities of the different solvents, however it is possible to set a lower limit on its value.

It has previously been stated that S=4 for the case of a liquid drop in another solvent, but this includes the assumption that the drop has a viscosity of 0. If in fact the drop has an appreciable viscosity then the slip factor will always be above 4 and we can calculate this for the solvents present in our experiment to give a lower limit of the possible values for S. The equation for the slip factor for a drop of one solvent in another [63] is

$$S = 6\frac{1 + \frac{2\eta_d}{3\eta_s}}{1 + \frac{\eta_d}{\eta_s}} \tag{6.2}$$

where η_s and η_d are the viscosities of the suspending solvent and the drop respectively. Clearly when the viscosity of the drop is 0 then S=4 and ideal slip boundary conditions are achieved and when $\eta_d \gg \eta_s$ (when the drop becomes a solid) S=6 and stick boundary conditions are recovered.

For our case where the viscosity of cisdecalin is 3.38 cp and the viscosity of petrol is 0.21 cp at room temperature the lower limit that S can have in our system is around 4.1.

The entire experiment was repeated a number of times, preparing a new set of samples in the same way each time, and it was found that, while the samples with particles from petrol stock always gave values for the diffusion coefficient that were faster than expected, the precise values varied from one sample to the next suggesting that the final form of the coating was delicately linked to the preparation. However the values found for S are always between 4 and 6, and in this case were always above the lower limit of 4.1.

These kind of unusual colloid dynamics observations have to our knowledge never been previously documented, and serve as a warning as to the potential importance of preparation procedure on the final behaviour of the particles. The next few sections shall now concentrate on some of the particular details that have emerged concerning the exact nature of the coating.

6.2.2 Size of the coating

Clearly the thickness of the solvent coating surrounding the particles will have a direct effect on their final dynamics, with thicker coatings leading to boundary conditions which resemble the case of pure slip. In our system though there are restrictions on how thick the coating could possibly be.

Because the coating solvent (petrol) has a lower refractive index than the PMMA particles, any significant size of coating should be detectable when Static Light Scattering measurements are performed. Even coatings of a few nanometers will affect the form factors such that it is noticeably different from its usual shape. Because the form factors measured for particles with and without coatings were almost identical we can deduce that the coating must be thin enough so that its appearance is not detectable through the form factor.

We can go someway to quantify this by modelling our system of a particle with a

solvent coating with a core-shell model in the same way as we initially modelled the PMMA core and PHSA hairs. The model for our particle can now be seen in Fig 6.3 and the theoretical form factor for this can be found with Eqn 4.16. This can be plotted fitting parameters such as particle size, polydispersity and coating thickness.

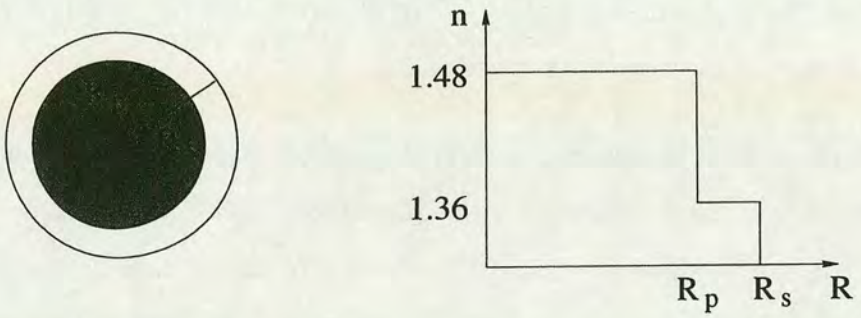

Figure 6.3: Schematic diagram for the two-step refractive index profile of the colloidal particle.

We can therefore compare experimental data with theoretical form factors, controlling parameters including the coating thickness, allowing us to see the effect different sized coatings will have as is seen in Fig 6.4

It is clear from the two graphs that while a coating thickness of 3nm gives a form factor which is similar to what was obtained experimentally, a coating thickness of 5nm means the form factor departs drastically from what is expected. Because the form factors for coated and un-coated particles were virtually identical it means that the coating thickness can not be more than about 3nm if this model is to be believed.

There is a number of problems with this model however that throw uncertainty upon its ability to accurate predict the size of the coating. Firstly, even the presence of a small coating shifts the minima of the form factor slightly towards higher Q. This coupled with the fact that there are many parameters to fit to, including particle radius, polydispersity and coating thickness,means there is a

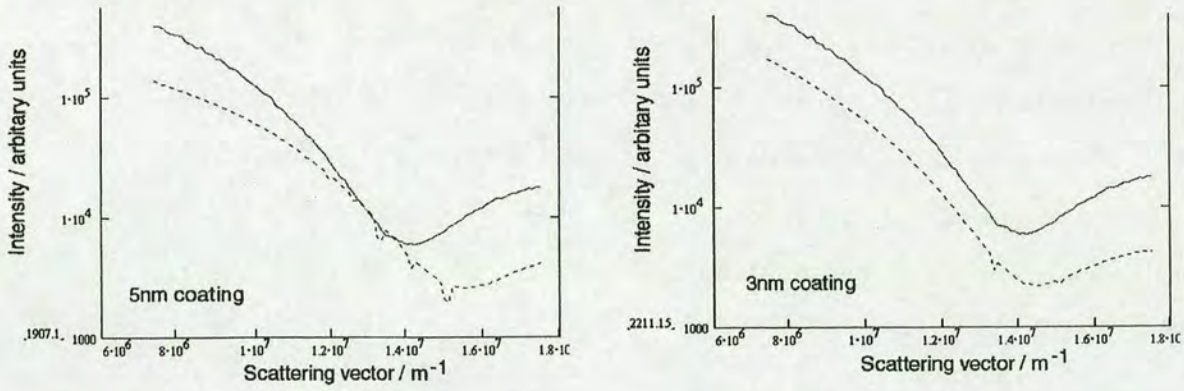

Figure 6.4: Two different examples of experimental data (solid lines) compared with the theoretical form factor for coated spheres (dotted lines). In the first case the experimental form factor is created with the physical radius of the particles (known from previous SLS experiments) and a coating thickness of 5nm. The second graph shows the same experimental data compared with a theoretical form factor with a coating thickness of 3nm. In both cases the physical radius of the particles was 317nm and the refractive index of the coating was 1.36.

high source of error when fitting to the experimental data.

There is also the question of how applicable this theoretical model is to our case. In the model the particles are thought of as having a two step refractive index profile of a PMMA core and a solvent coating, but we know that the particles are also covered with polymer hairs. There is no way of knowing how the solvent behaves around the polymer hairs as it may soaked into them or merely attach near the surface. The chemistry at this level will be crucial in respect to the SLS measurements obtained and the final boundary conditions that the particle has, but unfortunately there was no way of investigating this further within the limited time restraints and so caution must be used when making claims for the precise nature of the coating.

However along with the evidence from the data fitting to theoretical form factors comes the intuition that would suggest that only thin coatings would be possible,

as it seems unlikely that any thick coating ($\geq 10nm$) would exist in a stable state surrounding the particles even after there were kept at high temperatures. So it seems sensible to conclude that the coating thickness is limited to a few nanometers and in the later hydrodynamic model of this system which is used this is the assumption that is made.

6.3 The effect of time

It was noticed that while all samples gave anomalously high diffusion coefficients when DLS was performed at first, that in a matter of weeks this decreased for the same samples, suggesting a slowing of the diffusion towards what is expected of un-coated particles of the same size. An example of this can be seen in Fig 6.5 where measurements of the diffusion coefficient of the particles are made on the same sample two weeks apart with no interference between the two measurements.

A large difference in the diffusion coefficients of the two sets of results is clear and this is reflected in the hydrodynamic radii shown in the inset. After two weeks there is marked decrease in the diffusion coefficient of the particles suggesting that the conventional stick boundary conditions are returning and the coating is desorbing away from the surface of the particles.

Because the exact nature of the coating/particle/polymer hair relationship is not known it is impossible to propose a definitive mechanism for this but experimentally it is found that in all cases the diffusion slows with time to varying degrees.

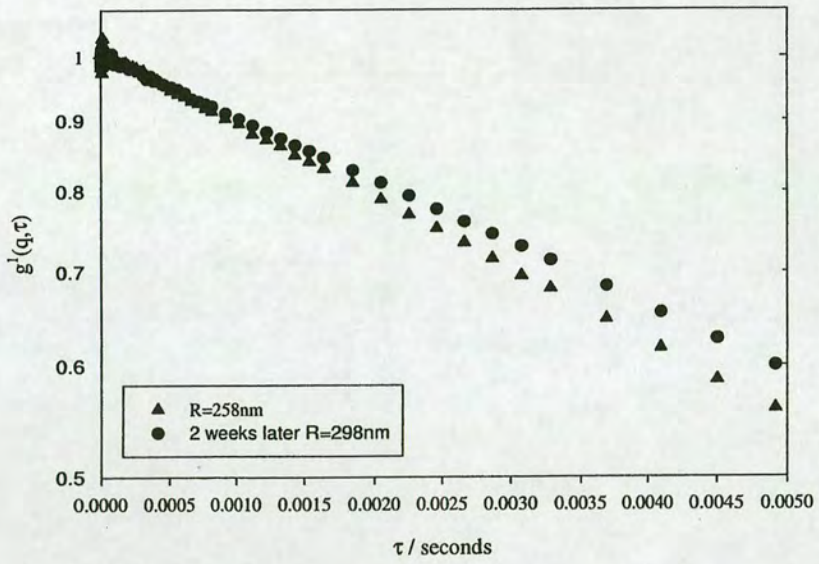

Figure 6.5: A graph of the correlation function for the same sample of coated colloids two weeks apart. Clearly the diffusion is significantly slower after two weeks pointing to a desorbtion of the coating from the particle surface with time, which regains its stick boundary conditions and slows its diffusion.

6.4 Effect of particle size

When successive batches of samples were made from the same stock it was often found that the diffusion constants of the particles varied significantly implying that the preparation procedure was sensitively linked to the final boundary conditions of the particles. It was also found that particles of different sizes gave different results when the boundary conditions were examined. In general it was found that larger particles showed a larger discrepancy between the hydrodynamic and physical radius than the smaller particles.. A graph of hydrodynamic radius against physical radius for various different particle sizes can be seen in Fig 6.6.

It is clear that the larger particles show a much larger discrepancy between the

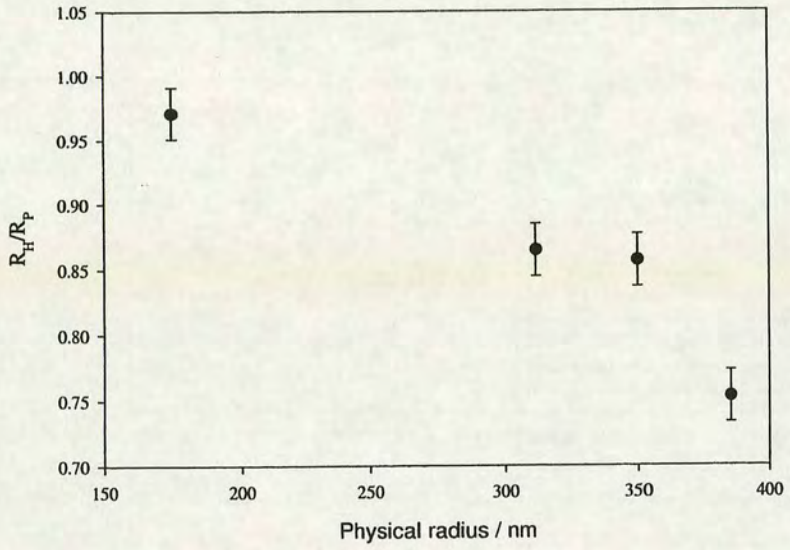

Figure 6.6: Comparison of the physical and hydrodynamic radii for a number of different sized particles.The data points shown are for typical values of the hydrodynamic radius, but it should be noted that different samples prepared with the same particles can give significantly varying radii, especially when using large particles.

physical and hydrodynamic radii whereas the smaller ones are barely indistinguishable within experimental error. Because the physical radii of the particles is known from SLS experiments it is possible to calculate the "slip" factor S from the Stokes-Einstein expression using the values for hydrodynamic radii simply from

$$S = 6\frac{R_h}{R_p} \tag{6.3}$$

and the results of this can be seen in Table 6.4

While it has been seen in repeated experiments that particle size affects the size of the coating, the reasons for this are not clearly understood. The interaction between the two solvents the PMMA core and the PHSA hairs is clearly vital to the end boundary conditions, but there is no way of understanding this from the present experiments.

R_p(nm)	R_h(nm)	S	Bulk Solvent	Coating solvent
175	170	5.83	5CB	Heptane
312	270	5.20	Cisedecalin	Petroleum ether
350	300	5.14	5CB	Heptane
385	310	4.83	5CB	Heptane

Table 6.1: Table showing a series of results taken from SLS and DLS showing the physical radius of particles alongside the measured hydrodynamic radius, and the slip factor implied. The combinations of solvents used for both the bulk and the coating are also shown. Note that for the case of the liquid crystal 5CB it was always used in the isotropic phase.

6.5 A Hydrodynamic model

In order to make predictions as to the validity of the proposed coated colloid model we began investigating a hydrodynamic model of our coated colloid system. The fluid dynamics of Stokes flow past a sphere has been known for well over a hundred years. What shall be presented in this section begins with the basic premise that the simple fluid dynamics of this case are well understood [64–67]. The theoretical treatment which follows contains a basic review of a previously used model and it's applications to our system, but the theoretical treatment shall not be examined in depth as the focus shall concentrate on how it can be used to compare with results acheived from experiment. Proposed by Hodgdon and Stillinger [68] the model uses a so called 2-step model of the colloidal particle surrounded by two solvents of different viscosities as can be seen in Fig 6.7. This model was initially used to describe Stokes-Einstein violation in glass forming liquids but here it is used in a completely new context to explain the effects that were observed experimentally.

Before we can begin to solve the hydrodynamic problem a number of common assumptions must be made in order to simplify the equations involved. The

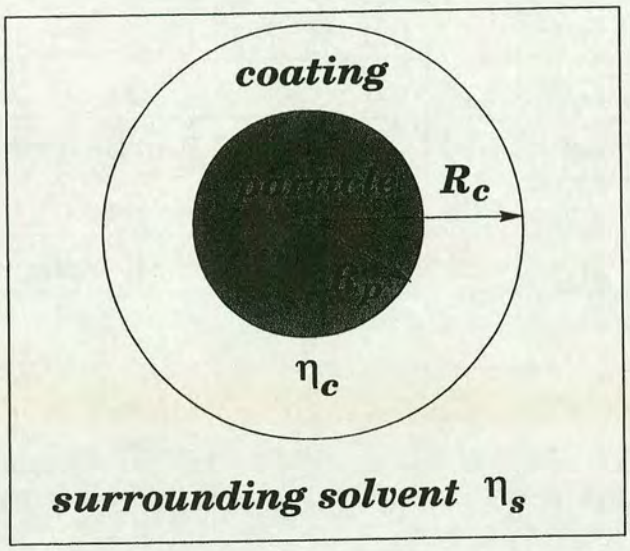

Figure 6.7: Diagram of the 2 zone model used for the hydrodynamic calculations of the coated colloid dynamics. The particle of radius R_p is surrounded by a region of solvent of viscosity η_c which in turn is surrounded by another solvent of viscosity η_s. The size of the coating is measured from the centre of the particle and is denoted as R_c so the actual coating thickness is given by $R_c - R_p$.

first of these is the assumption that the fluid is incompressible, meaning that any variations in pressure do not produce any significant variations in density. The second assumption is that the fluid flows with low Reynolds number. The Reynolds number is used as a measure of the type of forces which dominate the flow, with high Reynolds number flows being more turbulent than low Reynolds number flows which are laminar [69], and the assumption of low Reynolds flow for our system of colloidal particles diffusing in a normal solvent is reasonable.

These assumptions for steady-state flow around our particle lead to two partial differential equations for the fluid velocity ν_i. The first is the linearized Navier-Stokes equation

$$\eta \frac{\partial^2 \nu_i}{\partial x_k^2} = \frac{\partial p}{\partial x_i} \tag{6.4}$$

where p is the pressure and repeated indices imply summation, and the second is

the equation of continuity which comes directly from the assumption of incompressible flow

$$\frac{\partial \nu_i}{\partial x_i} = 0 \tag{6.5}$$

However to solve these equations for our system they must be used in spherical polar coordinate (r, θ, ϕ) form which is allowed because of the axisymmetric flow of the liquid. This gives a continuity equation of the form

$$\frac{1}{r^2}\frac{\partial}{\partial r}(r^2 \nu_r) + \frac{1}{r sin\theta}\frac{\partial}{\partial \theta}(sin\theta \nu_\theta) = 0 \tag{6.6}$$

The boundary conditions at the surface of the sphere must also be considered if an understanding of the hydrodynamics is to be had. In the case of a sphere in a single solvent there are two possible extreme cases. For slip boundary conditions there is no tangential force or normal velocity of the fluid at the particle surface, whereas for stick boundary conditions the fluid velocity vanishes completely at the surface. The other boundary condition which holds true in either case is that far from the sphere the velocity of the fluid is unperturbed by the particle.

For most colloidal systems stick boundary conditions are usual and in fact solving the two equations above with these boundary conditions eventually leads to the Stokes-Einstein expression. However cases of drops of one liquid suspended in another, as in emulsions, are described by slip boundary conditions at the surface because of the internal flow of the drop. For the case above, where a rigid particle is surrounded by two solvents, then it is reasonable to expect that the boundary conditions here will fall somewhere between the two extremes. Here both the Navier-Stokes equation and the equation of continuity still hold, as do the boundary conditions, but an additional boundary condition that states that the fluid velocity and transmitted force must be equal at the interface between the two fluids is needed.

As with the case for an ordinary sphere suspended in a single solvent the solution

to the hydrodynamic equations has the form

$$\nu_r = u(cos\theta)f(r) \tag{6.7}$$
$$\nu_\theta = -u(sin\theta)g(r)$$

where the boundary conditions determine the final form of f(r) and g(r). To satisfy Eqn. 6.6 the following condition is needed.

$$g(r) = \frac{r}{2}f'(r) + f(r). \tag{6.8}$$

Looking at the Navier-Stokes equation we can immediately identify that the right hand side of Eqn. 6.4 which contains the gradient of the pressure is unknown. However using the fact that $curl(\nabla F) = 0$ means that the equation can be satisfied whenever the curl of the left hand side is 0. We can now find the form of our Navier-Stokes equation by using the components of ν found in Eqn 6.8 and taking the curl of both sides to give

$$\frac{4}{r^2}f'(r) - \frac{4}{r}f''(r) - 4f'''(r) - \frac{r}{2}f''''(r) = 0 \tag{6.9}$$

for all r, and the solution of which can be found by repeated integration to be

$$f(r) = C_1\frac{r^2}{R^2} + C_2 + C_3\frac{R}{r} + C_4\frac{R^3}{r^3} \tag{6.10}$$

where the C_n are dimensionless constants. To determine the values of these constants requires the application of the boundary conditions in each of the two regions: inside the coating and outside of the coating.

Inside the coating the function takes the same form as Eqn 6.10 , whereas outside the boundary condition that as $r \to \infty$ then the velocity of the fluid is unperturbed by the particle means it has the form

$$f^o(r) = 1 + C_5\frac{R}{r} + C_6\frac{R^3}{r^3} \tag{6.11}$$

The boundary conditions can now be applied to these equations to give six linear equations for the six constants C_n. The drag force can be found in terms of either

C_3 or C_5 but the most useful form for us is

$$F = -4\pi\eta^s RuC_5 \tag{6.12}$$

where η_s is the viscosity of the bulk solvent, and C_5 has the form

$$C_5 = \frac{3l[-2 - 3l^5 + 2\xi(1 - l^5)]}{4 + 6l^5 + \xi(-8 + 9l - 10l^3 + 3l^5 + 6l^6) + \xi^2(l-1)^4(4 + 7l + 4l^2)} \tag{6.13}$$

where $l = \frac{R_c}{R_p}$ and $\xi = \frac{\eta_s}{\eta_c}$ and we assume stick boundary conditions between the particle and the coating at $r = R_p$. As a check on this we can see that if $\xi = 1$ or $l = 1$ then the drag force reduces to the familiar Stokes drag force at it should.

The determination of C_5 for the various parameters effectively equates to the "slip-factor" which was introduced earlier in the modified Stokes-Einstein expression.

6.6 Using the model

Now that we have introduced the finished model it should be possible to use it in order to make some predictions as to the nature of the coating in our experimental systems.

We have experimentally determined the hydrodynamics of our coated particles and so determined the slip-factor so it should be possible to work back with the help of the model to get an idea of the coating thickness.

The first step in this is to plot a graph of the theoretically obtained slip factor against l for the various parameters in our experimental system including particle size, coating viscosity and bulk solvent viscosity. A number of different combinations of bulk solvents and coating solvents were used and the respective viscosities can be found below.

Heptane (coating) viscosity $\eta_c = 0.32cp$ at 40^oC

Petroleum ether (coating) viscosity $\eta_c = 0.22$ cp at 20^oC

Cis-decalin (bulk solvent) viscosity $\eta_s = 3.38$ cp at 20^oC

5CB (bulk solvent) viscosity $\eta_s = 20$ cp at 40^oC

The values for the viscosities of Heptane and 5CB are both shown at 40^oC as it was necessary for the liquid crytsal to be in the isotropic phase when performing experiments. Because samples that used Cis-decalin as the bulk solvent were always combined with petroleum ether coatings and samples where the liquid crystal 5CB was used as the solvent always used heptane coatings we can calculate the two experimental values for $\xi = \frac{\eta_s}{\eta_c}$ to be ≈ 15 and 64.

From the previous investigation into the maximum coating size it was possible to put a limit on the coating thickness itself at around 2 - 3nm so in the following discussion a coating size of 2.5nm is assumed at all times. With the particle sizes used it would imply an l of no greater than about 1.008 for the 312nm particles and l=1.007 for the larger 385nm particles. With the above data and the hydrodynamic equations it is now possible to calculate a value for the coating size which gives values for the slip factor S that agree with the experimental data and a graph of this can be seen in Fig 6.8.

Now that predictions as to the slip factor have been made using the hydrodynamic model and some of the parameters used in the experiments it is possible to compare those with the actual experimentally measured values for S.

$\xi = \frac{\eta_s}{\eta_c}$	Theoretical S	Experimental S
15	5.4	5.2
64	4.9	4.8

Table 6.2: Comparing experimentally measured values of S with the theoretical predictions made for a 2.5nm coating of solvent surrounding the particle.

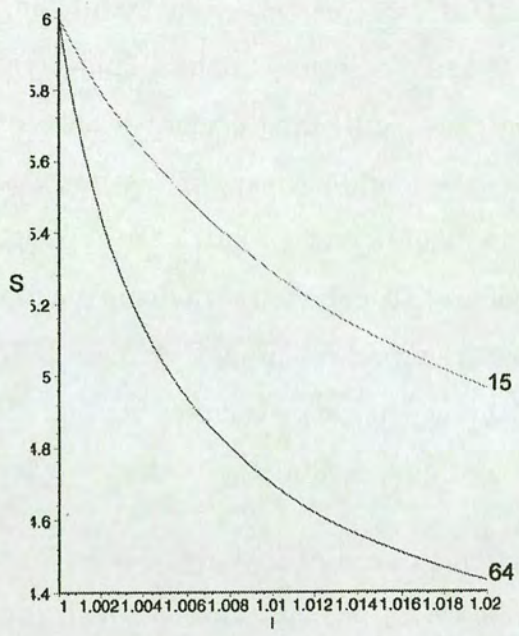

Figure 6.8: A plot of l ($\frac{R_c}{R_p}$) against the slip factor S for 2 values of ξ:15 and 64. For a 2.5nm coating we can see that $\xi = 15$ gives a value for S of around 5.4 while for $\xi = 64$ produces a S value of 4.9.

It can be see that while the theoretical and experimental predictions are not in total agreement the values predicted for S are similar, and in the discussion section of this chapter the many complications that may cause this discrepancy are examined further.

6.7 Coated colloids in a liquid crystal

In a previous chapter the phenomena of orientational pre-wetting was discussed, where liquid crystal molecules order at the surface of a colloidal particle in the isotropic phase. We have also just discussed how coated particles in a liquid crystal have altered dynamics as a result of changed boundary conditions, so it is now pertinent to ask how these two separate observations affect each other.

It was previously shown that colloidal particles that exhibited a solvent coating still showed a slowing of their diffusion as the liquid crytsal cooled from the isotropic to the nematic phase, providing evidence that even coated particles can act as defect sites in the liquid crytsal. In the last chapter samples of coated colloids suspended in a liquid crytsal which gave slip factors of $S = 5.45$ ($R_H = 318nm$ and $R_P = 350nm$) still showed significant molecular ordering at the particle surface. However, this was not always the case as it was frequently observed that particles which demonstrated a larger coating did not show any change in their diffusion as the liquid crystal approached the nematic phase.

To examine this further a number of samples were prepared in the usual manner until one that showed particles with an anomalously low hydrodynamic radius was found. The lower the radius the larger the solvent coating and the more pronounced the changes in boundary conditions at the particle surface will be. In Fig 6.9 shown below the particles used had a physical radius of 312nm but when measured with the standard techniques of DLS were shown to have a hydrodynamic radius of approximately 272nm leading to a slip factor S of 5.2.

The figure shows that for samples where the particles have large coatings then it is common that no increase in the hydrodynamic radius is seen as the liquid crystal approaches the nematic phase, unlike the uncoated particles where the radius does increase. This suggests that the large coating has the effect of making it impossible for the liquid crystal molecules to order at the particle surface because of the partially slip boundary conditions. This is unsurprising as the whole concept of orientational pre-wetting relies on the fact that the liquid crystal molecules attach themselves homeotropically at the particle surface in the isotropic phase. Slip boundary conditions would prevent this and so any ordering at the surface would become difficult.

A coating around the particles has other implications when a liquid crystal solvent is used. Because the molecules cannot attach on the particle surface they will no

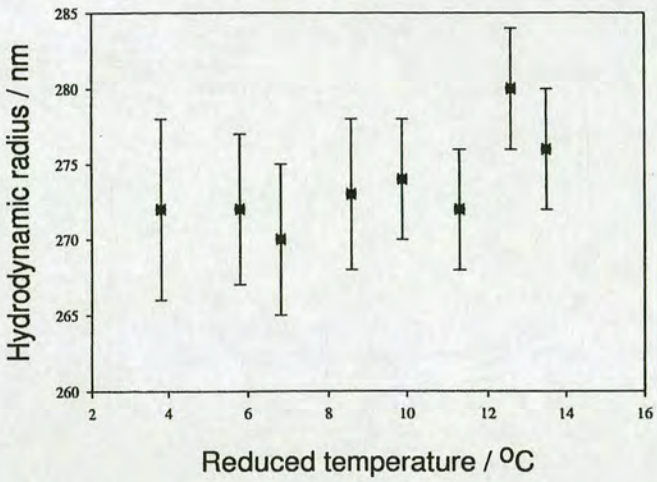

Figure 6.9: Measurements of hydrodynamic radius against reduced temperature ($T - T_c$) for 312nm coated particles in 5CB. No increase in the hydrodynamic radius is seen as the temperature is decreased indicating the large coating on the particles prevents any orientational pre-wetting at the particle surface.

longer act as defect sites, and may not affect the phase transiton temperature. Fig 6.10 shows the scattering intensity profiles as a function of temperature for 3 different samples: pure liquid crystal, liquid crystal with uncoated particles and liquid crystal with coated particles. It is obvious that the uncoated particles cause a marked decrease in the phase transition temperature whereas the coated particles leave the phase transition temperature practically the same as for the case of pure liquid crystal. This agrees with the theory that coated particles prohibit liquid crystal ordering at the surface.

While we have showed that large coatings have a profound effect on the particle dynamics and consequently their behaviour in the liquid crystal, but orientational pre-wetting is still observed for particles with smaller coatings, identified through a hydrodynamic radius which is close to the physical one, so it seems that a small coating does not completely rule out the possibility of ordering at the surface. To explain this further requires a discussion about the exact nature of the coating at

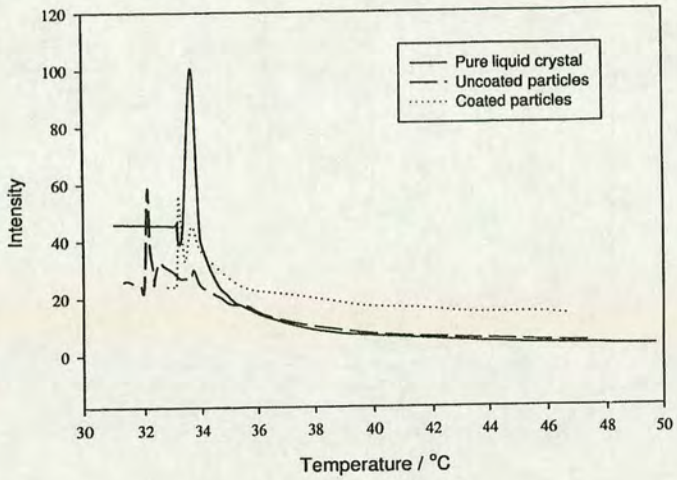

Figure 6.10: Intensity against temperature for 3 samples. The sample containing uncoated particles shows a delayed phase transition temperature while the samples prepared with coated particles have a transition which is practically identical to the pure liquid crystal.

the particle surface which shall be the topic of the final section in this chapter.

6.8 Discussion

In this chapter the dynamics of coated colloids have been discussed focusing on the possibility that a small solvent coating, caused by the particular preparation procedure, could have the effect of radically changing the boundary conditions at the surface of the particle and therefore their dynamics.

This began by the realisation that certain samples gave an anomalously low hydrodynamic radius when they were examined with Dynamic Light Scattering, and this led to a further examination of the preparation of the samples and how the existence of a solvent coating would lead to partial slip boundary conditions at the surface, resulting in an anomalously fast diffusion and consequently low hy-

drodynamic radius. Static Light Scattering measurements revealed no presence of a coating which in itself was useful as it allowed us to place a maximum thickness on the coating size as a large coating would have changed the form factor visibly. By comparing experimentally measured form factor with those given from theory it was possible to say that a coating of more than around 3 nm would change the form factor such that it would clear from Static Light Scattering. However even at this stage there were a number of complications regarding estimated of the coating thickness. The procedure of fitting experimental data to a theoretical form factor has a large number of unknown parameters. Factors like exact particle size and polydispersity clearly define the form factor and while these can be found from other methods the sensitivity of these parameters coupled with the other parameter of coating size means that fitting a theoretical form to the experimental data is difficult.

There is also the issue of variation in behaviour between different samples prepared from the same particles and in the same manner. It was observed that different samples gave different particle dynamics suggesting that the coating sizes were different in each case. This is perhaps unsurprising as the mechanism for coating the particles seems extremely sensitive but it raises the question that perhaps within each individual sample the particles themselves have different sized coatings. This is supported when the correlation functions in DLS are examined, as fitting to a single exponential was difficult. Particles with different sized coatings would have different boundary conditions and therefore diffuse at different speeds effectively introducing an exaggerated version of polydispersity which further complicates an already complicated system.

As important is the nature of the coating itself. The theoretical model used for the form factor fitting assumed that the particle is a core of PMMA of one refractive index surrounded by a coating of another refractive index in a two-step model. This is a large assumption as it completely ignores the presence of the

PHSA hairs at the particle surface and how the solvent interacts with this. If the solvent is entangled inbetween the hairs it would mean that the refractive index would be different to the pure solvent and any prediction to its size from the theoretical form factor is uncertain. Unfortunately without a closer examination of the particle surface/coating interface it is impossible to make more precise claims as to the size of the coating and so throughout the rest of the experiments and coating of approximately 3nm is assumed.

Further experiments were performed which offered a clearer picture of the coating phenomena. The coating itself seems to desorb away from the particles over a matter of days and the particles regain their stick boundary conditions, and particle size also seems to play a part with larger particles demonstrating a larger change in their dynamics, but again the reasons behind this are unclear at this time.

The latter half of the chapter was devoted to the development of a hydrodynamic model of coated colloids with the view to a comparison with experimental results. A two-zone model initially developed by Hodgon and Stillinger [68] was employed and used with parameters appropriate for our system to predict a value for the slip constant S in the modified Stokes-Einstein expression. It was found that a coating of the order of 3nm gave a value for the slip factor which although slightly higher than experimental data did agree reasonably well with the results, and as stated earlier it is possible that taking all of the relevant factors into account a slightly larger coating may be more realistic.

The last part of the chapter studied the effect that coatings surrounding particles have on their behaviour on liquid crystals. It was seen that while uncoated particles demonstrated an ordering of liquid crystal molecules at the particle surface, coated particles showed no such ordering as a result of the partial slip boundary conditions. This was also manifest when examining the phase transition temperature. For the uncoated particles a depression in the phase transition temperature

was observed as the particle act as defect sited disrupting the nematic order, but this phenomenon was not seen with the coated particles which resulted in a phase transiton temperature practically identical to that of the pure liquid crystal.

Chapter 7

Concentrated liquid crystal colloids

7.1 Introduction

So far all of the system we have been looking at have involved dilute colloidal suspensions in liquid crystal solvents. However there is also a lot of interesting behaviour to be found when we increase the concentration of the colloidal particles. This chapter shall be devoted to the study of these materials and the remarkable effects that are seen in these more concentrated systems.

It shall be shown that adding relatively concentrated amounts of colloidal particles to liquid crystal drastically alters the structure of the material and this is evident both through rheological measurements and microscopy observations. This is done using two liquid crystals: one nematic and another smectic to investigate the effects that molecular ordering have on the final composite structure, and the chapter begins the with the case for the ordinary nematic liquid crystal and then move onto the case where a smectic phase was also possible.

7.2 Effects of the nematic phase

7.2.1 Sample preparation

Because of the complications involved with preparing samples where the particles initially come from a solvent stock, it was decided that all samples should be prepared with dried particles. While this wasn't a practical solution for very small amounts of colloids due to the difficulty in completely re-dispersing small amounts of dried particles, the larger amounts used here meant it was viable.

First the final volume fraction of the samples was decided upon, and the amount of particles needed to produce that volume fraction for a given sample mass calculated. For example, a total sample mass of 5g requires a particle mass of 0.288g of particles to give a final volume fraction of 5%. It was therefore easy to measure 0.288g of dried colloidal particles and simply add enough liquid crystal to bring the total sample mass to 5g. The liquid crystal was added in the nematic phase at room temperature and then the entire sample was spun on a mixer in an oven at a suitable temperature for the isotropic phase (around 45^oC). The samples were then left mixing in the isotropic phase for approximately a week to ensure complete re-dispersal of the dried particles in the liquid crystal, and checked to see that no more particle aggregates were visible by eye. Once this was confirmed the samples were then ready to be used in the experiments. In these set of experiments the PMMA particles had a radius of 250nm, the liquid crystal was again 5CB, and the volume fraction was always 5%.

7.2.2 Direct observations and microscopy

It was immediately apparent once the samples were prepared that the presence of the colloidal particles had a profound effect on the final behaviour of the

solution. In the isotropic phase the liquid crystal appeared normal although slightly cloudier than normal due to the presence of the particles. However, when this was cooled to the nematic phase the sample "solidified" into a waxy solid which was rigid enough to be sliced with a knife, and an example of this can be seen in Fig 7.1.

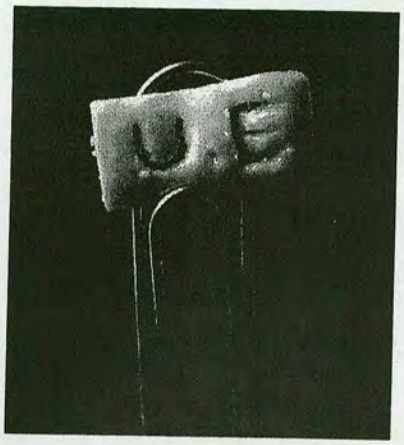

Figure 7.1: A slice of colloid liquid crystal composite. This particular sample was made from with a particle volume fraction of 20%, and at room temperature is so rigid that it can be cut with a knife. Picture courtesy of S. Meeker.

To examine this further bright field microscopy observations were performed on the samples as they were taken from the isotropic to the nematic states. To do this they were first kept and mixed in the isotropic phase and then, using a heated pipette, transferred onto an already heated slide and coverslip. This ensured that at no time was the sample ever cooled into the nematic phase. This was crucial because it was possible the samples would be irreversibly changed once they had entered the nematic phase once and it was necessary to observe the samples in the isotropic state under normal conditions. The liquid crystal colloids were then loaded into the hot stage connected to the microscope at $45°C$, well into the isotropic phase, again avoiding any cooling of the sample. Once the samples were successfully loaded onto the microscope observations could begin.

It was seen that in the isotropic phase the particles seemed to behave as they

would in any other solvent, where they diffuse around randomly in Brownian motion, and no evidence of any aggregation or other external forces was seen. A fixed cooling rate was then set and the sample cooled until room temperature. The nematic-isotropic transition was clearly identified by the rapid emergence of the birefringent thread-like texture associated with the disclination lines of the nematic phase. Below the phase transition temperature, where the structural change of the composites takes place, it was impossible to determine how the particles were behaving as the birefringence obscured everything else. To determine the particles structure within it was necessary to rapidly heat the sample (at around $15^{o}Cmin^{-1}$) into the isotropic phase where the disclination lines disappear. It was then possible to observe the underlying particle structure that was responsible for the huge increase in the solidity of the substance. This appeared as a honeycomb-like aggregate network of particles spanning the entire sample as can be seen in Fig 7.2.

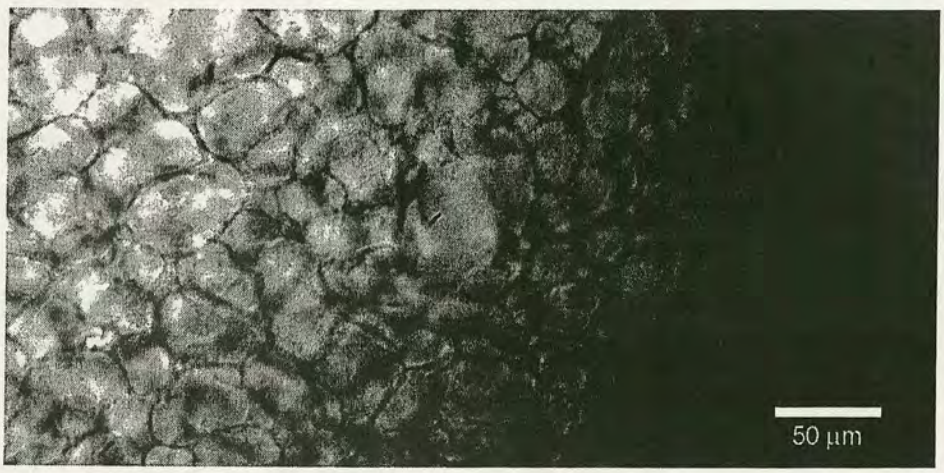

Figure 7.2: Microscope image of the honeycomb-like structure of aggregated particles that occurs when the liquid crystal undergoes the nematic phase transition. This image was taken using brightfield microscopy after reheating into the isotropic phase to eliminate the birefringent texture of the nematic which obscures the particles.

Clearly it is this particle network that is responsible for the sudden increase in solidity of the material when it is taken into the nematic phase. However, once

the sample has been taken into the isotropic phase the particle network begins to break up in a matter of a few minutes. The structure breaks down but the particles remain stuck in large aggregates and never fully re-disperse, and this confirmed the importance for the sample to be loaded into the apparatus in the isotropic phase without ever having entered the nematic.

7.2.3 Structural properties of network

To investigate this effect further rheology measurements were performed on a sample of this material as it was taken from the isotropic to the nematic phase. The samples used were again 5% volume fraction of 250nm particles in 5CB and taken from the same batch as the previous microscopy experiments.

Similarly to the microscopy observations above, it was decided that the liquid crystal colloid should be loaded in the isotropic phase and avoid the nematic phase altogether until measurements were to be made. This would prevent the possibly irreversible aggregation of the particles and give a better insight into the mechanism at work. Accordingly, the Peltier plate which the sample sits upon in the rheometer was first heated to 45^oC and the sample loaded onto this with a heated pipette. The sample was then pre-sheared at a shear rate of $100s^{-1}$ for about 2 minutes in order to mix the sample and re-disperse any particles that had aggregated together or got stuck to the cone or plate. A small amplitude oscillation was then applied to the material at 1Hz and a strain amplitude of 2% as the sample was cooled from 45^oC to 15^oC at a rate of $2^o min^{-1}$. The results of the measurements of the storage and loss modulii can be seen in Fig 7.3.

Looking at the graph we can see that at high temperatures the material behaves as expected. The loss modulus G'' which details the viscous nature of a substance is much higher than the storage modulus G' which contains information about the elasticity of the material. This is obvious by the general observation

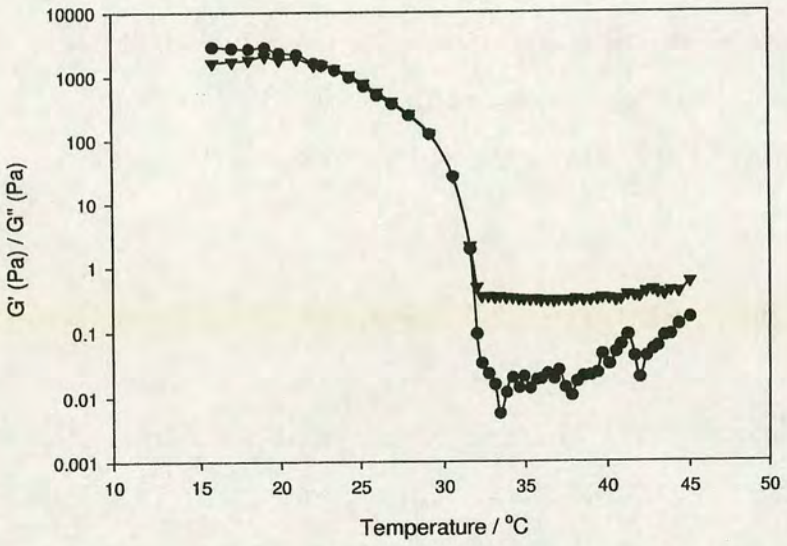

Figure 7.3: Oscillatory viscoelastic measurements of the storage and loss modulii of the liquid crystal colloid compound as it is cooled from the isotropic phase to the nematic phase at a rate of 2^oCmin^{-1}. The material undergoes a transformation from a viscous liquid to a waxy solid at the isotropic-nematic transition and this is evident by the huge increase in G' (circle data points) and G'' (triangle data points).

of the substance as a fairly unremarkable cloudy fluid at these temperatures. The interesting results occur when the material is cooled to a point approaching the isotropic-nematic phase transition. Here we see a dramatic increase in both the storage and loss moduli as the liquid crystal enters the nematic phase and while the nematic phase is more viscous than the isotropic and an increase in the loss modulus is to be expected the magnitude of the increase (a factor of 10^5) here means another mechanism must be responsible. As the system is cooled further we eventually see a levelling off of the storage and loss modulii to values around 1000 Pa and notice a slight decrease in the loss modulus at the lowest temperatures.

This data combined with the microscopy images provides compelling evidence

that the cause of the increased viscoelasticity of the composites is the particle network that is formed at the isotropic-nematic transition, and the honeycomb particle structure is strong enough to produce a solid with a storage modulus of over 1000 Pa.

Also of interest is the temperature position of the isotropic-nematic phase transition, as this provides insight into the relationship between the particles and the liquid crystal. The pure liquid crystal has a phase transition temperature of $\approx 35^oC$ but in the above graph the point at which we see an increase in G' and G'', and so presumably the phase transition, is lower at around $32-33^oC$. This is in agreement with our earlier results on more dilute systems where the presence of the particles affected the phase transition temperature and suggests that there exists liquid crystal ordering around the particles above the isotropic-nematic transition.

7.2.4 Developing a model for network formation

It is clear from the microscopy experiments performed previously that the formation of the particle network is responsible for the final viscoelasticity of the material, so the mechanism by which it is formed must now be understood. We can start by ruling out a number of possible explanations of the particle interactions at work in order to gain a more complete understanding of the system.

Any two particle dispersed in a solvent naturally have a van der Waals attractive force between them, but this force is present in the isotropic phase and no aggregation of the particles is seen here even over long periods of time so this can be excluded as a means of inducing the particle aggregation. In fact when samples are reheated from the nematic phase into the isotropic the particle network gradually begins to break up and the particles redisperse, however the process is not completely irreversible as shall be seen later.

Another possible cause for the particle network could be the effect of the particles disturbing the order in a nematic liquid crystal. As mentioned in a previous chapter particles will come together into "chains" in order to minimise the elastic distortion energy of the director field. The attraction is due to the interactions between particles and their associated satellite defects, which form dipolar configurations, attracting other particles along certain preferred directions. In a nematic crystal where the particles exhibit a radial hedgehog director structure two particles will repel each other along certain directions and attract along other directions leading to the chaining of particles, and this has been seen experimentally by Poulin *et al* [34] where drops of water are suspended in larger drops of nematic liquid crystal which are themselves suspended in a volume of water. The average energy associated with this attraction is $U \sim KR$ where K is the usual Frank constant ($\sim 10^{-11} Jm^{-1}$) and R is the particle radius which in this case is 250 nm. This gives an attractive energy between particles of $\sim 1000 k_B T$ from which we can estimate the storage modulus $G' \sim \phi U/R^3 \sim \phi K/R^2$ to be approximately 10 Pa, much smaller than we see in the experiments, and so this theory can not fully explain the process that leads to the particle network either.

A more plausible explanation for the behaviour observed, developed by Terentjev *et al* [16,17], requires looking at the mechanics of the isotropic-nematic transition. If pure liquid crystal is observed with a microscopy and crossed polarisers in its isotropic state nothing is seen as all light is extinguished. As it is cooled into the nematic phase small domains of nematic liquid crystal form which grow and coalesce as they touch, leading to the complete formation of the nematic phase. Now it is known that the presence of a colloidal particle will disturb the order of a liquid crystal and because of this the nematic phase will often try and expel the particle if possible. This is not seen when particles are suspended in drops of liquid crystal (as in the emulsions used earlier and in the Poulin experiments) because the boundary conditions differ, but in the case of a large volume of nematic with no imposed boundary conditions at the edges particles are seen to

be expelled. When a large concentration of these particles are present in the liquid crystal and it goes from the isotropic to the nematic phase the particles will be expelled from the growing nematic drops and aggregate as can be seen in Fig 7.4. In between the aggregated particles the liquid crystal will be "melted" in the isotropic phase as can be seen from Fig 7.5 and it is believed that this also contributes to the mechanical strength of the material.

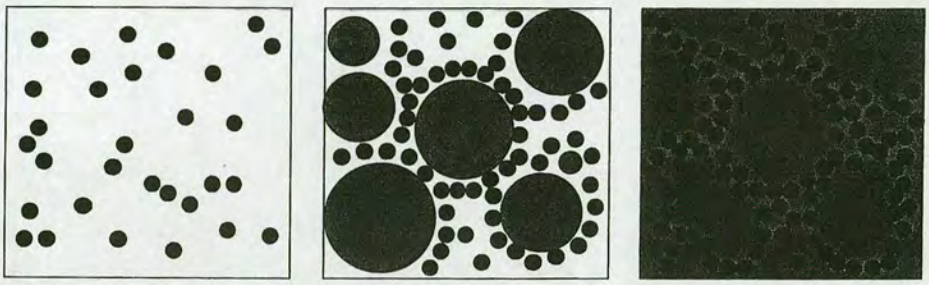

Figure 7.4: A series of schematic diagrams describing the formation mechanism of the particle network. In (a) the system is seen in the isotropic phase with the particles (black dots) diffusing in Brownian motion throughout the sample. As it is cooled into the nematic phase in (b) domains of nematic liquid crystal nucleate and expel the particles, pushing them together. In (c) the liquid crystal has completely changed into the nematic phase and the particles have aggregated into the rigid network which gives rise to the increase in viscoelasticity.

With the model in place we can begin to understand the huge elastic strength of our materials. Clearly densely packed colloidal particles will create a strong structure in itself, but the role of the liquid crystal is also important. In between the packed particles the liquid crystal is melted in its isotropic phase, but outside of the particles the liquid crystal remains in the nematic state. This creates an imbalance in the energy density between the nematic on either side of the cell walls and the isotropic inside the walls, which in turn creates an effective pressure pushing the particles together and strengthening the network even further. It is believed that these effects go some way to describing the structural strength of the materials that has been experimentally observed.

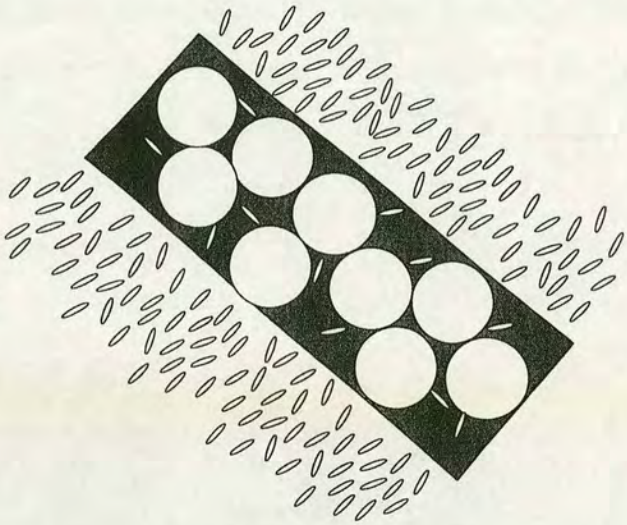

Figure 7.5: Close-up schematic of the cell wall of particle network, showing the molecular behaviour of the liquid crystal. Either side of the wall the liquid crystal is in the pure nematic state but "inside" the close packed particle wall (shaded region) the liquid crystal is melted, in its isotropic state. This leads to an effectively pressure on either side of the walls which pushes the particles together more increasing its viscoelastic strength.

From this we can see that the mechanism that creates the particle network is intrinsically linked to the mechanism of the isotropic-nematic transition itself so anything which affects the transition will probably have an effect on the final particle structure. One such factor that alters the dynamics of the transition is the cooling rate and so the next section investigates this further.

7.3 The effect of different cooling rates

The final viscoelastic strength of the liquid crystal colloids is linked to the particle network, which itself is linked to the process of the nematic-isotropic transition. Because of this anything which affects the dynamics of the transition will affect the particle structure, and one example of this is the rate of cooling from the isotropic to the nematic phase. To investigate this a number of samples were

prepared from the same stock and in the fashion described above. The samples were all prepared with a volume fraction of 5% and 250nm particles in 5CB.

Without performing any detailed experiments it is possible to see by eye that samples that are cooled from the isotropic to the nematic phase at a fast rate are more rigid than samples that are cooled at a slow rate. This is easily visible as the samples which are prepared with a slow cooling rate are softer and more "liquid-like" than the waxy solids produced when the cooling rate is fast. To quantify this more rheology and microscopy experiments, similar to the previous ones, were then performed to determine the effect of cooling rate on the viscoelasticity of the materials.

7.3.1 Relationship between cooling rate and microstructure

Bright field microscopy with crossed polarisers was then performed on the samples in order to gain insight as to how the cooling rate affects the particle structure. The samples were loaded onto the microscope in the isotropic phase at around 45^oC, and cooled at a set rate until the nematic phase was reached. Images were taken every few seconds as the phase transition was reached. Once the samples were taken into the nematic and the particle network had formed the samples were quickly heated at around 10^oCmin^{-1} into the isotropic phase as this allowed us to view the particle structure briefly and allowed for images to be taken. Images of the particle network in the isotropic phase, prepared with different cooling rates, can be seen in Fig 7.6

While it may appear at first glance that the two images are relatively similar there are subtle differences. The sample cooled at 1^oCmin^{-1} shows a particle network which has thicker aggregates and larger domain sizes than the one cooled at 3^oCmin^{-1} which is more regular. It is believed that these changes have a large effect on the rigidity of the material as shall be seen in the next section detailing

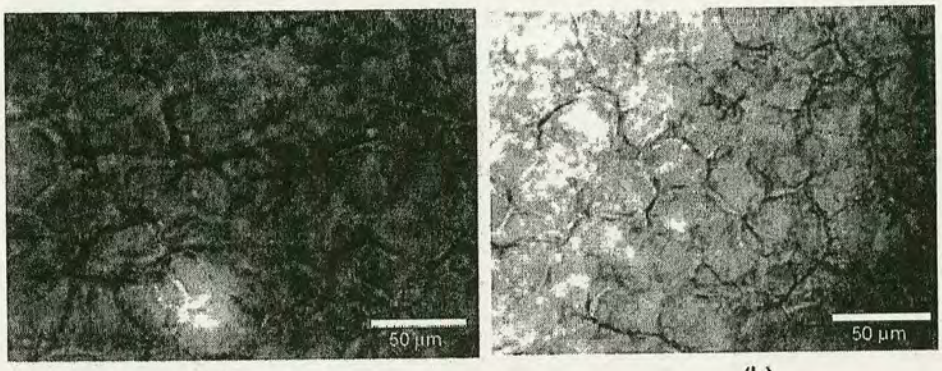

(a) (b)

Figure 7.6: Two microscopy images of the particle network taken in the isotropic phase after reheating. In (a) the initial rate of cooling from the isotropic to the nematic phase was 1^oCmin^{-1} and in (b) it was 3^oCmin^{-1}. The domain sizes in (a) are about $50\mu m$ on average which is significantly larger than in (b) where the domain sizes are around $35\mu m$. The aggregates are also thicker and more irregular in shape and size for the slower cooling rate. The fast cooling rate leads to a more regular network with smaller domain sizes. It is thought it is this difference in particle network which is partially responsible for the different viscoelastic properties.

the rheological investigation of this phenomenon.

But the microscopy can also tell us about the mechanism for the particle network creation in the first place and why different cooling rates lead to the different networks. As the samples were cooled a number of images were taken as the nematic domains were beginning to form amongst the bulk isotropic phase and further images were taken rapidly as the phase transition continued. Images of this can be seen in Fig 7.7.

Although the two images are quite blurry due to a lack of focus of the microscope it is possible to see the regions of nematic forming and coalescing. The sample which cooled at 1^oCmin^{-1} shows much larger bubbles than the one which cooled at 3^oCmin^{-1}. Because the particles disrupt the nematic order they are expelled from the nematic bubbles as they form, pushing them together in the aggregate network observed. Large bubbles will mean that the final domain sizes of the particles network will be large while the converse is similarly true. This gives

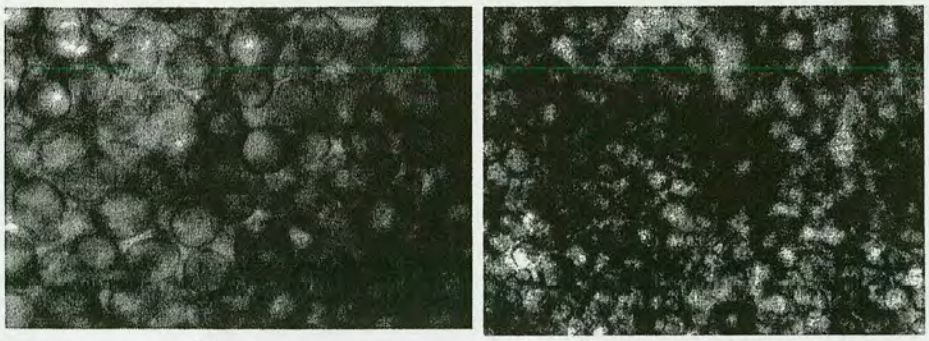

(a) (b)

Figure 7.7: Two microscopy images taken just below 35^oC when the nematic domains nucleate in the isotropic and eventually coalesce to completely form the nematic phase. In (a) the rate of cooling was 1^oCmin^{-1} and in (b) it was 3^oCmin^{-1}. It is clear that the bubbles in (a) are much larger than in (b). This is due to the slower cooling rate allowing the domains more time to grow.

an explanation for the cooling rate dependency on the elasticity of the liquid crystal colloids. A final structure which has small regularly shaped domains will be stronger than one where the domains are larger and more irregular, and a fast cooling rate means these structures are more likely to form.

While this model provides a mechanism for the dependence of rigidity on cooling rate, to examine it further requires rheological measurements. This method is also inherently flawed by the fact that the network can only be observed in the isotropic phase meaning a rapid heating of the structure into this phase was necessary in order for images to be taken. While in this state the structure quickly breaks up (in a matter of minutes) and so all images must be taken quickly. A method that allowed for the observation of the particle network in the nematic phase would be extremely useful and one such method shall be employed later.

7.3.2 Rheological study of the effects of cooling rate

A further series of samples were prepared in the manner described above, again with a volume fraction of 5%. These were studied individually using the rheometer with an oscillatory shear with a rate of 1Hz and a strain amplitude of 2%. The samples were initially loaded into the rheometer at 45^oC with a heated pipette so the liquid crystal colloids remained in the isotropic phase at all times, and were then subjected to a pre-shear at a rate of $100s^{-1}$ to ensure all the particles were well dispersed throughout the sample. The samples were then cooled at different rates from 45^oC down to 15^oC and the storage and loss modulii measured in order to quantify the effect that cooling rate had on the viscoelastic properties of the material. At first 3 different cooling rates were used: 1^oCmin^{-1}, 2^oCmin^{-1} and 3^oCmin^{-1} and the results for the rheological measurements for these can be seen in Fig 7.8.

As the graph shows the values for the loss modulus G'' are higher than the storage modulus G' at high temperatures, and this is to be expected as the sample behaves like a normal liquid at here. The interesting behaviour begins when the nematic phase transition is reached. As with the previous rheological results we see a huge increase in the values of G' and G'' as the particle network is formed and increases the rigidity of the substance, but we can also observe a difference in the magnitudes of the increases for the different cooling rates. For a cooling rate of $1^oC/min$ we still observe a large increase in the storage modulus up to a value of 200 Pa but this is significantly less than the values reached for $2^oC/min$ and $3^oC/min$ where the values for G' reach up towards 10000 Pa, an increase by a factor of 50. As a side note, the position of the nematic-isotropic phase transition for 5CB is well known to exist at about 35^oC but it appears that this is depressed in this case due to the particles acting as defect sites in the isotropic phase agreeing with some of the earlier experiments.

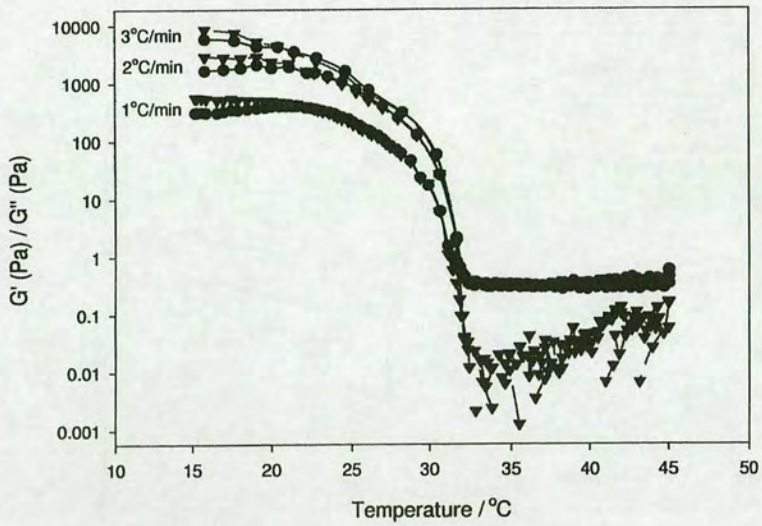

Figure 7.8: Rheology results for the storage (triangles) and loss (circles) modulii for samples cooled at 3 different rates. It is immediately apparent that faster cooling results in a stronger structure.

The reason for the sensitivity of the viscoelasticity on cooling rate can now be related to the domain sizes of the final particle network. A fast cooling rate results in a regular honeycomb particle network with small domain sizes and consequently a high elasticity while the slower cooling rate means the resultant network is irregular with large aggregates of particles and large domain sizes which leads to a lower elasticity.

7.4 Successive measurements

It was quickly discovered that after a rheology run had been performed, with the liquid crystal cooling to around 15^oC, that the samples were irreversibly altered. Upon reheating into the isotropic phase and a further period of vigourous pre-

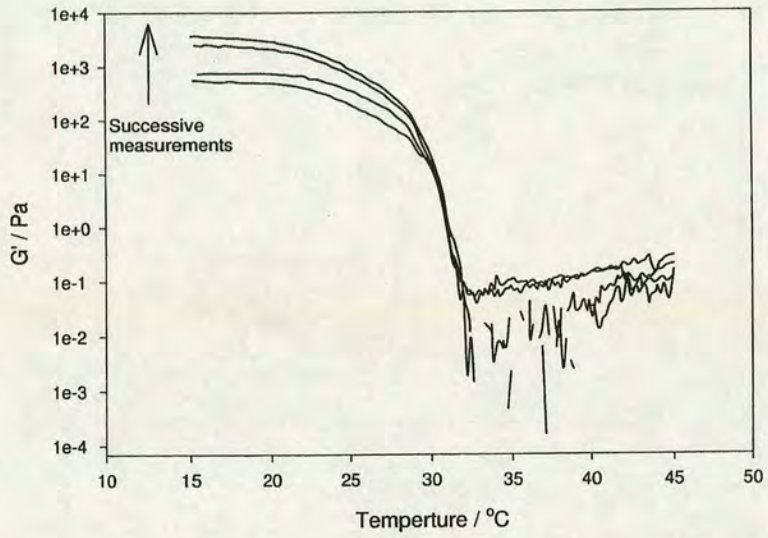

Figure 7.9: Rheological measurements of the storage modulus taken from the same sample where reheating into the isotropic phase and vigorously shearing for 5 minutes occurred between each run. Even with these precautions it appears that any particle structure which is formed when the liquid crystal enters the nematic phase is not completely destroyed upon return into the isotropic.

shearing the experiments were repeated with different results. It seems that with each successive experiment that the storage and loss moduli were increasing compared with the previous run. An example of this can be seen in Fig 7.9

The important point is that even when the material has been reheated into the isotropic phase and sheared again with the apparent return to the liquid state and re-dispersal of the particles that the process is not entirely reversible. It is probable that while the particle network breaks up upon reheating that the particles themselves stay together in smaller aggregates and upon cooling these aggregates come together to form stronger networks. It is likely that if the samples were vigorously shaken for a longer period of time that they would completely return to their original state and indeed this has been seen in recent experiments

[70]. Because of this, all of the results shown for rheology experiments were done with the samples never having been used before, ensuring that the tests are as accurate as possible. Indeed, when the above experiment regarding elasticity dependence on cooling rate is performed where the same sample has been used and reheated the results are drastically different as can be seen from Fig 7.10 If

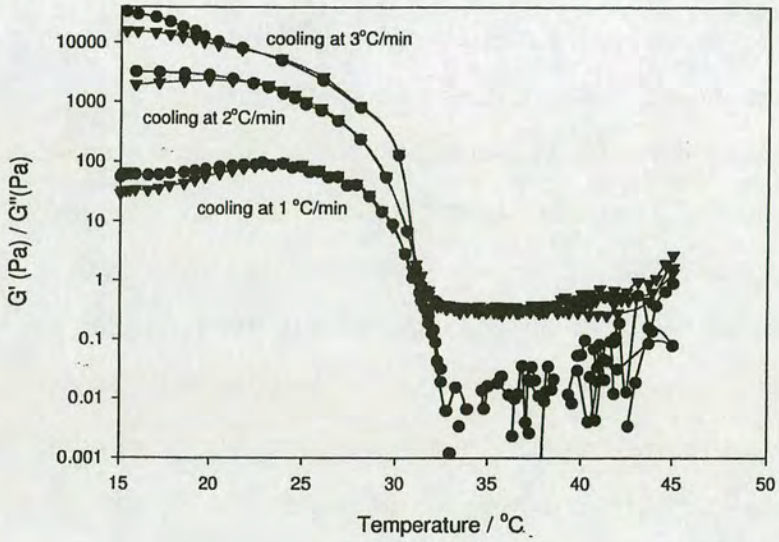

Figure 7.10: Successive storage and loss modulii measurements for a 5% volume fraction sample. Here the first run was performed with a cooling rate of $1^oC/min$ until 15^oC was reached. The sample was then reheated to 45^oC and sheared vigourously for 2 minutes in an attempt to redisperse the particles. The sample was then cooled at a rate of $2^oC/min$ and finally after repeating the above steps at $3^oC/min$.

the graph above is compared with that from the previous section, where a new sample was used each time, it is seen that repeating the experiment using the same sample leads to a much greater apparent increase in elasticity with cooling rate. In fact much of this increase is due to the impossibility of completely re-dispersing the particles between successive runs and proves that aggregation of the particles at least partially contributes to the elasticity of the final network structure.

7.5 Confocal microscopy of particle network

It has been previously mentioned that one of the biggest drawbacks of the conventional bright field microscopy used earlier is the need for the structure to be observed in the isotropic phase where the network itself quickly degrades. One method of microscopy which would eliminate this is confocal microscopy used with a laser which scans across the sample and only detects objects which fluoresce at a certain wavelength. This means that if the particles are dyed with a suitable dye then only they will be observed by the microscope even when they are in the nematic phase of the liquid crystal. In this case a common dye called Fluorescein was used, as this is excited by an illuminating wavelength of around 500nm which is suitable for the laser used. When the dyed particles are added to the liquid crystal, the microscope should only detect the particles even in the nematic phase where the particles are usually obscured by the disclination line texture, and so should allow for a more accurate analysis of the particle network than was possible with conventional bright field microscopy.

The first step was to dye the particles, and as with the previous experiments the particles used were 250nm radius and were dyed simply by adding a few drops of fluorescein to the stock solution of particles in heptane. This solution was then dried in a vacuum oven at a high temperature until the heptane had completely evaporated leaving only dried particles. These were then added to our 5CB and shaken vigourously for around a week in the isotropic phase to ensure complete dispersal of the particles.

Once the stock of liquid crystal colloid had been prepared a number of samples were made up with different cooling rates, and because the microscopy was possible at room temperature these were all prepared beforehand by adding a drop of the liquid crystal and particles onto a heated slide with a heated pipette, and placing a coverslip on top. When this was done the sample could then be cooled

at the desired rate to room temperature and stored until it could be examined using the confocal microscope. All samples were prepared from the same stock of liquid crystal colloid to minimise any possible variation from one sample to the next and the following cooling rates were used: $0.5^oC/min$, $1^oC/min$, $2^oC/min$, $3^oC/min$, $5^oC/min$ and $10^oC/min$.

There are a number of similarities and differences between these images and the normal bright field microscopy images taken of the particle network in the previous sections. We can see that as before the particles have aggregated together to form a network spanning the entire sample, but the advantage with this method is that it allows for all the imaging to be done in the nematic phase where the birefringent textures usually prevent conventional microscopy. This was only possible because of the particle labelling with a fluorescent dye, however from the final images it appears as though much of the dye has leaked from the particles into the surrounding liquid crystal making the isolation of the particles from the background difficult. It is still possible to discriminate the network from the liquid crystal though, and doing so reveals insight into the mechanisms that are involved in the formation of the network.

Perhaps the most obvious difference between the images taken of particles with and without dye is that the dyed particle networks show thicker walls. In the undyed case the network "walls" were very thin but it seems that the dye has the additional effect of increasing the tendency of the particles to naturally aggregate possibly by interfering with the stabilising layer around the particles which normally prevents aggregation. Indeed, even in the isotropic phase large visible aggregates of dyed particles are seen to form if the sample is left unmixed. This means that much larger clumps of particles will be formed in the network which in turn has an effect on the viscoelasticity of the material as shall be seen later. This implies that while the natural aggregation of the particles is at least connected in someway with the network formation it is not exclusively responsible

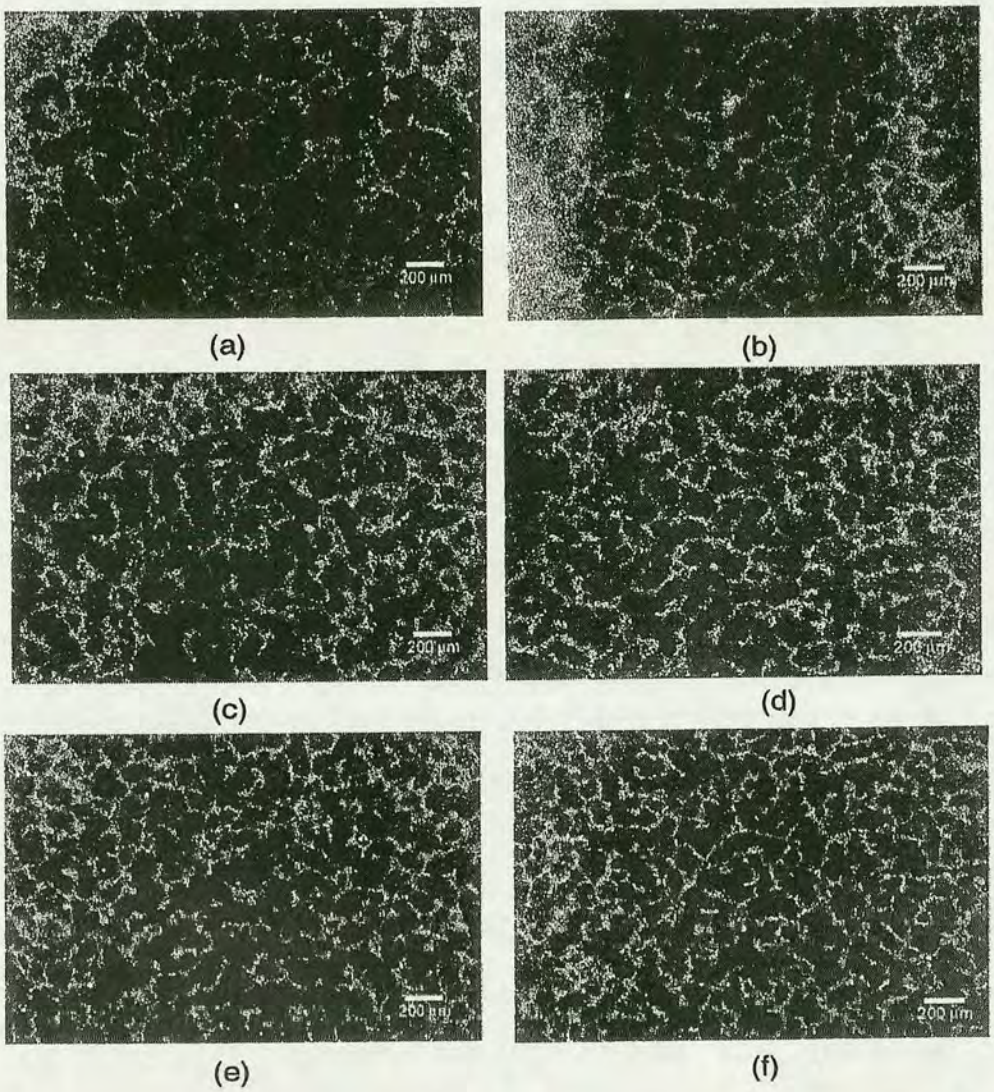

Figure 7.11: Confocal microscopy images taken from 5% volume fraction liquid crystal colloid composites for a variety of different cooling rates. Images (a) through to (f) show samples cooled at 0.5, 1, 2, 3, 5 and $10^oC/min$ respectively. The lighter regions are the dyed colloids aggregating to form a particle network while the darker regions represent the liquid crystal, here in its nematic state at room temperature. Unfortunately due to the preparation procedure much of the dye has leaked out from the particles into the liquid crystal making observation of the particles alone difficult. All images are shown alongside a $200\mu m$ scale bar.

for it as we see the network formation in samples with no aggregation, and this in turn gives weight to the idea that the network is formed due to the particle expulsion from the nucleating nematic drops in the isotropic phase.

7.5.1 Domain sizes of network

The effect of cooling rate on elasticity is linked to the strength of the particle particle network and one contributor of this is the domain size of the network caused by the nucleating nematic bubbles. As was previously shown a fast cooling rate will result in a network with small domain sizes and a rigid structure whereas a slow cooling rate cause large domains and a weaker structure, and from the confocal microscopy images we can begin and try to understand the link between cooling rate and domain size.

To this end the images of the particle networks obtained from the confocal microscopy experiments have been studied, measuring large amounts of individual domain sizes and averaging them. This was made difficult by two complications: due to the dye leaking from the particles into the liquid crystal solvent the network resolution is low and the nature of the network itself is very irregular making it difficult to accurately measure the domain sizes. As such the errors in domain size calculation are large but they still show an interesting trend as can be seen in Fig 7.12.

7.5.2 Rheology of dyed networks

The use of the dye on the particles has clearly had an effect on the final structure of the particle network with the larger aggregates presumably due to increased attractive forces between particles. If this is the case then the viscoelasticity of the material will also be affected and in order to examine this further the samples

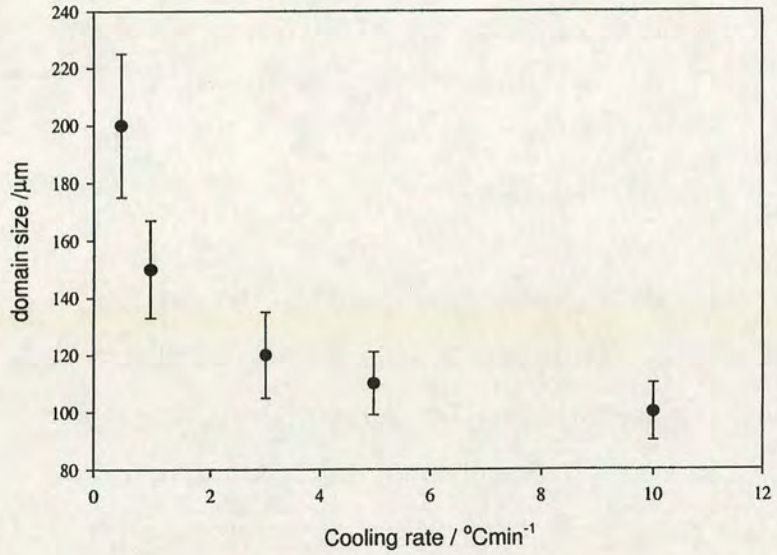

Figure 7.12: Results for the domain size against cooling rate from measuring and averaging over approximately 100 domains. While the errors are large for the slower cooling rates where the network is very irregular a clear pattern can be seen as the domain size seems to level off at around 100nm at higher cooling rates.

were investigated with the rheometer once more.

The samples were made from the same stock of dyed 250nm particles in 5CB at a volume fraction of 5%, and investigated with an oscillatory shear with strain amplitude of 2% and shear rate 1Hz. The sample was initially heated to 45^oC and subjected to a pre-shear at a rate of $100s^{-1}$ for 5 minutes to ensure complete dispersal of the particles and then cooled at a constant rate of $2^oC/min$ until 15^oC was reached. As before, the sample was loaded onto the rheometer with a heated pipette ensuring the liquid crystal remained in the isotropic phase throughout.

The results of G' and G'' against temperature can be seen in Fig 7.13 and show a very different form to the undyed particles. The first thing that is noticeably different is the magnitude of G' compared with G'' at high temperatures. In the

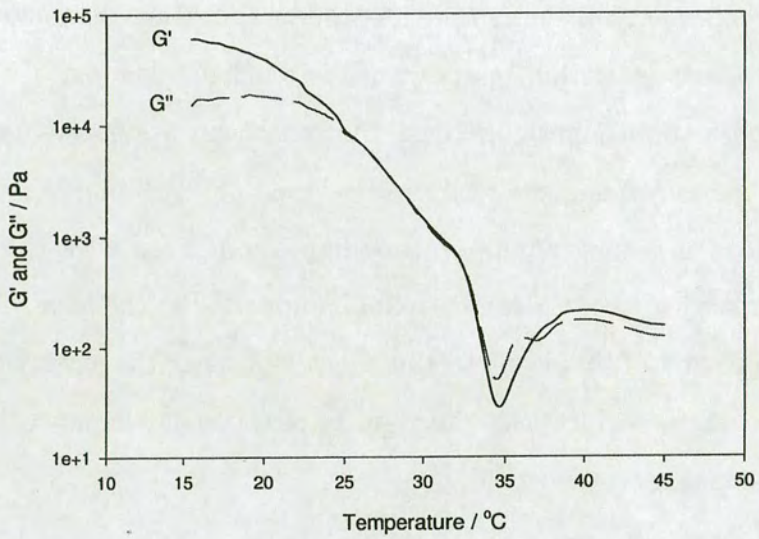

Figure 7.13: Rheology results for measurements of G' and G'' made on a sample of dyed particles in 5CB. The shape of the curve is markedly different to the one normally associated with the composites as the jump in the storage and loss modulii is spread out over a much greater temperature range and the magnitude of the jump itself is greater. Both of these observations can be attributed to the effects of dying the particles, as this seems to increase their tendency to aggregate thus changing the network formation mechanics.

previous samples using undyed particles the magnitude of G' was indicating that the sample had little elasticity to it in the isotropic state and was indeed acting as a viscous liquid. However with the dyed particles we see values for G' and G'' which are nearly equal at these temperatures and are also around 1000 times that seen in the case of undyed particles. This again suggests that the dye has caused some drastic change to the interactive forces between the particles, and that this attraction is causing the particles to aggregate even at high temperatures increasing the viscoelasticity of the sample. As the temperature is cooled and the isotropic-nematic phase transition temperature is reached a sudden drop in G' and G'' is seen before the dramatic increase that has been previously seen. The magnitude of this increased is greater, almost by a factor of 100 but the increase itself is spread out over a longer temperature range compared with the undyed particles where the majority of the increase in G' happened in the near vicinity of the phase transition. All of this leads to the conclusion that the extra attractive forces between the particles increases the rigidity of the particle network and so consequently the substance as a whole.

7.6 Effects of a smectic phase

Having examined the effect that the nematic phase had on the formation of the particle network, it seemed a natural extension of this to investigate the possible effects that the smectic phase would have. The smectic phase has an intrinsically higher elasticity due to the molecular structure so the possibility of increasing the rigidity of the material beyond that already seen was worthy of study. The liquid crystal that was used for these experiments was 8CB which exhibits a isotropic phase above 40^oC, a nematic phase between 33.5^oC and 40^oC, and a smectic phase below 33.5^oC and the particles used were the same as used in the previous experiments, having a radius of 250nm.

Because 8CB has a smectic phase which itself displays a very high viscosity, it was necessary to first measure this in order that any increase in the storage or loss modulii could be separated from this. To this end, pure 8CB was studied using the rheometer and an oscillatory shear as the temperature was cooled from 55^oC down to 15^oC and the results of the viscosity measurements can be seen in Fig 7.14.

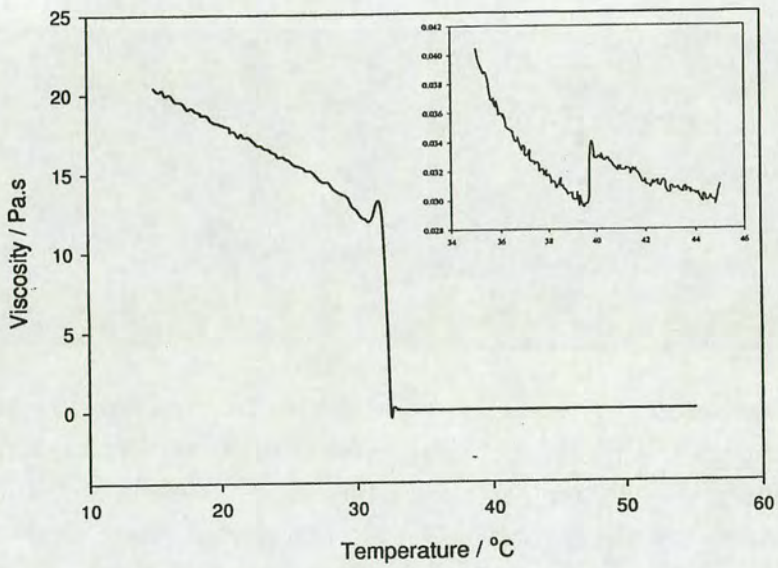

Figure 7.14: Viscosity measurements as a function of temperature for pure 8CB. The nematic-smectic transition is clearly defined by a large jump in the viscosity, while the isotropic-nematic (inset) is much smaller and cannot be seen on the larger scale.

It was decided that due to the complications of dying the particles for use in confocal microscopy that all microscopy should be performed using a conventional brightfield set up. This would allow us to see the effects that the two ordered phases had on the particle network but only after reheating into the isotropic phase. Rheology would then be performed on the samples to determine the viscoelastic properties of the new composites.

7.7 Microscopy images from 8CB samples

Samples of 5% volume fraction colloids in 8CB were prepared as before and loaded onto the microscope at around 45^0C, well into the isotropic phase. The sample was then cooled at a steady rate of $1^oC/min$ until the nematic phase was reached at around 40^oC and the particle network was seen to form, at which time the sample was reheated into the isotropic phase to allow for a clearer viewing of the network structure and an example of this can be seen in Fig 7.15.

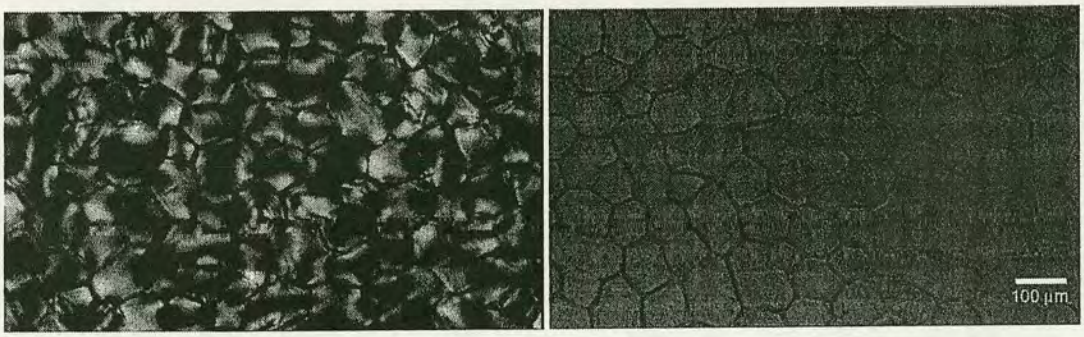

Figure 7.15: Two microscopy images of a 5% volume fraction liquid crystal colloid composite prepared with 8CB. The first image shows the liquid crystal as it first enters the nematic phase, and while the nematic texture obscures much of the image it is still possible to make out the particle network. The second image shows the same sample after reheating back into the isotropic phase to allow for a clearer view of the network, alongside a scale bar to give some idea of the domain sizes.

If the sample is then cooled to below 33^oC at the same rate we can see how the smectic phase of the liquid crystal affects the particle network after reheating into the isotropic phase. A microscopic image taken in the isotropic phase after reheating from the smectic can be seen in Fig 7.16.

It is evident from the above images the while the nematic phase of 8CB acts in the same way as 5CB, where the emerging nematic bubble pushed the particles together into the aggregated network, that once the network has been formed it is unaffected when the liquid crystal undergoes the phase transition into the smectic phase. This is not surprising as to alter the shape of the rigid network

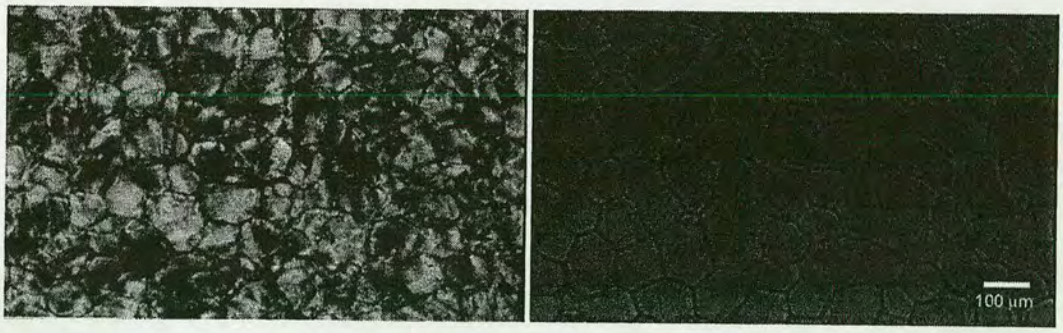

Figure 7.16: Microscopy image taken in the isotropic phase of the liquid crystal after the sample had been previously cooled into the smectic phase then reheated. The particle network is identical to that formed when the sample was only taken into the nematic phase suggesting that the smectic phase does not radically affect the network once it has been initially formed by the nucleating nematic phase.

would require large amounts of energy from the nematic-smectic transition.

7.8 Rheology results from 8CB samples

With the previous samples prepared with 5CB rheology was useful in understanding some of the properties of the particle network, and was therefore repeated for the samples prepared with 8CB in order to determine the elasticity effects that a smectic phase would cause.

The preparation procedure was identical to previous efforts with the 5% volume fraction samples loaded into the rheometer in the isotropic phase, and then subjected to a vigorous pre-shear for a number of minutes in order to fully disperse the particles. The sample was then cooled at a constant rate of $1^oC/min$ from 50^oC to 15^oC with measurements of G' and G'' being taken at regular intervals, the results of which can be seen in Fig 7.17.

The rheology measurements show that the nucleating nematic phase once again has the effect of creating a rigid particle network indicated by the initial jump

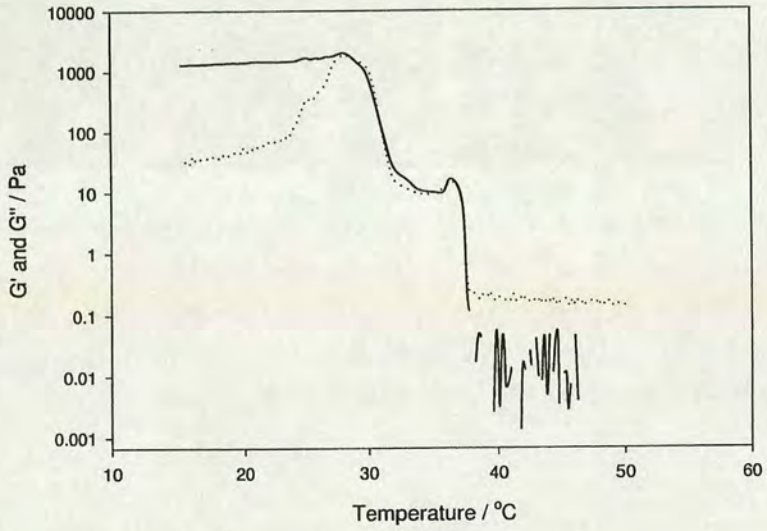

Figure 7.17: Rheological measurements of G' (solid line) and G'' (dots) taken as the sample is cooled from the isotropic to the smectic phase. At high temperatures the sample behaves as a normal liquid where the loss modulus is significantly higher than the storage modulus. The first jump in G' and G'' corresponds to the isotropic-nematic transition while the second corresponds to the nematic-smectic transition.

in both G' and G''. As the temperature is cooled further into the smectic phase there is another jump in G' and G'', but as the microscopy has shown the smectic phase does not affect the already established particle network so we can conclude that the second jump must be due mainly to the changes in viscoelasticity of the liquid crystal itself. This is supported by recalling the viscosity measurements of pure 8CB where a large jump in viscosity was seen at the nematic-smectic phase transition. A point should be made about the effect of the ordered liquid crystal, on either side of the cell walls, on the melted isotropic inside the walls. It was mentioned in a previous chapter that this could cause an "nematic pressure" which would have the effect of increasing the strength of the network further. It is also possible that while a smectic phase does not alter the shape of the network

that a "smectic pressure" could also partially account for the observed increase in rigidity.

7.9 Discussion

While there are numerous similarities between the samples prepared with 5CB, which demonstrates only a nematic phase, and 8CB, which demonstrates a nematic and smectic phase there are also significant differences which reveal information about the mechanism of the network formation. Perhaps the most obvious difference is the domain sizes of the respective networks created by the corresponding nematic phases of both liquid crystals. The average network domain size for the samples prepared with 5CB was around $50 \pm 10\mu m$ for a cooling rate of $2^oC/min$, whereas for the samples prepared with 8CB this was around $100 \pm 20\mu m$. This large difference in domain size contributes to a difference in the elasticity between the two types, with the small domain sizes of the 5CB type resulting in greater rigidity than the 8CB type. While this is not a direct consequence of the smectic phase it highlights another factor in determining the final strength of the network: the dynamics of the isotropic-nematic transition.

It was seen from the viscosity measurements of 8CB, where there was little change in the properties around the isotropic-nematic phase transition, that the transition itself must be more "weakly first order" in comparison to 5CB where there is a large jump in the viscosity at the transition. Physically this means that both isotropic and nematic phases coexist for a longer period of time for 8CB, implying that the nucleating nematic bubbles will have more time to grow. This would explain why the domain sizes are larger for the samples prepared with 8CB and why these samples form weaker composites.

There are other factors which are important in determining the network strength,

including the particle density of the cell walls. It is possible that in the case of the 8CB samples the particles are not packed as densely as in the 5CB particles due to the dynamics of the isotropic-nematic transition. It also mentioned previously that due to the external pressure cause by nematic liquid crystal on either side of the melted isotropic inside the cell walls that the particles could be pushed together further still increasing the mechanical strength. This effect would vary between different liquid crystals, so we must therefore exercise caution when discussing the role of domain size on final elastic strength of CLCC's. Indeed these considerations are also pertinent when discussing the role of cooling rate on the final elastic strength. Faster cooling rates may push the particles together more, forming a denser structure and increased network strength.

Though the network may be weaker for samples prepared with 8CB, it is also apparent that once the network has been formed as the nematic phase is reached that it is strong enough so that the phase transition into the smectic phase leaves it for the most part unchanged and any change to the viscoelastic properties can be mainly attributed to the changes in the liquid crystal itself.

The use of confocal microscopy was also useful in examining the behaviour of the particles in the network formation. A side effect of dying the particles was that they had an increased tendency to aggregate. This was clear as large aggregates could be seen in the isotropic phase of the liquid crystal, and is possibly due to a destabilisation of the polymer layer surrounding the particles. When these samples were cooled into the nematic phase the structures had a larger storage modulus compared with the samples that did not tend to aggregate. This tells us that while aggregation plays an important role in the network formation it is not the sole contributor and it also suggests that even low quality particle systems (ie polydisperse aggregating systems) could still be used to create strong composites. This may have important industrial consequences if they are ever to be used commercially.

Chapter 8

Conclusions

8.1 Summary of results

In this thesis we have presented results from a study of the behaviour of liquid crystal colloids and the dynamics of coated colloids. The first step in this project was to examine the dynamics of typical colloidal particles in the isotropic phase of a thermotropic liquid crystal. During the course of the investigations it was found that the colloidal particles were becoming coated in a low viscosity solvent which altered their dynamics and an off-shoot study was undertaken to study this further. Experiments were also performed in order to determine the behaviour of the coated colloids in a liquid crystal. The focus of the experiments then moved on to examining the remarkable structural properties of concentrated liquid crystal colloid composites, and a number of methods were employed to investigate their unusual elastic strength.

8.1.1 Dynamics of colloids in isotropic phase

Dispersing colloids in a liquid crystal was of interest to us for a number of reasons, but perhaps the biggest motivation with regards to the later work was that it allowed us to gain an insight into the forces at work between colloidal particles in a liquid crystal and how the molecules behaved near the particle as the liquid crystal underwent the phase transition. It was shown that as the liquid crystal was cooled from the isotropic phase towards the nematic that the particles demonstrated a slowing of their diffusion which was explained by the ordering of liquid crystal molecules at the particle surface. This molecular ordering, in the isotropic phase, results in higher local viscosity and consequently slower colloidal dynamics. It was shown that the ability of the particle to act as defect sites in this way also affected the position of the phase transition temperature, lowering it significantly.

8.1.2 Dynamics of coated colloids

The study of colloidal dynamics, while not completely relevant to the main examination of liquid crystal colloids, still demonstrated some novel colloidal behaviour and served as an important cautionary warning as to the importance of preparation procedure on the final behaviour of the system. Particles, initially suspended in a low viscosity solvent, were transferred directly to another higher viscosity solvent, and placed in an oven at such a temperature so as to remove the low viscosity solvent. However, this was found to be difficult as while the bulk of the low viscosity solvent could be easily evaporated there still remained a thin layer surrounding the particle which affects their dynamics dramatically. The coated particles showed a friction coefficient which was much lower than the 6 value associated with the usual stick boundary conditions in the Stokes-Einstein expression, with values being found as low as 4.8.

A hydrodynamical model of a coated particle, suspended in solvent was then used

to theoretically calculate the friction coefficients for our system. It was found that the friction coefficients predicted by the theory were in fairly good agreement with that measured from experiments but out of the whole thesis this area perhaps has the most unanswered questions. It is believed that any large coating would be detected experimentally with static light scattering and because it was never seen the coating was presumed to be very small. This assumption is open to discussion as the exact nature of the solvent coating/particle interface is a complicated one, and it may be possible that a slightly larger coating is possible than was first predicted. This may explain the small discrepancy between the results predicted by theory and those obtained by experiment, but without a rigorous study into the precise nature of the coating then it is impossible to elaborate further. What is known is that the coating does desorb away from the particle with time and that physical particle size has a bearing on the thickness of the coating, but again this is an area where further work is needed.

The final section of this chapter was devoted to the studying the effects that coating particles would have on their dynamics in a liquid crystal. It was seen that, where the particles acted as defect sites before, they no longer did so when coatings were present. Indeed no change in the colloid dynamics was observed as the liquid crystal approached the phase transition. This may prove as useful tool because if it was possible to accurately control the size of the coating then it effectively creates a mechanism of controlling the ability of the particles to work as defect sites. This would allow for the role of defects sites in the behaviour of liquid crystal to be examined more thoroughly.

8.1.3 Structure and rheology of liquid crystal colloid composites

The final results chapter involved an investigation into the structural qualities of liquid crystal colloid composites. Samples of 5% particles in two different liquid crystals were prepared:5CB, which has a nematic phase, and 8CB which has a nematic and a smectic. These were then cooled from the isotropic phase to the nematic and examined with rheology and microscopy. It was seen that as the nematic phase is reached a network particles is formed which spans the entire sample greatly increasing its elastic strength. This is created when the nucleating nematic domains expel the particles, which eventually cluster together into the particle aggregate network. This mechanism is extremely sensitive to the cooling rate as this effects the size of the nucleating nematic domains. As such, we find a large cooling rate dependence on final structural strength, with faster cooling rates resulting in higher elastic modulii. Confocal microscopy allowed as to study this further, and to get a measure of the relationship between the cooling rate and the domain sizes of the particle network.

When the smectic phase was examined it was found that while an increase in elasticity was seen that this was probably due to the inherently increase in elasticity of the pure liquid crystal itself and not because of any change to the particle network. It appears as once the network has formed in the nucleating nematic phase it is so rigid so as to remain that way even when the smectic phase is entered.

8.2 Future work

Having described the main conclusions of this work it is perhaps relevant to also discuss some of the areas in which further work needs to be done to clear

any remaining confusion, and some of the possible practical implications of the materials I have been studying.

Perhaps one of the ares that would benefit the most from further investigation is the behaviour of coated particles. Because this area of research began as an off shoot study it was not possible to dedicate as much time as we would have liked to exploring the exact nature of the coating. Although the dynamics of coated particles was comprehensively explored the behaviour of the coating itself at the molecular level on the particle surface is still uncertain. A closer investigation on this scale would hopefully reveal the relationship between the PMMA core, PHSA hairs and solvent coating which in turn would lead to a better predictability of the coated particle dynamics. This is useful because if coated particles are to be used as a means of testing the effect of defect sites in a liquid crystal then they boundary conditions at the surface of the particle must be well controlled. If it were possible to accurately control the boundary conditions of the particles then a mechanism has been introduced that effectively allows for controlled introduction of defect sites in a liquid crystal.

While introducing controlled defects into a liquid crystal is interesting from an academic point of view perhaps more useful from an industrial standpoint are the potential uses of the colloid liquid crystal composites (CLCC's). The vastly increased rigidity of the liquid crystal composites coupled with their electro-optical response have important implications in the field of liquid crystal displays. There are possibilities that a new type of display could be created with great mechanical strength as well as the fast switching associated with normal LCD's. These new displays would be flexible enough so that they could be rolled up making them extremely portable, and could be used in the construction of laptop computers or even televisions. However much work still has to be done understanding the electro-optical response of these materials in both the isotropic and nematic states if improved LCD's are to be made, and issues relating to the final mechan-

ical strength of CLCC's are also crucial.

It was seen during our investigations that the choice of liquid crystal was important in determining the final elasticity of the CLCC's with certain liquid crystals resulting in stronger materials. This is believed to be due to the complex molecular behaviour at the isotropic-nematic transition, some liquid crystals can be described as "better" nematics than others in that they lead to a higher elastic modulus of the CLCC. This appears to be closely related to the domain sizes of the particle network, as well as the mechanical strength of the network itself and further work in this area would give a clearer insight into these fascinating materials.

Bibliography

[1] Tschudi T. Kreuzer, M. and R. Eidenschink. *Mol. Cryst. Liq. Cryst.*, 223:219, 1992.

[2] F. Brochard and P.G. de Gennes. *J. Phs. (Paris)*, 31:691–708, 1970.

[3] S-H. Chen and N.M. Amer. *Phs. Rev. Lett.*, 51:2298–2301, 1983.

[4] A.M. Figueiredo Neto and M.M.F. Saba. *Phys. Rev. A*, 34:3483–3485, 1986.

[5] Frenkel E. Van de Riet E. Bottger, A. and R. Zijlstra. *Liquid crytsals*, 2:539–547, 1987.

[6] Fang J. Ming N. Sun, Z. and X. Tang. *Phys. Lett. A*, 145:284–286, 1990.

[7] Fang N. Hsia Y.F. Widatallah, H.M. and X.M. Lee. *Phys. Lett. A*, 215:326–330, 1996.

[8] S.V. Burylov and Y.L. Raikher. *Phys. Rev. E*, 50:358–367, 1994.

[9] M. Kreuzer and R Eidenschink. *Liquid Crystals in Complex Geometries.* Taylor and Francis, 1996.

[10] Raghunathan V.A. Poulin, P. and D. Roux. *J. Phys. France*, 4:1557–1569, 1994.

[11] E.M. Terentjev and R.W. Ruhwandl. *Phys. Rev. E*, 54:5204–5210, 1996.

[12] R.W. Ruhwandl and E.M. Terentjev. *Phys. Rev. E*, 56:5561–5565, 1997.

[13] R.W. Ruhwandl and E.M. Terentjev. *Phys. Rev. E*, 55:2958–2961, 1997.

[14] Pettey D. Stark H. Lubensky, T.C. and N. Currier. *Phys. Rev. E*, 57:610–625, 1998.

[15] Poon W.C-K. Crain J. Meeker, S.P. and E.M. Terentjev. *Phys. Rev. E*, 61:R6083–R6086, 2000.

[16] V.J. Anderson, S.P.-Crain J. Terntjev E.M., Meeker, and W.C-K. Poon. *Euro. Phy. J. E*, 4:11–20, 2001.

[17] V.J. Anderson, S.P.-Crain J. Terntjev E.M., Meeker, and W.C-K. Poon. *Euro. Phy. J. E*, 4:21–28, 2001.

[18] P.G. Petrov and M. Terentjev. *Langmuir*, 17:2942–2949, 2001.

[19] I-C. Khoo and F. Simoni. *Physics of Liquid Crystalline materials.* Gordon and Breach, 1991.

[20] P.G. de Gennes and J. Prost. *The Physics of liquid Crystals.* Oxford University Press, 1993.

[21] Gray G.W. *Thermotropic Liquid Crystals.* John Wiley and sons, 1987.

[22] Wojtowicz P.J. Priestly, E.B and P. Sheng. *Introduction to Liquid Crystals.* Plenum Press, 1976.

[23] S. Chandrasekhar. *Liquid crystals.* Cambridge University, 1977.

[24] P.J. Collings and M. Hird. *Introduction to Liquid Crystals.* Taylor and Francis, 1997.

[25] G. Vertogen and W.H. de Jeu. *Thermotropic Liquid Crystals: Fundamentals.* Springer-Verlag, 1988.

[26] S. Elston and R. Sambles. *The Optics of Thermotropic Liquid Crystals.* Taylor and Francis, 1998.

[27] D.H. Everett. *Basic Principles of Colloid Science.* RSC, 1988.

[28] P.N. Pusey. Colloidal suspensions. chapter 10.

[29] W.B. Russel, D.A. Saville, and W.R. Schowalter. *Colloidal Dispersions.* Cambridge University Press, Cambridge, 1948.

[30] J. Brandrup and E.H. Immergut, editors. *The Polymer Handbook.* Wiley, New York, Chichester, 1989.

[31] D.J. Fairhurst. *Polydispersity in Colloidal Phase Transitions.* PhD thesis, University of Edinburgh, 1999.

[32] K. Miyano. Cellular solid behaviour of liquid crystal colloids 1. *Phys. Rev. Lett*, 43:51, 1979.

[33] H. Stark. *Euro. Phys. J. B.*, 10:311–321, 1999.

[34] P. Poulin and D.A. Weitz. *Phys. Rev. E*, 57:626–637, 1998.

[35] L. Antl, J.W. Goodwin, R.D. Hill, R.H. Ottewill, S.M. Owens, and S. Papworth. The prepration of poly(methyl methacrylate) latices in non-aqueous media. *Coll. Surf.*, 17:67–78, 1986.

[36] P. M. Golz. *Dynamics of Colloids in Polymer Solutions.* PhD thesis, University of Edinburgh, 1999.

[37] W. Schaertl and H. Sillescu. *J.Stat.Phys.*, 77:1007–1025, 1994.

[38] Richetti P. Raghunathan, V.A. and D. Roux. *Mol. Cryst. Liq. Cryst.*, 288:181–187, 1996.

[39] V. ad Weitz D.A. Poulin, P. Cabuil. *Phys. Rev. Lett.*, 79:4862–4865, 1997.

[40] R.C. Weast, editor. *CRC handbook of Chemistry and Physics.* CRC Press, Baton Rouge, Florida, 1988.

[41] P Snabre and P. Mills. *Euro. Phys. J. E.*, 1:105–114, 2000.

[42] Hsiung H. Guyot-Sionnest, P. and Y.R. Shen. *Phys. Rev. Lett.*, 57:2963–2966, 1986.

[43] Weitz D. A. D. Stark H. Lubensky, T.C. and N. Currier. *Science*, 275:1770–1773, 1997.

[44] G. Maret. Diffusing wave spectroscopy. *Curr. Op. Colloid Interface Sci.*, 2:251–257, 1997.

[45] B.J. Berne and R. Pecora. *Dynamic Light Scattering.* Wiley, New York, 1976.

[46] P. Munk. *Introduction to Macromolecular Science.* Wiley, New York, Chichester, 1989.

[47] P.N. Pusey and W. van. Megen. *J. Chem. Phys.*, 80:3513–3519, 1984.

[48] V.C. Martelozzo. *Crystallisation and phase separation in colloidal systems.* PhD thesis, University of Edinburgh, 2001.

[49] Pusey P.N. and J.M. Vaughan. *Light Scattering and Intensity Fluctuation Spectroscopy.* London: The Chemical Society, 1975.

[50] P.N. Pusey. *Phil. Trans. R. Soc. Lond.*, 293:429–439, 1979.

[51] J.K.G. Dhont. *An Introduction to the Dynamics of Colloids.* Elsevier, Amsterdam, 1996.

[52] R. Pecora, editor. *Dynamic Light Scattering.* Plenum Press, New York and London, 1985.

[53] P.N. Pusey and J. Brown. *J. Chem. Phys.*, 62:1136–1144, 1975.

[54] Hutton J.F. Barnes, H.A. and K. Walters. *An Introduction to Rheology.* Elsevier, 1993.

[55] A.G. Fredrickson. *Principles and applications of rheology.* Prentice-Hall, 1964.

[56] M. Reiner. *Deformation, strain and flow: an elementary introduction to rheology.* London: H.K. Lewis, 1960.

[57] R.W. Whorlow. *Rheological techniques.* Ellis Horwood, 1992.

[58] L.A. Galloway. *Phase behaviour of colloid-micelle mixtures.* PhD thesis, University of Edinburgh, 2001.

[59] M.S. Elliot. *The optical microscopy of colloidal suspensions.* PhD thesis, University of Edinburgh, 1999.

[60] B. Savile. *Introduction to light microscopy.* Oxford, 1997.

[61] H. Haga and C.W. Garland. *Phys. Rev. E*, 56:3044–3052, 1997.

[62] Stark H. Borstnik, A. and S. Zumer. *Phys. Rev. E*, 60:4210–4217, 1999.

[63] B.K. Shivamoggi. *Theoretical fluid dynamics.* John Wiley, 19948.

[64] S. Kim and S. J. Karrila. *Microhydrodynamics.* Butterworth-Heinemann, 1991.

[65] A. Liggett. *Fluid mechanics.* McGraw-Hill, 1994.

[66] L.D. Landau and E.M. Lifshitz. *Fluid mechanics.* Pergamon Press, 1959.

[67] F. Chortlon. *Textbook of Fluid Dynamics.* Nostrand, 1967.

[68] J.A. Hodgdon and F.H Stillinger. *Phys Rev E*, 48:207–213, 1993.

[69] H. Ockendon and J.R. Ockendon. *Viscous Flow.* Cambridge Press, 1995.

[70] D. Vollmer. Private Communication.